DISSERTATION

MOLECULAR MECHANISMS REGULATING Kv2.1-INDUCTION OF ENDOPLASMIC RETICULUM / PLASMA MEMBRANE CONTACT SITES

Submitted by

Ben Johnson

Department of Biomedical Sciences

In partial fulfillment of the requirements

For the Degree of Doctor of Philosophy

Colorado State University

Fort Collins, Colorado

Summer 2019

Doctoral Committee:

Advisor: Michael Tamkun

Gregory Amberg
Santiago Di Pietro
Jessica Prenni
Susan Tsunoda

ABSTRACT

MOLECULAR MECHANISMS REGULATING Kv2.1-INDUCTION
OF ENDOPLASMIC RETICULUM / PLASMA MEMBRANE
CONTACT SITES

Kv2 voltage gated potassium channels localize to ‘clusters’ on the soma, axon initial segment, and dendritic arbor of hippocampal neurons. For decades the molecular mechanism behind this localization pattern was unknown. In 2015 our lab determined that this behavior was due to the channels interacting with an unknown endoplasmic reticulum resident protein and thereby forming endoplasmic reticulum / plasma membrane (ER/PM) junctions. The channel clusters covering the surface of cells represented those domains.

The work in this dissertation examines in increased detail the mechanism, regulation, and possible functions associated with these sites. ER/PM junctions are domains with a variety of roles. They regulate both calcium and lipid homeostasis, they are involved in vesicular trafficking, and they oversee a host of cell signaling pathways. Junctions represent 12% of the neuronal soma surface and are also present in both the axon and the dendritic arbor. These are sites that exhibit a high degree of dynamic flux, both in composition and in structure. Residency of junction proteins is governed by the calcium concentration of the ER, the calcium concentration of the cytosol, the activity of the excitable cell, and the lipid composition of the PM. In turn these residents influence the nature of the junction, determining the function and nanoarchitecture of these domains.

In this work we use a proximity-based biotinylation approach to identify VAMP-associated proteins (VAPs) as the Kv2 channel interactor responsible for the formation of ER/PM junctions.

We characterize the amino acid motif necessary to generate interaction between the two proteins, finding an unconventional FFAT motif located in the channel C-terminus. We examine the protein composition of these novel junctions by investigating their relationship with other known ER/PM tethers such as Nir2, STIM1 and the junctophilins. We use super resolution imaging techniques to observe ER membrane behavior at these locations and study how that behavior changes during the concentration of additional protein residents. Lastly, we investigate the mechanisms underlying Kv2-VAP junction disassembly during neuronal activity and insult. We find that Kv2.1-VAP unbinding during glutamate stimulation is mediated by serine residues downstream of the Kv2.1 FFAT motif. This dispersal of Kv2-VAP ER/PM junctions during calcium influx is mirrored by junctophilin-induced junction disassembly, suggesting a common mechanism regulating ER/PM junctions throughout the hippocampus.

This dissertation examines a novel microdomain formed by Kv2 channels and presents data describing how this domain is created and regulated on a molecular level. It represents the first in-depth study of this topic.

ACKNOWLEDGEMENTS

There are a number of people I would like to sincerely thank for making this work a possibility: my family, my friends, my peers, and my mentors. I could not have accomplished this work without all of you.

Denise and Patricia at Skidmore, thank you for taking me on that summer and letting me discover how much I loved research. Susan, your lab rekindled this love and taught me that, for some odd reason, late nights in the lab can be calming influence. Girma, thank you for being a friend, and teaching me everything I know about fly genetics. Noreen, your lab taught me to stay involved in the world, both in science and at large. Alexa, Dylan, Remi, Mal – remember that bowling and pie aren't just a suggestion, they're really the only pursuit of any merit.

Mike, I'm not sure I ever told you this, but the real reason I wanted to join your lab wasn't because of the techniques, or the questions being asked (although the localization pattern of Kv2.1 was immediately appealing). The reason was the way you approached problems, how you thought about the whole of things, and then how you came up with a wild and crazy approach that no one had ever tried before but in retrospect was the only thing that made any sense. This type of problem solving is clearly the combination of both immense knowledge, and immense creativity. To learn that way of thinking was the real reason you were my first choice.

Phil and Liz, you two paved a road so wide it would've been hard not to follow in your footsteps. You taught me so much about how to be a scientist. I can't thank you two enough. Laura, Emily, and Ashley, you three were incredible coworkers and even more incredible friends. Xevi, you're a backstabbing traitor and you always will be. Don't ever change that about yourself. All of you, keep up the Who, keep up the horror stories.

Ma, pa, Jill, Brian, Brady, Brooke, Bailey, Linda, Bob, Hunter, Katherine, James – you're the best family anyone could hope for. Amanda, Hopper, I can't wait to start this new chapter with you. I love you, and thank you for the socks.

DEDICATION

To my father, who taught me right from wrong.

TABLE OF CONTENTS

Chapter One: An Introduction

"[I]n order to achieve a satisfactory understanding of how any biological system functions, the detailed molecular composition and structure of that system must be known"

-Singer & Nicolson, 1972 (1)

The Kv2 channels: A History

Kv2.1 was first discovered by cDNA expression cloning from rat brain in Rolf Joho's lab in 1989 (2). This channel, originally designated drk1, encoded a classic delayed rectifier K^+ channel with a high activation threshold of -15 mV. These investigators postulated that the unusually large cytoplasmic C-terminus may be involved in both channel regulation and subcellular localization. As discussed below, these ideas were correct. Three years later in the Snyder lab, Kv2.2, first termed cdrk1, was cloned from rat taste buds using drk1 sequence to screen a cDNA library (3). Kv2.1 and Kv2.2 are conserved in the channel forming core, containing the six transmembrane domains and ion conducting pore, and within a limited region of the proximal C-terminus, but otherwise show little sequence identity (3). mRNA expression analysis indicated areas of overlapping expression in the CNS but suggested that cells predominantly use either Kv2.1 or Kv2.2 (4, 5). Studies of Kv2.1 have dominated the Kv2 literature, partially due to a Kv2.2 cloning artifact which wasn't realized for some time (6), and Kv2.1 is emphasized in the discussion presented below. However, Kv2.2 shares many properties with Kv2.1, as well as some intriguing differences, which are noted where appropriate.

RNA expression studies and antibody-based protein detection indicate that Kv2 channels are perhaps the most widely expressed voltage-gated K^+ channel genes in terms of tissue distribution. They are present in cortical (7), hippocampal (8), and α-motoneurons (9) but also in retinal bipolar cells (10), cardiac myocytes (11), vascular and gastrointestinal smooth muscle (12,

13), and pancreatic beta cells (14, 15). Kv2.1 protein expression is high not only in neurons but even in cell types such as vascular smooth muscle where the outward currents average 100-200 pA (12). From a functional standpoint, Kv2.1-derived K^+ currents regulate the action potential waveform in pyramidal neurons undergoing high frequency stimulation (16), cardiac action potential duration (17), vascular smooth muscle membrane potential and contraction (12), beta cell potential and insulin release (14, 15, 18), and cortical neuron apoptosis (19-22). Mutations altering Kv2.1 conductance are linked to epilepsy in humans (23, 24) and Kv2.1 knockout mice are epileptic, hyperactive, and display defects in spatial learning (25). Additionally, these mice have elevated serum insulin levels, a prolonged glucose-induced beta cell action potential duration and a diminished firing frequency (18).

Kv2 channels 'cluster' on the membrane

Two years after the cloning of Kv2.1 cDNA the Trimmer group used immunolocalization in rat cerebral cortex to explore the distribution of Kv2.1 (26). Immunoreactivity was described as neuronal specific, with staining present on the soma and both the apical and proximal dendrites. Importantly, Kv2.1 immuno-staining was described as having a "punctate, membrane-associated nature" as opposed to a fully diffuse localization across somato-dendritic compartments. This was the first evidence that Kv2.1 adopts a unique and enigmatic subcellular localization pattern on the neuronal plasma membrane. Two years later these findings were both supported and expanded upon by the Snyder group that first identified Kv2.2 (4, 5). Whereas the Trimmer group initially focused on pyramidal cells of the rat cortex, Hwang et al. also found α-Kv2.1 staining in Purkinje and granule cells of the cerebellum and granule cells of the olfactory bulb. Furthermore, the Snyder group reported molecular layer staining consistent with stellate and basket cells. Again, Kv2.1

immunoreactivity was described as “punctate” in nature. Given the additional finding that Kv2.1 migrates heterogeneously during SDS gel electrophoresis, the Snyder lab postulated that differences in cellular localization could be due to either Kv2.1 posttranslational modification or “may result from some intrinsic targeting information contained within the amino acid sequences of the two K^+ channels that directs them to the different subcellular compartments where they are then post-translationally modified” (5). These hypotheses would prove especially apt in the years to come.

In 1996, evidence suggesting a specific domain of Kv2.1 is important for its localization, as well as the putative role of posttranslational modification, began to solidify (27). The Trimmer group generated two Kv2.1 C-terminal truncation mutants, ΔC187 and ΔC318, and found that while wildtype Kv2.1 and the ΔC187 mutant both formed 0.5-1.0 μm “clusters” on the cell membrane of MDCK cells, removal of additional amino acids from the C-terminus abolished clustering, as the ΔC318 construct was uniformly distributed. It was also revealed that while wildtype Kv2.1 would cluster in MDCK cells, the clustered phenotype was reported absent in COS-1 cells. Concomitantly, Scannevin et al. noted differences in the gel mobility of Kv2.1 in the two separate cell types, i.e. Western analysis revealed a higher molecular weight in the clustering MDCK cells compared to a lower molecular weight in the non-clustering COS-1 cells, consistent with a link between channel posttranslational modification and clustering. Given earlier findings using *in vivo* ^{32}P-labeling (28), it was deemed likely a portion of these posttranslational modifications represented phosphorylation events.

At this time, the mechanism by which Kv2.1 localized into clusters was poorly understood, for all that was known was that a portion of the C-terminus was critical and that clustering may be phosphorylation-dependent. Then in 2000, the Trimmer lab used a series of truncation and internal

deletion mutations to identify a 26 amino acid region within the C-terminus of Kv2.1 that was responsible for clustering (29). They called this 26 amino acid region the proximal restriction and clustering (PRC) domain. The addition of this domain to the C-terminus of Kv1.5 endowed a clustering phenotype to its otherwise fully diffuse membrane localization while its removal completely abolished clustering in Kv2.1. In addition, several point mutations within the PRC domain also abrogated the clustering phenotype.

Kv2.2 also contains a PRC-like domain and clusters on the membranes of neurons, however it would take 18 years from the time it was first cloned for the field to recognize this fact due to an unfortunate single-nucleotide deletion that resulted in a diffuse truncated protein (6).

As it was previously established that Kv2.1 channels are capable of shaping dendritic $[Ca^{2+}]_i$ transients (8), Antonucci et al. in 2001 (30), examined whether Kv2.1 colocalized with Ca^{2+} signaling proteins. They reported colocalization between Kv2.1 clusters and both calsequestrin and ryanodine receptors in pyramidal neurons. In addition, overexpression of a GFP-Kv2.1 construct via adenovirus altered the localization of both calsequestrin and ryanodine receptors, causing them to more closely resemble the exact distribution of Kv2.1 macroclusters. This effect of Kv2.1 overexpression suggested a direct or indirect association between Kv2.1 and these two Ca^{2+} signaling proteins.

Kv2 clustering is regulated by neuronal activity and insult

In 2004, Misonou et al. (31), proposed a link between neuronal electrical activity, Kv2.1 phosphorylation, and somatic clustering. First, they observed that the induction of class 5 motor seizures by kainate injection declustered Kv2.1 *in vivo* (see Figure 1.2). Next, 10 μM glutamate treatment of cultured hippocampal neurons to increase spontaneous bursting activity caused a

similar declustering with no effect on the total surface level of Kv2.1 protein. These two findings effectively coupled the electrical activity of the cell with the subcellular localization of Kv2.1. The

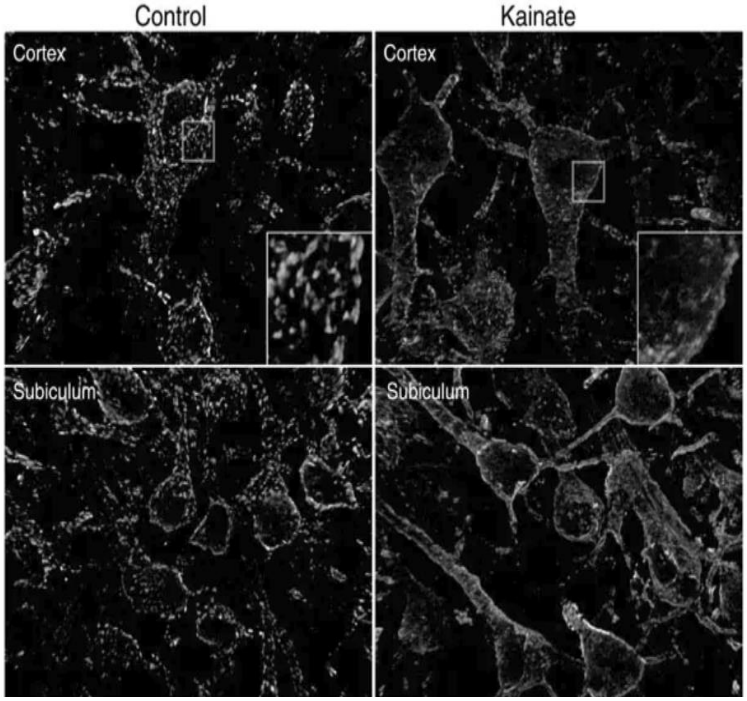

Figure 1.2. Rats injected with 15 mg/kg kainite display declustered Kv2.1. Brain sections were taken from cortex and subiculum, from treated and control rats. Insets are higher magnification views of the boxed regions. Figure taken from Misonou et al., 2004.

glutamate-induced declustering was also associated with a coincident decrease in the phosphorylation state of the channel; both dephosphorylation and declustering were dosage- and time-dependent and reversible with glutamate washout. Pre-incubation with 100 µM AP-5 (D-2-amino-5-phosphonopentanoate) and 10 µM CNQX (6-cyano-7-nitroquinoxaline-2,3-dione) prior to glutamate treatment blocked dephosphorylation and declustering, suggesting that glutamate was signaling these downstream events through NMDA and AMPA-kainate glutamate receptors. In addition, removal of Ca^{2+} from the media or Ca^{2+} channel block with $CdCl_2$ blunted glutamate-induced dephosphorylation and declustering.

Misonou et al. next identified the protein phosphatases responsible for Kv2.1 dephosphorylation. Treatment with okadaic acid, an inhibitor of protein phosphatase 1 and protein phosphatase 2A increased phosphorylation in unstimulated cultures, but failed to prevent glutamate-induced dephosphorylation of the channel. Cyclosporin A, on the other hand, an inhibitor of calcineurin, had no effect on phosphorylation in unstimulated cultures, but did abolish glutamate-induced dephosphorylation and declustering. This led to the conclusion that "glutamate-induced dephosphorylation of Kv2.1 and lateral translocation of Kv2.1 from a clustered to uniform localization are tightly coupled and occur by means of ionotropic glutamate receptor stimulation, leading to Ca^{2+}-dependent activation of calcineurin." In two 2005 papers (32, 33), Misonou and coworkers discovered that Kv2.1 cluster dispersal also occurred after hypoxic or ischemic insult. They postulated that "Kv2.1 clusters form specialized 'micro-signaling domains' to regulate somatodendritic Ca^{2+} signaling at these sites" (32). The glutamate-induced declustering of Kv2.1 is illustrated in the top row of Figure 1.

Contrary to Kv2.1, Kv2.2 is largely resistant to insult-induced declustering. In both mouse brain sections and HEK293 cells, Kv2.2 clusters largely remain intact after hypoxia and elevated cytoplasmic Ca^{2+} (7). This resistance to declustering is paired with less phosphorylation at rest, as well as less dephosphorylation during insult (7). The significance of this difference in sensitivity to declustering stimuli, if one exists, has yet to be examined.

Relationship between Kv2.1 clustering and channel activity

Throughout early studies of Kv2.1 localization there were few solid ideas with respect to the physiological significance of Kv2.1 clustering. However, glutamate treatment affected more than just the phosphorylation state and subcellular localization of Kv2.1. In the final finding of the

Misonou et al., 2004 paper, they concluded that glutamate-induced declustering resulted in a >20 mV hyperpolarizing shift in the $V_{1/2}$ of neuronal I_K, from +15.5 ± 0.5 mV to -8.4 ± 0.5 mV. This shift was reversible after a 2 hour glutamate washout and was blocked by calcineurin inhibitors. This last conclusion shaped the field's thinking in regards to the physiological significance of Kv2.1 clustering, effectively linking the channel's voltage-sensitivity to its subcellular localization. The next year Misonou et al. went further, hypothesizing that clusters on the soma and proximal dendrites acted as "on/off" switches that regulated the intrinsic excitability of the cell (33). It was thought at the time that clusters represented reservoirs of high-threshold Kv2.1 channels, ready to be hyper-activated upon cluster release when needed. Throughout the early 2000s, the overall hypothesis was that Kv2.1 was tethered to cytoskeletal elements adjacent to the ER and near ionotropic receptors, kinases, and phosphatases that served to either maintain or disrupt Kv2.1 clustering and thus regulate channel voltage-dependence (34). As is often the case, a more complex picture arose as we learned more.

Working under the assumption that Kv2.1 clustering regulated the voltage-dependence of channel activation, our group, the Tamkun laboratory, began cell biological studies of Kv2.1 behavior on the membrane surface to better understand the mechanism and dynamics underlying Kv2.1 localization and the regulation of channel function. Surprisingly, both traditional FRAP approaches and newly developed single molecule, quantum dot-based, imaging indicated that Kv2.1 channels were not statically tethered within clusters at the cell surface as originally proposed (34), but rather were corralled within a cytoskeletal fence (35). Here the clustered channels had a lateral mobility similar to Kv2.1 outside the clusters, which agreed with that expected for freely diffusing membrane proteins. Thus, it seemed likely that phosphorylation of the C-terminus allowed Kv2.1 to interact with an additional unknown protein and this additional mass prohibited

the channel from diffusing through the cluster's perimeter boundary. Non-clustered channels did not have this posttranslational modification, could not interact with this unknown accessory protein, and therefore were too small to be hindered by the cytoskeletal architecture and were free to diffuse into and out of clusters. Supporting this hypothesis were the dual findings that in HEK293 cells Kv2.1 clusters tend to be entirely bordered by actin filaments and that disruption of actin with swinholide A dissolved Kv2.1 clusters (35). A mechanism by which Kv2.1 was corralled in a phosphorylation-dependent manner by a cytoskeletal perimeter fence neatly fit all available data at the time.

Since these data cast doubt onto the prevailing model for Kv2.1 clusters, i.e. where static tethering regulates the voltage-dependence of activation, O'Connell et al. decided to directly examine the function of clustered Kv2.1 using HEK293 cells expressing GFP-Kv2.1 and a cell-attached patch clamp approach (36). While cell-attached patches on membrane regions devoid of Kv2.1 clusters, but populated with freely diffusing Kv2.1 channels, exhibited macroscopic delayed rectifier currents, little to no channel activity was detected when the patch clamp pipet was placed directly onto Kv2.1 clusters, as if the clustered channels were non-conducting even at +60 mV. When comparing the whole cell gating current magnitude to ionic currents in transfected HEK293 cells a striking mismatch was found, suggesting that all the Kv2.1 channels responded to a depolarizing stimulus with a moving S4 domain but only a small percentage of these transitions resulted in pore opening. This finding agreed well with early work from the Pongs lab (37) that indicated a discrepancy between Kv2.1 gating and ionic current in *Xenopus laevis* oocytes, where less than 1% of the gating channels actually opened. To test whether Kv2.1 clusters acted as reservoirs of non-conducting channels that were activated upon release, O'Connell et al. next measured whole cell currents before and after inducing Kv2.1 declustering via either actin

depolymerization to dissolve the hypothesized diffusion-limiting fence, or alkaline phosphatase in the patch clamp pipet to dephosphorylate the clustered channel (36). Both treatments resulted in declustering, however while the alkaline phosphatase treatment resulted in the expected shift of voltage dependence, declustering via actin depolymerization did not. Neither treatment increased current density, which would be expected if non-conducting channels suddenly became conducting once declustered. These findings were contrary to the prevailing theories about the channel, as they demonstrated that clustering per se has little impact on channel function. While phosphorylation seems to both govern some aspects of channel electrical activity as well as clustering, location and conductance were not inextricably linked.

Following studies would confirm these findings. Baver and O'Connell (38) showed that the NMDA receptor-based regulation of Kv2.1 activity occurs in the absence of Kv2.1 clustering. In addition, our group would later find that the non-conducting state was regulated by surface channel density and not location on the cell surface (39). The non-conducting state existed in C-terminal truncation mutants that lack the PRC domain and cannot cluster and the percentage of non-conducting channels increased as a function of surface channel number (39). Further supporting a separation between localization and conductance, in 2015 the Trimmer lab found that the cell cycle-dependent regulation of Kv2.1 clustering in COS-1 cells, which is due to changes in Kv2.1 phosphorylation, does not affect Kv2.1 currents (40). While we now know that uncoupling of S4 movement from pore opening is regulated by channel density, the exact mechanism underlying this disconnect remains a mystery.

Non-conducting functions of Kv2.1 clusters

If the clustered channels are not, and do not become, conducting upon declustering, what is their purpose, especially considering the gating current data that indicates non-conducting Kv2.1 channels still sense changes in membrane potential? The high levels of Kv2.1 protein in multiple cell types suggest a structural role and these high levels would also mandate the non-conducting state, for without this, neurons would be electrically silenced.

Non-conducting Kv2.1 had already been linked to exocytosis, for the Lotan group found that Kv2.1 facilitates dense core vesicle release from neuroendocrine cells independently of potassium flux via Kv2.1 interaction with syntaxin (41, 42). Unfortunately, since this work did not employ imaging, no relationship was drawn between these results and Kv2.1 localization. Motivated by this Lotan work, our lab next asked whether the Kv2.1 clusters acted as insertion platforms for membrane protein delivery to the plasma membrane (43). Approximately 85% of both Kv2.1 and Kv1.4 channel plasma membrane insertion events occurred at the Kv2.1 cluster perimeter. As Kv1.4 is freely diffuse, this localized delivery is not specific to cluster-resident proteins. In addition, since endocytosis was also observed at the perimeter of Kv2.1 clusters, these microdomains were postulated to act as membrane trafficking hubs (44). Very recent work from the MacDonald and Gaisano labs (14, 15) further demonstrates that Kv2.1 clusters regulate insulin exocytosis in pancreatic beta cells.

Du and colleagues (8), using a combination of immunohistochemical and electron microscopy approaches, had previously found that Kv2.1 clusters were often localized on neuronal cell membranes directly apposed to both ER/PM junctions and astrocyte membranes. These junctions, or discs of flattened cortical ER located 5-8 nm from the intracellular side of the cell membrane, were continuous with either the smooth or rough ER. This association between Kv2.1

clusters and membrane junctions had also been reported in rat α-motoneurons where the Kv2.1 clusters are apposed to cholinergic C-type synaptic terminals (9). As discussed above, the Trimmer group had reported association between Kv2.1 clusters and ER proteins such as ryanodine receptors. Thus, still searching for non-conducting functions associated with Kv2.1 clusters, our lab returned to the idea that Kv2.1 clusters existed at sites of ER/PM junctions as first seen by Du et al. in 1998. Given that the clustered, but non-conducting, Kv2.1 channels still likely responded to voltage, and being influenced by the work of Kurt Beam (45), we wondered whether they could act in a fashion similar to L-type Ca^{2+} channels at the skeletal muscle triad junction where Ca^{2+} channels couple membrane depolarization to Ca^{2+} release from internal stores via mechanical activation of ryanodine receptors. Therefore, we further examined the relationship between Kv2.1 and the ER.

In untransfected HEK293 cells, endogenous ER/PM junctions were small in size and transient in nature as observed using TIRF imaging of fluorescent ER markers as well as electron microscopy (46). In contrast, following Kv2.1 expression, cortical ER adjacent to the Kv2.1 clusters was dramatically remodeled. These results suggested that Kv2.1 binds to the ER surface and tethers the ER to the PM. This tethering generates the observed Kv2.1 cluster phenotype and explains the high Kv2.1 mobility within the clusters, assuming the ER binding partner, whether it be protein or lipid, is mobile within the ER membrane. Thus, Kv2.1 channel bound to the ER is corralled by the edge of the ER membrane at the point where this organelle turns inward towards the more internal cytoplasm. Further confirming a non-conducting role of Kv2.1 is to induce ER/PM junctions, glutamate-induced Kv2.1 declustering in cultured hippocampal neurons resulted in concomitant retraction of ER localized under Kv2.1 clusters after cluster dispersal (46). The next obvious step required to understand the Kv2.1-ER relationship was for us to identify the

Kv2.1 binding partner on the ER cytoplasmic face, be that protein or lipid. As both Kv2.1 and Kv2.2 form clusters, our lab privately hypothesized that a common mechanism behind this clustering existed and that Kv2.2 also likely interacted with an unknown ER resident to form ER/PM junctions. Indeed, recent efforts have confirmed that cortical ER remodeling is a function of both Kv2.1 and Kv2.2 (47, 48).

A Neuron-within-a-Neuron: The Endoplasmic Reticulum

"Since the endoplasmic reticulum is a continuous network distributed throughout the cell, it may be considered as a neuron-within-a-neuron, a concept that becomes all the more interesting because the endoplasmic reticulum, like the plasma membrane, has both integrative and regenerative properties that could play important roles in neural signaling."

-Berridge, 1998 (49)

While the PM is often emphasized as the principal membrane in the neurosciences due to its excitable nature and role in the action potential, the ER comprises close to 50% of the total membrane area of the animal cell (50) and forms a continuous endomembranous system that stretches from the nuclear envelope, throughout the soma, down the length of the axon to the terminal, and into the very spines of distal dendrites (51) (See figure 1.3). It displays a wide array of organization, structurally assembling into tubules, flattened cisternae, stacks of sheets, and crystalloid assemblies (52), although recent work suggests what were historically considered to be sheets may actually be dense tubular networks (53). Befitting such an extensive organelle, the ER performs a number of tasks integral to the health and function of the neuronal cell alongside its

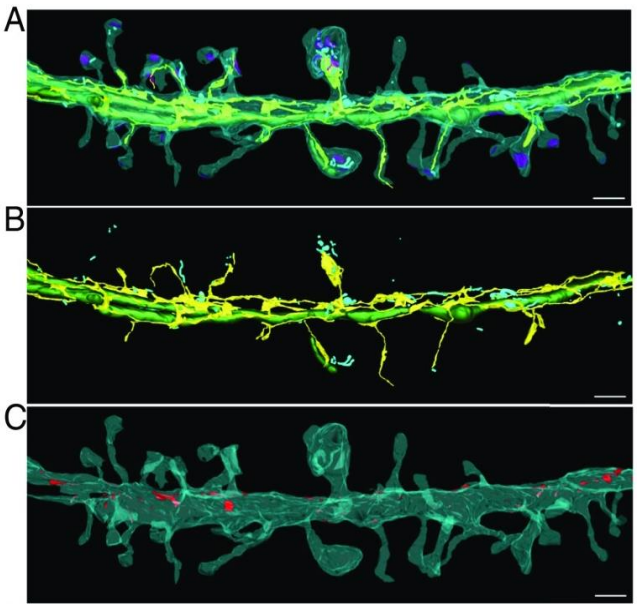

Figure 1.3. ER organization in dendrites. Three dimensional model created from a FIB-SEM image stack. (A) All membranous organelles. (B) ER in yellow, mitochondria in green, endosomes in cyan. (C) Plasma membrane with contact sites with the ER in red. Scale bars represent 400 nm. Image taken from Wu et al., 2017.

more ubiquitous cellular functions of protein synthesis, lipid generation, calcium storage and signal integration (54). The neuronal ER coordinates ischemia-induced cell apoptosis (55), there are reports it may be involved in controlling neurotransmitter release (56), it is integral to long-term potentiation through calcium-induced calcium release (57) and the neuronal ER membrane propagates waves of calcium flux in a manner so reminiscent of the sodium and potassium flux of the PM that it has been described as being a 'neuron-within-a-neuron' (49, 52). ER dysfunction in neurons is involved in a number of human diseases, including Parkinson's (52), Alzheimer's (58), amyotrophic lateral sclerosis (59), the prion diseases (60), and hereditary spastic paraplegia (61, 62), to name a few. This plethora of disease manifestations only speaks to its central role in the proper functioning of the neuronal cell.

Endoplasmic Reticulum / Plasma Membrane Junctions

ER/PM junctions represent locations where the activities of the PM and those of the ER can be coordinated and where specialized functions unique to this domain can be performed. ER/PM contact sites were first described in muscle cells by Porter & Palade in 1957 (63) and their existence in neurons would be described just five years later by Rosenbluth (64). Contact sites in these two cell types display remarkable similarities and as early as 1976 were hypothesized to couple intracellular processes with the electrical activity of the PM (65). Defined as close apposition of the ER and PM membranes at a distance of 15-25 nm without membrane fusion (66), contacts between the ER and the PM represent up to an impressive 12% of the neuronal soma in the intact rodent brain (51). These junctions are also found in the AIS, the synaptic terminal, throughout the dendritic arbor, and within dendritic spines (51, 67). ER/PM contact sites are known to regulate calcium homeostasis (68, 69), non-vesicular lipid transport (70, 71), phosphoinositide metabolism (72), cell signaling regulation (73), stress responses (74), vesicular trafficking (43, 44, 75, 76), and cytokinesis (77, 78).

These are sites that not only organize proteins within the ER, but also serve to organize proteins on the PM. ER/PM junctions serve as tethering sites (79), they affect the PM diffusion landscape (80, 81), and there are reports that ER/PM junctions are also sites of cell-cell contact, suggesting they may be organizing complexes that span cells in certain cases (8, 51)

While it has been found that loss of junction stability, or the loss of specific ER/PM tethers, results in deficits in learning and memory (82-84), redundancy and compensation are common with ER/PM tethers and knockout of a single tether often results in no discernable phenotype as other tethers are able to maintain junction coherence (73, 85-89). In yeast, concurrent knockout of Ist2, Tcb1, Tcb2, Tcb3, Scs2 and Scs22 must be performed in order to observe any change in

ER/PM junction morphology (73). It has been hypothesized that this redundancy serves to ensure ER/PM junction structural integrity even as individual components may exhibit shifting tethering behavior (50).

The ER/PM Junction: A Complex Microdomain with Many Constituents

> "For instance, do the various families of tethers described above collaborate in establishing one contact between the ER and the PM, or does each type independently form a specific apposition destined for a specialized function? And consequently, can a MCS change its functional specificity, depending on spatial and/or temporal regulation? Identifying the full catalog of proteins and lipids functioning at MCSs will be pivotal in deciphering how interorganelle exchanges of materials and signals are modulated and coordinated and in understanding how MCS plasticity underlies these events."
>
> -Gallo, Vannier, & Galli, 2016 (50)

Endoplasmic reticulum / plasma membrane junctions are home to a wide variety of proteins, and the list of known residents only continues to grow. The internal milieu of these sites is highly dynamic, with protein composition of junctions influenced by the calcium concentration of the ER (90), the calcium concentration of the cytosol (91, 92), the activity of the excitable cell (93, 94), the lipid composition of the PM (72), as well as a whole host of other signals and cell states. How the functionality of the junction is altered depending on protein residency, as well as how multiple residents may or may not coordinate in that functionality, is only now beginning to be investigated (50). Below is a brief discussion of a few of the many ER/PM junction resident

proteins. Those outlined will be those that this dissertation will focus on the most in the upcoming chapters.

ER/PM Junction Components: VAPs

VAMP [Vesical-associated membrane protein]-associated protein (VAP) was first discovered in *Aplysia californica* and was originally referred to as VAP-33 as the polypeptide migrated at 33 kD during SDS gel electrophoresis (95). Four years later, three mammalian homologues were uncovered: VAPA, VAPB, and VAPC (96). While VAPA was almost identical to the *Aplysia* VAP-33, VAPB and VAPC were novel homologues with the latter, VAPC, being a VAPB splice variant that lacks the transmembrane domain found at the C-terminus of VAP A and B (96, 97). All VAP proteins contain an immunoglobulin-like β sheet on their N-terminus followed by a coiled-coil domain (98). A VAP consensus sequence, FK(V/I)KTT(VA)**P**(K/R)(K/R)YCV(K/R)P, within their N-terminal major sperm protein (MSP) domain may contribute to VAP oligomerization (99) in addition to the transmembrane domain (96, 100). A missense mutation within VAPB (P56S; highlighted in the above sequence), which results in a proline to serine substitution, causes intracellular aggregation of the VAPB mutant and is associated with late-onset spinal muscular atrophy and amyotrophic lateral sclerosis (101). This mutation recruits both wildtype VAPB and VAPA to these immobile aggregates and results in cell death in culture systems (102). In addition, the P56S mutation interferes with VAPBs ability to interact with other proteins via its MSP domain (103). Deletion of the *Drosophila* homolog, DVAP-33A, results in a decrease in the number of synaptic boutons while overexpression leads to an increase in bouton number and decrease in average size (104). There is also a rich literature

connecting the VAPs to viral replication which raises the question of whether Kv2-induced ER/PM junctions are in some way co-opted for viral transmission (105-107).

The interaction between the VAPs and their partners occurs through the binding of the MSP domain within VAP to an FFAT (two phenalalanines in an acidic tract) motif located on the binding partner. The consensus sequence for FFAT motifs is EFFDAxE, though this sequence can tolerate a high degree of variability (108). A negative upstream flanker region aids in the interaction between VAP and the FFAT motif although serine phosphorylation can replace acidic residues in this region, thus allowing activation by phosphorylation (109-111).

The VAPs interact with a number of proteins to form ER/PM junctions, most notably Nir2 (100), where it works to coordinate phosphatidylinositol-phosphatidic acid exchange (70, 71).

ER/PM Junction Components: Junctophilins

JPH1, JPH2, and JPH3 were first identified in 2000 (112). Identification of a fourth junctophilin, JPH4, occurred in 2003 (113). JPH1 and JPH2 are expressed in the heart and skeletal muscle, JPH3 is expressed in brain and to a lesser degree in the testis (112). Expression of JPH4 is brain specific (113). Structurally, all the JPHs contain a transmembrane domain, an α-helical linker sequence, and a series of eight membrane occupation and recognition nexus (MORN) domains (114). While their transmembrane domains are embedded in the ER membrane, the JPH MORN domains allow them to bind phospholipid within the PM, thus tethering these two membranes together (112). The consensus MORN motif is as follows: YxGxWxxGKRHGYG (115). MORN motifs bind strongly to phosphatidic acid, and to a lesser extent to both PI4P and $PI(4,5)P_2$ (116).

It is hypothesized that differences in the α-helical stalk length between the JPHs carries functional significance, determining the distance at which the PM and ER membranes are tethered (115). This distance between membranes has been experimentally confirmed to influence protein composition of the ER/PM microdomain (117), although functional differences in the JPHs due to stalk length have not been studied nor found to date.

The JPHs are known to stabilize both L-type calcium channels and ryanodine receptors at sites of junctions (118-121). JPH3/4 double knock-out mice display deficits in memory and hind-limb reflex (83) and the JPHs are becoming recognized as potential therapeutic targets for a number of neurological diseases (122).

ER/PM Junction Components: STIM/Orai1

Representing possibly the best studied ER/PM junction proteins, STIM1 and Orai1 coordinate the store-operated calcium entry (SOCE) signaling pathway (69, 90, 123-133). Under conditions of low ER calcium concentration, the ER protein STIM1 will relocalize to ER/PM junctions (69) and bind Orai1. Named after the Greek mythological keepers of the gates of heaven, the three Orais (Orai1, Orai2, and Orai3) were first identified in 2006 (134). Orai1, or CRACM1 (Calcium Release-Activated Calcium Modulator 1) is a calcium selective ion channel responsible for the calcium release activated calcium (CRAC) current (131). Together, these proteins are responsible for generating the calcium entry necessary for store refilling after ER calcium depletion.

Endoplasmic Reticulum / Plasma Membrane Architecture

The nanoarchitecture of neuronal ER/PM junctions is quickly emerging as an area of extreme interest. Hints that this microdomain is far from homogenous in structure have circulated

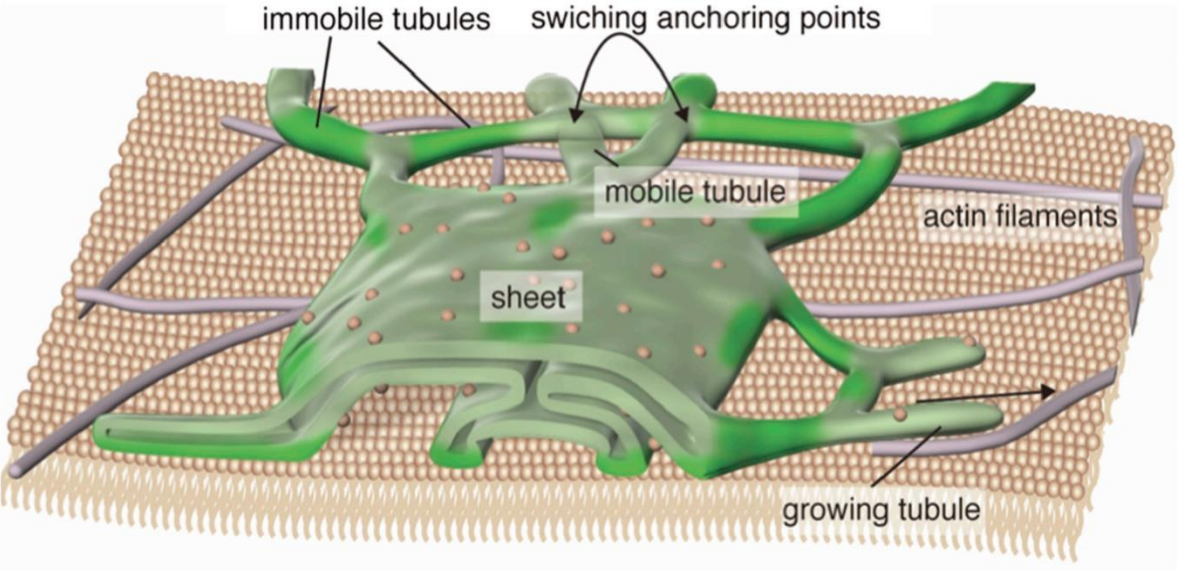

Figure 1.4. 3D model of ER/PM contact site in *Arabidopsis*. ER/PM junctions (deep green) tend to be localized to immobile ER tubules. Mobile tubules are driven by actin filaments (purple). Ribosomes (beige balls) can be seen dotting the ER but are not localized to ER/PM junctions. Image taken from Ishikawa et al., 2018.

for the past several years, but what exactly this structure is, and how it may change in response to stimuli, remains elusive. EM micrographs have captured ER/PM junctions that appear to be flat sheets (51), junctions that possess stacks of internal cisternae adjacent to the contact site (51, 135), and junctions where the ER varies in volume, with thinner ER at the center of the contact site and more voluminous ER at the periphery (8). This last type of structure has been observed in Kv2.1 containing junctions (8). The intramembrane distance between ER and PM is also varied. Junctions have been observed with uniform distances and junctions have been observed that seem to vary in this intramembrane distance (135-137). In Arabidopsis, models of ER/PM junctions have become especially complex (138) (see figure 1.4).

Reports have already confirmed instances where ER structure confers functional significance to these sites (77, 78) and it's easy to imagine how ER invaginations could aid in the creation of signaling hubs, and could prove especially useful in to optimize calcium pathways. Ultimately, the exact structure of any given ER domain or junction rests with the protein composition of that space. For instance, tethers of different lengths are known to create different intramembrane distances, excluding one another from these sites based on this distance (117). The extended synaptotagmins are known to regulate this distance (136), as is STIM1 once activated during SOCE (137). There are a number of proteins which regulate ER curvature as well (66, 139, 140).

Unfortunately, while EM provides an incredible window into what these domains look like as a frozen snapshot, it fails to capture how these microdomains truly operate as a dynamic whole in live cells. Recently however, the nanoarchitecture of these junctions has been brought to the forefront, displaying nanoscale organization (120). This new push has been aided immensely by the creation of new, super resolution imaging techniques.

Tricks of Light: Modern Microscopy Techniques

"We happened to leave one of the protein aliquots on the laboratory bench overnight. The next day, we found that the protein sample on the bench had turned red, whereas the others that were kept in a paper box remained green. Although the sky had been partly cloudy, the red sample had been exposed to sunlight through the south-facing windows."

-Ando et al., 2002 (141)

Light microscopy is inherently restricted by the diffraction limit. With typical fluorescent imaging systems, this confines the optical resolution to ~200 nm (142). While electron microscopy can surpass this level of resolution, it is incompatible with live-cell imaging. The last decade has ushered in a number of super resolution fluorescent techniques, allowing researchers to circumvent the diffraction limit and better peer into the dynamics of cellular processes that have laid beneath the confines of the light-induced theoretical resolution barrier. These techniques often take advantage of being able to identify the max peak of the point spread function (PSF) and thus define a molecules position to a more restricted space than its light signature would otherwise allow. Techniques that use this method, such as photoactivated localization microscopy (PALM) and stochastic optical reconstruction microscopy (STORM), require the separation of PSFs in order to identify them, and thus rely on sparsely labeled fields of view with easily identifiable single molecule light sources that are at distances beyond the Abbé diffraction limit away from one another. Both PALM and STORM obtain these conditions through photoactivation of a few particles at a time, either by using photoactivatable fluorophores or conditions that induce 'blinking' behavior in the fluorophores utilized (143, 144). The creation of better and more stable photoactivatable fluorophores has aided this endeavor (145, 146). Using the PSF of these spaced single point light sources, a super resolution image can be built frame by frame, providing resolution that would otherwise be impossible.

Super-resolution radial fluctuations (SRRF) analysis is a new super-resolution approach (147, 148), but unlike PALM or STORM, it does not rely on visualizing single point sources. SRRF instead takes a raw image stack, divides each pixel into subpixels, then calculates the degree of local gradient convergence (radiality) to define and identify fluorophore PSFs (147). This approach means that super-resolution images can be built from areas of dense fluorescence, live

cell dynamics can easily be examined, and the algorithm can be applied to most fluorescence images if collected at a fast frame rate.

Of course, techniques such as super resolution imaging depend on knowing the identity of protein residents *a priori*. Afterall, one cannot visualize an ER/PM component if one does not know what that component is. And there are, of course, a wide variety of techniques to solve this very problem.

Painting the Town Red: Proximity-Based Biotinylation

To better investigate the protein composition and organization of various subcellular microdomains such as ER/PM junctions, investigators have begun to turn to proximity-based biotinylation techniques (149-154). These approaches rely on the unusually strong non-covalent interaction between biotin and avidin, having a dissociation constant of 10^{-13} – 10^{-15} (155, 156). While historically this interaction has been used to tag proteins by genetically engineering a protein of interest to contain a biotin acceptor domain (BAD) then labeling with an avidin-conjugated fluorophore (157), recently researchers have developed 'promiscuous' biotin ligases. These promiscuous ligases contain a catalytic site mutation that allows the activated biotin molecule (biotinoyl-5'-AMP) to dissociate and biotinylate proteins within a within a 10 nm radius at exposed lysine residues (158, 159). The following steps describe this reaction (155):

1. Biotin + ATP ⇄ Bio-5'-AMP + PPi
2. Bio-5'-AMP + apo-Protein → Biotinoyl-Protein + AMP (1)

These biotinylated proteins can then be purified through the use of avidin-coated beads allowing researchers to explore the protein composition of subcellular areas using mass spectrometry analysis (153). The success of this technique has given rise to second generation ligases (160), as well as the creation of functionally related methods (151, 154, 161-163).

APEX-based proximity biotinylation acts by generating a freely diffusing biotin-phenoxyl radical in the presence of H_2O_2. This radical is short lived (<1 ms) and reacts with electron-rich amino acids such as tyrosine, tryptophan, cysteine, and histidine (159). This approach offers the advantage of being faster to generate robust biotinylation than more standard promiscuous ligases, and has already been used to identify new regulators within ER/PM junctions such as STIMATE (150).

An Overview of this Dissertation

This dissertation examines the structure, regulation, and protein composition of ER/PM junctions with an emphasis on a novel type of contact site first described in this work, the Kv2-VAP junction. Chapter 2 provides data demonstrating that Kv2 channels create ER/PM junctions through a regulated interaction with the ER resident proteins VAPs. The VAPs were identified using a promiscuous biotinylation scheme that relied on proximity-based biotinylation by APEX2 conjoined to the Kv2.1 beta subunit AMIGO. Interaction between Kv2 and the VAPs was confirmed using FRET and siRNA knockdown experiments, and the minimal interaction domain within Kv2.1 was mapped using a CD4-chimeric protein approach, resulting in the identification of an unconventional FFAT motif within the channel c-terminus.

Chapter 3 examines additional proteins that may reside, either ubiquitously or through a regulated manner, within Kv2-VAP ER/PM junctions. JPH-induced ER/PM junctions are also

examined. This chapter focuses on proteins known to reside in ER/PM junctions, such as Nir2 and STIM1.

Chapter 4 investigates the architecture and nanostructure of Kv2-VAP junctional microdomains using TIRF microscopy, spinning disk microscopy, and super-resolution techniques such as STORM and SRRF analysis. Actin filaments surrounding ER/PM junctions were resolved, and the internal dynamics of the ER at these microdomains were observed.

Chapter 5 elucidates the mechanisms behind the activity-driven regulation of ER/PM junctions with emphasis on tethers known to create contact sites in excitable cells. Within this chapter the amino acid sequence governing Kv2-VAP junction sensitivity to glutamate was examined using a combination of fluorescence imaging paired with chimeric protein creation as well as phosphomimic substitutions. In addition, junctophilin sensitivity to glutamate was revealed, and a cursory investigation into the mechanism underlying the regulation of junctophilin-induced ER/PM junctions during activity is provided as well as conjecture as to the consequences of this regulation.

Chapter 6 summarizes the pertinent findings of this dissertation and presents a few future directions that are of particular interest.

Chapter Two: Identification of the VAPs as Kv2 Channel Interactors that form Endoplasmic Reticulum / Plasma Membrane Junctions

Chapter Overview

Kv2.1 exhibits two distinct forms of localization patterns on the neuronal plasma membrane: one population is freely diffusive and regulates electrical activity via voltage-dependent K^+ conductance while a second localizes to micron-sized clusters that contain densely-packed, but non-conducting, channels. We have previously established that these clusters represent endoplasmic reticulum/plasma membrane (ER/PM) junctions that function as membrane trafficking hubs and that Kv2.1 plays a structural role in forming these membrane contact sites in both primary neuronal cultures and transfected HEK cells. Clustering and the formation of ER/PM contacts is regulated by phosphorylation within the channel C-terminus, offering cells fast, dynamic control over the physical relationship between the cortical ER and PM. The present study addresses the mechanisms by which Kv2.1, and the related Kv2.2 channel, interact with the ER membrane. Using proximity-based biotinylation techniques in transfected HEK cells we identified ER VAPs as potential Kv2.1 interactors. Confirmation that Kv2.1 and 2.2 bind VAPA and VAPB employed colocalization/redistribution, siRNA knockdown and FRET-based assays. CD4 chimeras containing sequence from the Kv2.1 C-terminus were used to identify a non-canonical VAP motif. VAPs were first identified as VAMP Associated Proteins required for neurotransmitter release in *Aplysia* and are now known to be abundant scaffolding proteins involved in membrane contact site formation throughout the ER. The VAP interactome includes AKAPs, kinases, membrane trafficking machinery, and proteins regulating non-vesicular lipid transport from the

ER to PM. Therefore the Kv2-induced VAP concentration at ER/PM contact sites is predicted to have wide ranging effects on neuronal cell biology.

Introduction

Kv2.1 and Kv2.2 are abundant voltage-gated K^+ channels in the mammalian brain. Kv2.1 is the predominant channel in the hippocampus while both channels are differentially expressed in the cortex (7). Both channels localize to micron-sized clusters on the neuronal surface of the soma, proximal dendrites, and axon initial segment (AIS) *in vivo* and *in vitro* (164). Clustered Kv2.1 channels disperse in response to ischemic or hypoxic conditions, neuronal activity and glutamate-induced excitotoxity via calcineurin-dependent dephosphorylation of the channel C-terminus (165, 166). While Kv2.1 clustering was first proposed to regulate channel voltage-dependence (34), several studies indicate little connection between channel clustering and regulation of conductance (36, 38, 39). In fact, our evidence suggests that the freely diffusive channel population provides the voltage-dependent K^+ conductance that regulates neuronal electrical activity while clustered channels are non-conducting and have other functions. We previously reported that the clusters represent trafficking hubs where membrane protein insertion and retrieval at the cell surface is localized (43). These findings agree with results from the Lotan group (41) that indicate one non-conducting function of Kv2.1 is to enhance dense core vesicle release from neuroendocrine cells. Recent studies also indicate Kv2.1 clusters regulate insulin exocytosis from pancreatic beta cells (14, 15). Taken together these studies strongly suggest that Kv2.1 clustering plays a structural role related to the cell biology of the neuronal surface. Indeed, we recently determined that the clustered localization pattern is due to Kv2.1 interacting with the cortical ER and inducing stable ER/PM contact sites (46). In rat hippocampal neurons this cortical ER remodeling is regulated by activity,

for glutamate treatment induces Kv2.1 declustering that is shortly followed by cortical ER retraction from the cell surface (46). While ER/PM contacts are best understood for their role in store-operated calcium entry and non-vesicular lipid transfer from the ER to the cell surface (167), additional research indicates these microdomains regulate neuronal burst firing (168) and plasma membrane PIP2 levels (72). In addition, a recent study from the Hess and De Camilli groups (51) reveals that neuronal ER/PM contact sites represent approximately 12% of the somatic surface *in vivo*. Given the abundance and functional significance of neuronal ER/PM contacts, and the likelihood that processes within these domains are influenced by the Kv2.1-ER interaction, it is paramount to understand the mechanisms underlying the activity-dependent interaction between Kv2 channels and the cortical ER.

Our present work demonstrates that Kv2 channels interact with VAMP-associated proteins (VAPs) embedded in the ER membrane. VAPs were first discovered in *Aplysia* where they are required for fast neurotransmitter release (95). VAPs are now known to be ubiquitous ER scaffolding proteins with a large and growing list of interactors, including AKAPs, protein kinases, Rabs, lipid transfer proteins, and kinesins (110, 169). Interestingly, single amino acid substitutions in VAP-B cause late-onset Spinal Muscular Atrophy and Amyotrophic Lateral Sclerosis (ALS)-type 8 (170, 171), which is intriguing given that Kv2.1 clustering over the cortical ER also exists in alpha motor neurons (9). Both the clustering of the Kv2 channels and induction of ER/PM junctions occurs via a non-canonical VAP motif contained within Kv2 channel C-terminus. This motif contains phosphorylation sites that are known to regulate Kv2 clustering and cortical ER remodeling. The balance of phosphorylation/de-phosphorylation at these sites likely governs affinity for VAPs, thus explaining the phosphorylation dependence of the Kv2/ER interaction.

Since Kv2 channels concentrate VAPs at the ER/PM contact site, the Kv2-VAP interaction summarized in the present work is likely to have a major influence on neuronal physiology.

Materials & Methods

DNA Constructs Plasmids encoding fluorescent protein- and biotin acceptor domain- tagged Kv2.1 have been described previously (35, 172, 173). Briefly, the fluorescent proteins are attached to the channel N-terminus and the biotin acceptor domain (BAD) inserted into the extracellular loop between the first and second transmembrane domains. Co-transfection with the BirA biotin ligase in the pSec vector was performed as previously described in order to biotinylate a specific lysine within the BAD sequence (173-175). Kv2.1 contains two methionine residues five residues apart, at the beginning of the coding sequence, each of which have each been selected as the starting amino acid in different publications. Thus there are two separate numbering systems currently in use in the Kv2.1/KCNB1 literature. For the sake of consistency between this manuscript and previously published work concerning Kv2 sequence critical for clustering (29, 176), we have opted to retain the original amino acid numbering which sets the second methionine as amino acid 1. Synthetic full length Kv2.2 sequence was obtained from Genewiz and inserted into the peGFP-C1 expression vector (Clontech). AMIGO in pDONR221 was obtained from DNASU (plasmid ID HsCD00296150) and from this AMIGO-YFP was created by using ApaI and XhoI cut sites and placing the AMIGO fragment into a peYFP-N1 vector.

VAPA-GFP and VAPA(K87D/M89D)-GFP were provided by Axel Brunger via Addgene (Addgene plasmids 18874 and 18875, respectively). VAPB-GFP has been previously described (177). From these initial constructs, VAPB-mRuby2, VAPB-Clover, VAPA-paGFP, and VAPB-paGFP were created using standard DNA manipulation techniques.

For the proximity biotinylation experiments AMIGO-YFP-APEX was generated from the APEX2-NES vector obtained from Alice Ting (Addgene plasmid # 49386). Overlap PCR was used to insert an EcoRI cut site (5'GACGGAGAATTCAAGGGATGGACTACAAGGATGAC3') in the APEX2-NES vector at the 5' end of APEX2 allowing the resulting XbaI and EcoRI APEX DNA to be added to the 3' end of AMIGO-YFP to form AMIGO-YFP-APEX.

pcDNA3.1-Clover-mRuby2 was a gift from Kurt Beam (Addgene plasmid # 49089), mRuby2-C1 was from Michael Davidson (Addgene plasmid # 54768) and pcDNA3-Clover was from Michael Lin (Addgene plasmid # 40259). An mClover-C1 construct was generated by digesting pcDNA3-Clover and mRuby2-C1 with NdeI and BsrGI and exchanging Ruby2 with Clover. Ruby2-Kv2.1 was generated from mRuby2-C1 and the previously described GFP-Kv2.1 (172) by replacing the NheI to EcoRI GFP encoding fragment in GFP-Kv2.1 with mRuby2. Clover-Kv2.1 was generated from mClover-C1 and a Ruby2-Kv2.1 by inserting the XhoI to XmaI fragment containing Kv2.1 into mClover-C1.

Generation of the CD4-based chimeras relied heavily on synthetic DNA obtained from Genewiz. CD4-Kv2.1:445-609 was created using synthetic DNA (amino acids 445-609 of Kv2.1) which were appended to wildtype CD4 using SacII and NotI restriction sites. The CD4-Kv2.2:452-911 was made using the same approach. In both of these constructs the VAP motif was the same distance from the CD4 transmembrane domain. The other CD4 Kv2.1 minimal FFAT sequence constructs (see Fig. 7) were based on work done in the Bjorkman laboratory (178), where the CD4 transmembrane domain was separated from the Kv2.1 channel sequence by using a combination of $(Gly_4Ser)_n$ linkers, to confer flexibility, with β2-microglobulin sequence to provide a more rigid structure. β2-microglobulin is a monomeric 12 kD protein with an N- to C-termini separation distance of ~3.5 nanometers (179). The Gly_4Ser linkers were of variable length so as to keep the

total amino acid number from the CD4 transmembrane domain to the Kv2.1 FFAT motif consistent between the CD4-chimeric constructs and wildtype Kv2.1. For the oxysterol-binding protein (OSBP) FFAT motif (110) and flanker construct (CD4-OSBP(FFAT)), a single serine in the OSBP FFAT flanker region was changed to aspartic acid to *a priori* nullify any possible phosphorylation effects on VAP interaction. All synthetic DNA segments were inserted into the CD4 backbone using SacII and XbaI restriction sites. All constructs terminated in a stop codon inserted into the sequence immediately after the last amino acid of interest.

The luminal ER marker dsRedER has been previously described (39, 46). mCherry-JPH4 was provided by Yousang Gwack (Addgene 79599).

Cell culture, transfection, and labeling of surface Kv2.1 and CD4 chimeras HEK 293 cells [American Type Culture Collection (ATCC), passage 45-48] were cultured, transfected with the indicated DNA constructs via electroporation and plated onto Matrigel coated 35 mm glass bottom coverslip dishes (Matsunami Glass Corporation) as previously described (46). BirA cotransfection was used to induce biotinylation of the biotin acceptor domain (BAD) containing Kv2.1 constructs, e.g. GFP-Kv2.1-BAD. Imaging was performed 24 h after transfection. In order to label the surface Kv2.1-BAD, cells were incubated with a 1:1000 dilution of CF640-conjugated streptavidin (CF640-SA) (Biotium) for 10 minutes in HEK physiological imaging saline (146 mM NaCl, 4.7 mM KCl, 2.5 mM $CaCl_2$, 0.6 mM $MgSO_4$, 1.6 mM $NaHCO_3$, 0.15 mM NaH_2PO_4, 0.1 mM ascorbic acid, 8 mM glucose, and 20 mM 4-(2-hydroxyethyl)-1-piperazineethanesulfonic acid (HEPES), pH of 7.4). Unbound CF640-SA was removed with imaging saline washes. CD4 chimeras on the cell surface were specifically detected by incubating the transfected cells with a 1/1000 dilution of CF640-conjugated anti-CD4 antibody targeting an extracellular epitope for 10 minutes.

Hippocampal neurons were isolated from embryonic (E18) animals deeply anesthetized using isoflurane in accordance with a protocol approved by the Institutional Animal Care and Use Committee of Colorado State University (Protocol ID: 15-6130A). Embryos of both sexes were collected and thus the neuronal cultures contain a mixed population of male and female cells. Neurons were dissociated as previously described (46, 174, 175) and plated onto glass bottom coverslip dishes coated for 1 h with poly-L-Lysine (P4707, Sigma) diluted 1:2 in 0.15 M borate buffer pH 8.4. After 2 washes with water, $5x10^5$ cells were seeded per dish, and cells were fed with Neurobasal media (Gibco by Life Technologies, REF# 21163-049) supplemented with 1:100 GlutaMAX(100x) (Gibco by Life Technologies, REF# 35050-061), Pen-Strep (HyClone, CAT# SV30010, 100 units/mL, 100 µg/ml respectively) and 1:500 NeuroCult SM1 (Stem Cell Technologies, CAT# 05711). On DIV6, rHN cultures were transfected with 2 µl of Lipofectamine 2000 and 1µg of Kv2.2/Kv2.1/CD4 chimera and 300ng of VAPA/B-GFP/Ruby per/dish. On DIV7 rHN dishes were washed with neuronal imaging saline (126 mM NaCl, 4.7 mM KCl, 2.5 $CaCl_2$, 0.6 mM $MgSO_4$, 0.15 mM NaH_2PO_4, 0.1 mM ascorbic acid, 8 mM glucose, and 20 mM HEPES, pH 7.4), followed by incubation with either CF640-conjugated streptavidin or anti-CD4 antibody as described above. Anti-neurofascin monoclonal antibodies were used to identify the axon initial segment when required. Here anti-NF186 antibody (Neuromab) was used at a 1/1000 dilution for 10 min, followed by 2 rinses with NIS and a 10 min incubation with fluorescent (Alexa 594 or 647) goat anti-mouse secondary antibody diluted 1/1000. Dishes were rinsed 3 times and imaged immediately.

APEX-based proximity biotinylation Promiscuous biotinylation of ER/PM junction components was accomplished by transfecting HEK cells with AMIGO-YFP-APEX, in reality APEX2, (154) with or without other plasmids as indicted. At 24 hours post transfection the cells were incubated

with 500 μM biotin phenol in DMEM + 10% FBS for 30 minutes, treated with 1 mM H_2O_2 for 1 minute, then fixed in 4% formaldehyde for 15 minutes prior to labeling with 2 ng/ml CF640-conjugated streptavidin (CF640-SA) and subsequent imaging. For Western blot analysis unfixed cells were scraped from plates in phosphate-buffered saline (PBS) containing Complete Mini protease inhibitor (Roche), centrifuged, and the cell pellet resuspended in SDS gel Laemmli sample buffer (Biorad) containing β-mercaptoethanol. Following sonication and boiling for 10 minutes the non-purified samples were fractionated by standard SDS-polyacrylamide gel electrophoresis on a 10% gel. After transfer to nitrocellulose membranes, the proteins were probed with either mouse anti-Kv2.1 (Neuromab) at a 1:1000 dilution or mouse anti-AMIGO antibody (Neuromab) at 1:1000 dilution. Antibody binding was detected with LiCor IRDye800CW goat ant-mouse antibody. Biotinylated proteins were detected with LiCor IRDye 680RD streptavidin used at 1:10,000. Imaging was performed using a dual color Odyssey CLx LiCor system. In this manner any biotinylated ER-resident proteins were visually separated from any potential Kv2.1 or AMIGO protein degradation products.

Microscopy Laser scanning confocal microscopy was performed using an Olympus FluoView 1000 inverted microscope equipped with two spectral detectors and one filter based detector in addition to an Ar laser (458/488/515 nm) and 543 nm and 633 nm HeNe lasers. Stage and objective temperatures were maintained at 37ºC and all images were collected using a 60X PlanApo, 1.4 NA, objective. Spinning disk confocal microscopy was performed using a Yokogawa-based CSUX1 system built around an Olympus IX83 inverted stand coupled to an Andor laser launch containing 405, 488, 561, and 637 nm diode lasers, 100-150 mW each. Images were collected using an Andor iXon EMCCD camera (DU-897) and 100X Plan Apo, 1.4 NA objective. This system is equipped with the ZDC constant focus system and a Tokai Hit chamber and objective

heater. The entire system is controlled by Metamorph imaging software. Unless stated otherwise, all images were acquired taken via spinning disk microscopy. When indicated, TIRF microscopy was performed on a Nikon Eclipse Ti fluorescence microscope with 405, 488, 561, and 633 nm diode lasers, 100 mW each, split evenly between TIRF and photoactivation unit pathways. However, 405 nm based activation of the photoactivatable GFP-VAPA presented in Fig. 5 was performed in TIRF to limit the activated GFP fluorescent to within 100 nm of the plasma membrane. TIRF images were collected using an Andor iXon EMCCD DU-897 camera through a Plan Apo 100x, NA 1.49, TIRF objective. Both the objective and dish are temperature controlled and z-drift was mitigated through the use of the Nikon Perfect-Focus system. The entire system is run by NIS AR software. With all three systems the appropriate use of spectral detectors, sequential excitation, dichroics and bandpass filters permitted fluorophore separation. Additional details regarding our microscopy have been previously described (46, 174, 175).

Förster resonance energy transfer (FRET) Sensitized-emission FRET imaged in living cells employed Clover-Ruby2 pairs analyzed as described by (180). HEK 293 cells were transfected using Lipofectamine 2000 (2 µl; Invitrogen, Carlsbad, CA) and 100 µl OptiMEM (Life Technologies, Carlsbad, CA) per dish using the following DNAs: 1 µg Clover-Kv2.1, 1 µg Ruby2-Kv2.1, 200 ng pcDNA3.1-Clover-Ruby2 (tandem), 200 ng mClover-C1, 200 ng mRuby2-C1, 600 ng Ruby2-VAPA, 600 ng Ruby2-VAPAmut, and 600 ng Ruby2-VAPB. FRET images were obtained on the Olympus/Andor spinning disk confocal microscope described above. For each cell, 4 images were collected: 1) excitation with 488 nm paired with a 500/25 bandpass filter (Donor image), 2) excitation with 488 nm paired with a 600/50 bandpass filter (FRET image), 3) excitation with 561 nm paired with a 600/50 bandpass filter (Acceptor image), and 4) a DIC image. Using ImageJ, 15 3px by 3px ROIs were placed on Kv2.1 clusters (or randomly in the case of

tandem and soluble conditions) and the fluorescence intensity of each channel was measured. Cells expressing only the donor (Clover) or acceptor (Ruby2) constructs alone were imaged to calculate bleed-through coefficients for the FRET efficiency calculations. Bleed-through coefficients (BT_{Clover} or BT_{Ruby2}) were calculated as the average intensity of the FRET channel (I_{FRET}) divided by the average intensity of the donor or acceptor (I_{Clover} or I_{Ruby2}). For our experimental conditions, $BT_{Clover} = 11\%$ and $BT_{Ruby2} = 4.3\%$. Although there are many options for the calculation of FRET, we decided to use NFRET, due to its correction for expression levels of donor and acceptor and its utility in the study of intermolecular protein interactions (181). To calculate FRET (N_{FRET}), the following relationship was used as previously described (180):

$$N_{FRET} = \frac{(I_{FRET} - BT_{Clover} \times I_{Clover} - BT_{Ruby2} \times I_{Ruby2})}{\sqrt{(I_{Clover} \times I_{Ruby2})}} \quad (2)$$

FRET efficiency images were created using the image calculator in ImageJ and applying mathematical transformations to FRET, Donor and Acceptor images as described in the equation above. After all transformations were performed, the royal look up table (LUT) in ImageJ was applied to each image.

siRNA-based knockdown of VAPA and VAPB HEK 293 cells plated in either 100 mm tissue culture dishes or 35 mm coverslip dishes were transfected with 250 nM siRNA (Dharmacon) using DharmaFECT transfection reagent as per the manufacturer's directions. After 24 h the cells on the 35 mm coverslip dishes were transfected again with the siRNA and with the GFP-Kv2.1loopBAD and BirA plasmids, 1 µg and 0.5 µg, respectively. The cells on the 100 mm dishes did not receive the Kv2.1-encoding plasmid DNA during second round of siRNA transfection. After another 24 h the cells on 35 mm coverslip dishes were imaged to assess Kv2.1 clustering while the cells on 100

mm plates were collected as described above for western blot analysis of VAP expression. Incubation with anti-VAPA and VAPB mouse antibodies (1:1000 and 1:2000 dilutions, R&D Systems, MAB5820 and MAB58551, respectively) followed by HRP-conjugated goat anti-mouse antibody and detection with SuperSignal West Dura (Thermo Scientific, product #34075) was used to assess VAP expression in the presence of various siRNAs.

Image processing and analysis Image processing was performed with ImageJ. Images were pseudo-colored, cropped, and adjusted for contrast and brightness. Image analysis was completed using either ImageJ or Volocity analysis software. Details specific to each experiment are presented in the Results section or Fig. legends. Unless noted single confocal planes are presented.

Experimental Design and Statistical Analysis The majority of our experiments were performed in HEK 293 cells as opposed to cultured hippocampal neurons since these cells are well suited for demonstrating protein-protein interactions that only occur within specific compartments of living cells. In addition, HEK 293 cells lack ion channel subunits that that could assemble with the expressed constructs and are less heterogeneous than neuronal cultures. Our primary concern with respect to experimental design focused on over-expression issues, for high level expression could induce protein interactions that are otherwise non-existent. The levels of Kv2.1 expressed in both transfected HEK 293 cells and neurons are similar to the level of the endogenous Kv2.1 as previously described (35, 43, 44) where immunostaining of transfected cells was compared to that against the endogenous channel in cultured hippocampal neurons. The CD4-chimera expression levels were similar to those of the endogenous channels. We did not use higher expression levels to avoid potential artifacts and our goal was to express just enough fluorescent protein tagged VAP to act as a tracer for the endogenous proteins, especially since any VAP redistribution is lost with over-expression. In addition, VAP overexpression alters ER morphology as previously described

(98), something we did not observe with our transfected VAP expression levels. Note that high expression levels were not necessary given the sensitivity of our TIRF and spinning disk microscopes, which are both capable of imaging single molecules.

For statistical analysis, one-way analysis of variance (ANOVA) with ad hoc Tukey's tests were performed. For the data presented in Fig 8, Kruskal-Wallis ANOVAs were performed. Number of regions of interest and cells examined and p values are indicated in the results section.

Results

Identification of VAPs as the putative Kv2 ER binding partner

Previous studies employing antibody-based affinity purification of Kv2.1 from either transfected HEK cells or rat brain isolated the channel protein free of any abundant interacting proteins (182). This result is not unexpected since a majority of Kv2.1 is insoluble in the non-ionic detergents used for affinity purification (27, 172, 182) and macromolecular complexes containing Kv2.1 are likely to reside in this detergent insoluble fraction. Indeed, when imaging GFP-Kv2.1 clusters in transfected HEK cells during the application of 1% TX-100 at 37ºC, conditions which solubilize putative lipid raft structures (183), the clusters remained intact as the rest of the membrane was solubilized. Since attempts to biochemically purify these detergent insoluble microdomains using a variety of fractionation procedures were unsuccessful, we used APEX proximity-biotinylation techniques (162) in transfected HEK cells in order to identify putative Kv2.1-interacting ER-resident proteins responsible for the formation of ER/PM junctions. APEX, in the presence of biotin-phenols and hydrogen peroxide, generates freely-diffusing, but short-lived, biotin radicals that non-discriminately biotinylate near-by proteins. In order to maximize the

biotinylation of neighboring proteins, as opposed to Kv2.1 itself, APEX was appended to the cytosolic end of the Kv2.1 beta subunit AMIGO as diagramed in Fig. 2.1A.

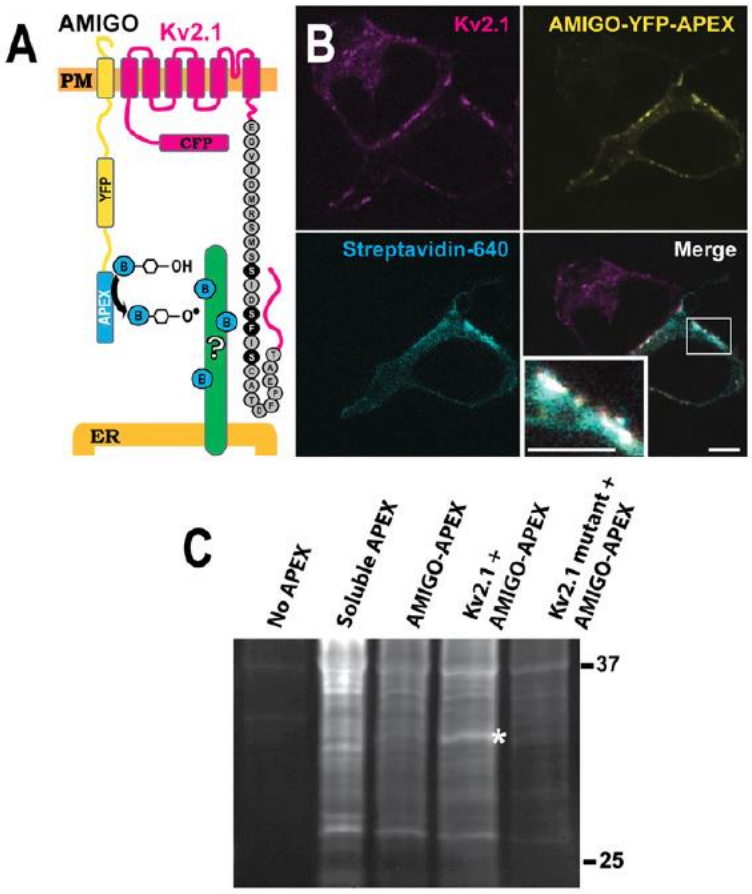

Figure 2.1. Use of proximity biotinylation to identify potential Kv2.1 interactors. (A) Diagram of the approach. APEX was attached to the C-terminal end of the Kv2.1 beta subunit, AMIGO. (B) Localization of APEX-mediated biotinylation. HEK cells were transfected with Kv2.1 and AMIGO-YFP-APEX, treated with biotin and H2O2, and then fixed using formaldehyde and labeled with CF640Rconjugated streptavidin to visualize biotinylated proteins as imaged with a laser scanning confocal microscope. Biotinylation localized at ER/PM junctions occurs only in cells expressing AMIGO-YFP-APEX and Kv2.1 (see Lower Right Inset for an enhanced view of biotinylation at a Kv2.1 cluster). (Scale bar: 5 μm.) (C) Parallel samples were collected and subjected to Western blot analysis without affinity purification, using streptavidin–horse radish peroxidase to visualize all biotinylated proteins. A 33-kDa band is present when AMIGO-YFP-APEX is coexpressed with the WT Kv2.1 channel (asterisk). This band is absent from the indicated control lanes, i.e., without any APEX transfection, with soluble APEX expression, and when AMIGO-YFP-APEX is expressed alone or expressed with a mutant Kv2.1 channel which is unable to form ER/PM junctions.

The C-terminal Kv2.1 sequence known to be involved in the clustering and ER-binding phenotype is indicated with previously described point mutations that abolish soma clustering and ER interaction highlighted in black (29). AMIGO, a single transmembrane cell adhesion molecule, associates with the clustered Kv2.1 channels when co-expressed (184, 185). Importantly, in our HEK cells AMIGO on the PM does not cluster nor associate with the cortical ER when expressed alone. As shown in Fig. 2.1B, co-expression of CFP-Kv2.1 and AMIGO-YFP-APEX induced protein biotinylation in the vicinity of Kv2.1 clusters as indicated by the binding of CF640R-conjugated streptavidin. The streptavidin binding was most prominent at Kv2.1 cell surface clusters, indicating localized biotinylation (see inset in lower right panel). Next, a Western blot analysis was performed in order to characterize the biotinylated proteins. Non-transfected cells and cells expressing soluble APEX were examined in addition to cells where AMIGO-YFP-APEX was expressed either alone, with Kv2.1, or with the non-clustering Kv2.1(S586A) point mutant (46). Western blots were probed with fluorophore-conjugated streptavidin to detect the biotinylated proteins. As indicated by the asterisk in Fig. 2.1C, a 33 kD protein was detected in cells co-transfected with AMIGO and Kv2.1 but not in cells transfected with either AMIGO alone or AMIGO plus the Kv2.1(S586A) point mutant that does not interact with the ER. **V**AMP - **a**ssociated **p**roteins (VAPs) are abundant ER proteins of 33 kD that function in membrane contact site formation between the ER and a variety of organelles (110). Thus, VAPs became an obvious candidate.

VAPs specifically redistribute to Kv2-induced ER/PM junctions

While our previous work (46) demonstrated Kv2.1-induction of ER/PM junctions, no direct binding partner was known at that time. Our first approach to determining whether VAPs interact

with Kv2.1 was to perform co-localization experiments. VAPA-GFP or VAPB-GFP were expressed either alone or with a Kv2.1-loopBAD construct that allowed for CF640-streptavidin labeling of only surface channels. Since all cells express endogenous VAPs the exogenous GFP-tagged VAPs act as a marker for endogenous proteins when expressed at low levels (110). As illustrated in Fig. 2.2A, when expressed alone, VAPA-GFP displayed a uniform distribution throughout the ER as expected. Fig. 2.2B shows that in the presence of Kv2.1 the VAPA-GFP localization was dramatically altered, with an obvious redistribution in favor of the Kv2.1-induced ER/PM junctions. We next used junctophilin 4 (JPH4) to induce ER/PM junctions independent of Kv2.1 to rule out the possibility that VAP favors all ER/PM contacts, regardless of molecular composition. JPH4 is an ER membrane protein which induces membrane contacts by binding PM lipid (115). When co-expressed with mCherry-JPH4, the VAPA-GFP remained evenly dispersed throughout the ER, showing no concentration at the JPH4-induced ER/PM contacts (Fig. 2.2C). Thus, the presence of ER/PM junctions per se had no effect on VAPA-GFP distribution. We also co-expressed GFP-Kv2.2 with VAPB-Ruby2 since Kv2.2 also clusters over the ER (7, 184). Fig. 2.2D shows that Kv2.2 also concentrates VAPs at its induced ER/PM contact sites. When Kv2.1 and Kv2.2 were co-expressed with VAPB all three proteins co-localized within the same ER/PM contact sites as illustrated in Appendix I. In order to determine whether the VAP redistribution to Kv2.1-induced ER/PM contacts is dependent on FFAT motif binding by VAP we co-expressed the K87D/M89D VAPA mutant (110), which is unable to bind FFAT motifs, with Kv2.1 as shown in Fig. 1.2E. This VAP mutant showed less redistribution to Kv2.1-induced ER/PM junctions but was still slightly enriched at the Kv2.1 clusters. Taken together, these data suggest that VAP concentration at ER/PM junctions is dependent on the presence of Kv2 channels and that this localization is largely dependent on a functional FFAT motif within the VAP protein.

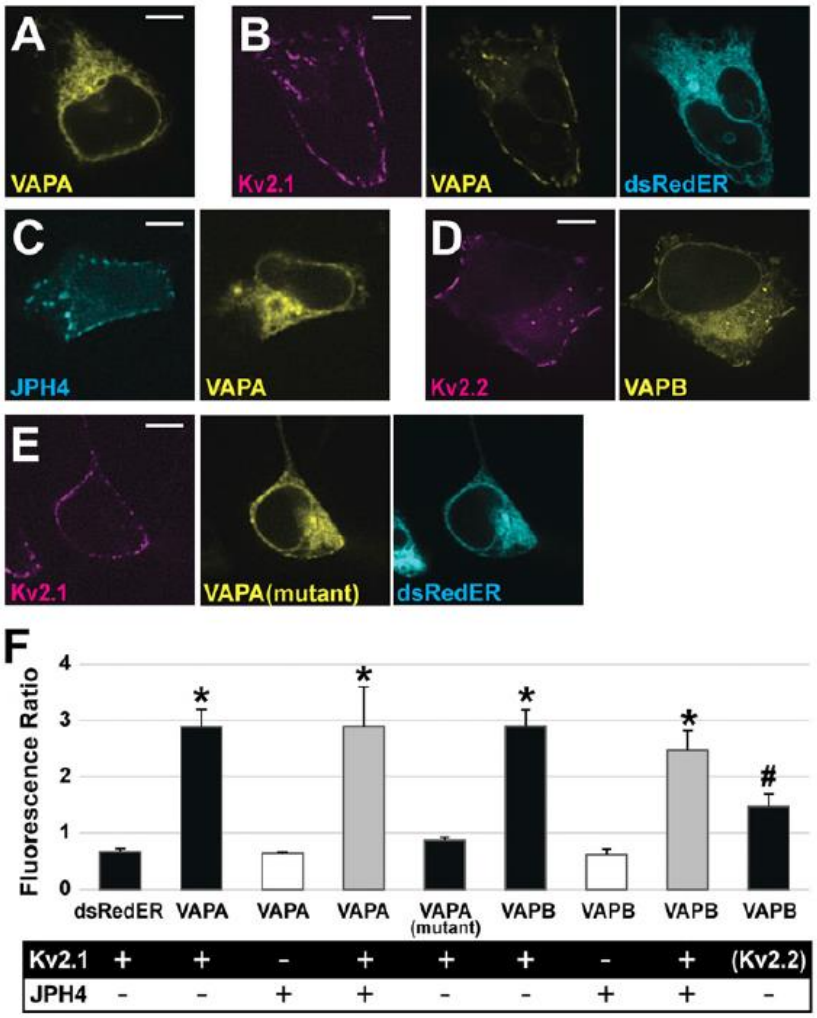

Figure 2.2. Kv2 channels impact localization of VAPA and VAPB in HEK cells. (A) VAPA-GFP expressed alone displays uniform localization across the ER. (B) VAPA-GFP expressed with Kv2.1-loopBAD redistributes to Kv2.1-induced ER/ PM junctions. (C) VAPA expressed with the ER/PM junction forming protein, JPH4, does not redistribute to junctions. (D) Kv2.2 coexpressed with VAPBGFP redistributes this VAP to the induced ER/PM junctions. (E) VAPA(K87D/ M89D) has a reduced ability to redistribute to Kv2.1-induced ER/PM junctions. (Scale bars: 5 μm.) (F) Bar graph summarizing VAP redistribution by calculating the ratio of fluorescence at ER/PM junctions to that at ER deeper within the cell when junctions are formed using Kv2 and/or JPH4 as indicated. Only Kv2.1 and Kv2.2 increase the ratio of VAP fluorescence. For analysis, a log transformation was used to satisfy the homogeneity of variance condition and a one-way ANOVA was performed, $F(8, 36) = 25.699$, $P = 1.106 \times 10{-}12$ with post hoc pairwise Tukey's tests. *$P < 0.0001$, significant difference relative to the dsRedER control,. #$P < 0.01$ significance. Error bars represent SEM. Twenty-five ROIs from five cells were examined in each case.

The effect of Kv2.1 expression on VAP localization is summarized in Fig. 2.2F. Here we calculated the ratio of VAP-GFP fluorescence at the PM to the cytoplasmic ER signal located further within the cell (Junctional/Internal ER Intensity Ratio) to quantify the degree to which VAPs were concentrating to ER/PM junctions formed by the various proteins. DsRed-ER, a soluble ER marker, had a ratio of 0.67, indicating a lower ER intensity at Kv2.1 clusters on the PM as compared to signal in the ER deeper within the cell. This ratio was not significantly different than the ratios of VAPA or VAPB when co-expressed with JPH4 (ratio of 0.64, $p = 1$, for VAPA and ratio of 0.62, $p = 0.9996$ for VAPB). In contrast to what was observed with JPH4-induced junctions, the VAPs were significantly more concentrated at Kv2.1 ER/PM junctions (ratio of 2.9, $p \leq 0.0001$ for VAPA and ratio of 2.9, $p \leq 0.0001$ for VAPB, unpaired student's t-tests). Note that JPH4 and Kv2.1 form ER/PM junctions that are similar in appearance (Fig. 1.2C) and in fact, Kv2.1 and JPH4 co-localize within the same junctions when expressed together as illustrated in Appendix I. The presence of Kv2.1 alongside JPH4 at ER/PM contact sites results in significant VAPA redistribution not seen when JPH4 is forming junctions alone (ratio of 2.90 vs 0.67, $p = \leq$ 0.0001, compared to JPH4 alone). Note that while the ratio, 0.87, for VAPA(K87D/M89D) was not statistically significant compared to the DsRed-ER control there was a trend towards increased concentration, with this redistribution being visibly noticeable in some cells. These data support the idea that FFAT motif interaction is critical for VAP redistribution to Kv2.1-induced ER/PM junctions, however a secondary mechanism by which VAPs concentrate to Kv2.1-containing ER/PM junctions that is independent of FFAT motif-binding may exist.

FRET analysis supports a direct Kv2.1-VAP interaction at Kv2.1-induced ER/PM junctions

The data presented thus far support a relationship between Kv2 channels and VAPs but do not demonstrate direct binding between the two proteins. Therefore, we used Förster resonance energy transfer (FRET), to determine whether these two proteins are likely in direct contact. We attached the FRET acceptor (mRuby2) and donor (Clover) to the VAP cytoplasmic domains and the N-termini of Kv2.1, respectively. A mRuby2-Clover linked tandem construct was used as a positive control while co-expression of soluble unlinked mRuby2 and Clover served as a negative control. The FRET signals obtained from these two controls, and the FRET observed between Kv2.1 and VAPA, are shown in the right-hand panels of Fig. 2.3A.

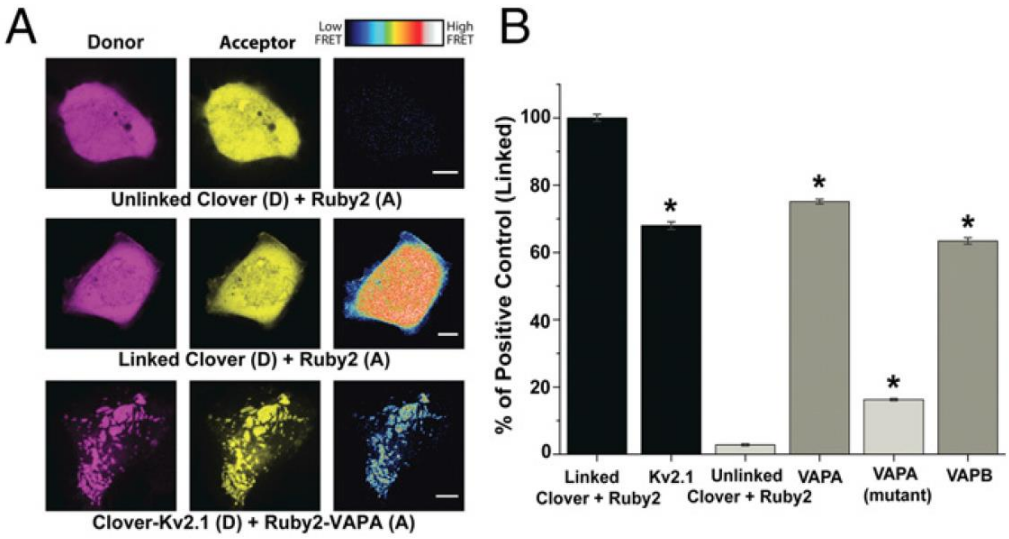

Figure 2.3. FRET between Kv2.1 and both VAPs in transfected HEK cells. (A) Representative images of donor, acceptor, and FRET efficiency between the indicated constructs. FRET efficiency magnitude is illustrated by the representative heat maps. (Scale bars: 5 μm.) (B) Quantified FRET efficiency. Here the FRET signals were standardized to that obtained with the linked CloverRuby2 positive control. Positive controls are indicated by the black bars, negative controls are in light gray, and the Kv2.1/VAP interactions are in darker gray. A one-way ANOVA was performed, $F(5, 481) = 195.7$, $P = 1.81 \times 10{-}133$ with post hoc Tukey's tests to examine significance. *$P < 0.000001$, significant difference relative to the unlinked negative control. Error bars represent SEM. n = 109 linked, 104 VAPA, 76 VAPA (mutant), 48 VAPB, 75 Kv2.1, and 58 unlinked cells. Each cell had 15 ROIs examined.

The FRET signals observed in all experiments are summarized in Fig. 2.3B. We observed significant FRET efficiency between Kv2.1 and both VAPA and VAPB (75% of linked control and 63% of linked control, $p \leq 0.000001$ and $p \leq 0.000001$ compared to unlinked control, respectively), indicative of protein-protein interaction. By contrast, unlinked Clover and mRuby-2 displayed FRET efficiency values that were only 3% of the linked control. An additional positive control examined the FRET efficiency existing between Kv2.1 subunits within a heteromeric channel, i.e. Ruby2- and Clover-Kv2.1 subunits (68% of linked control). The decreased FRET between Kv2.1 subunits, relative to the linked Clover-Ruby2 positive control, is likely due to the random assembly of the channel tetramer. Interestingly, a second negative control, the VAPA(K87D/M89D) mutant, which is incapable of binding FFAT motifs (98), displayed a diminished, but still significant (16% of linked control, $p \leq 0.000001$ compared to unlinked control) FRET efficiency. This signal, which is consistent with the diminished but still significant relocalization of the VAPA(K87D/M89D) mutant seen in Fig. 2.2E, could be due to oligomerization with endogenous VAPs via the transmembrane domain as has been previously described (186). In essence, the VAPA(K87D/M89D) mutant which is incapable of binding Kv2.1 is oligimerizing with endogenous VAPs that are bound to the channel. Such a mechanism would allow for the accumulation of VAPs with available FFAT-motif binding domains within the Kv2.1-induced ER/PM contacts.

Knockdown of VAP protein impacts the clustering behavior of Kv2.1

In order to confirm that VAPs are directly involved in Kv2.1 clustering over the ER we used a siRNA approach to reduce endogenous VAP expression in HEK cells. As illustrated in Fig. 2.4A, while the scrambled siRNA control had no effect on either VAPA or VAPB expression,

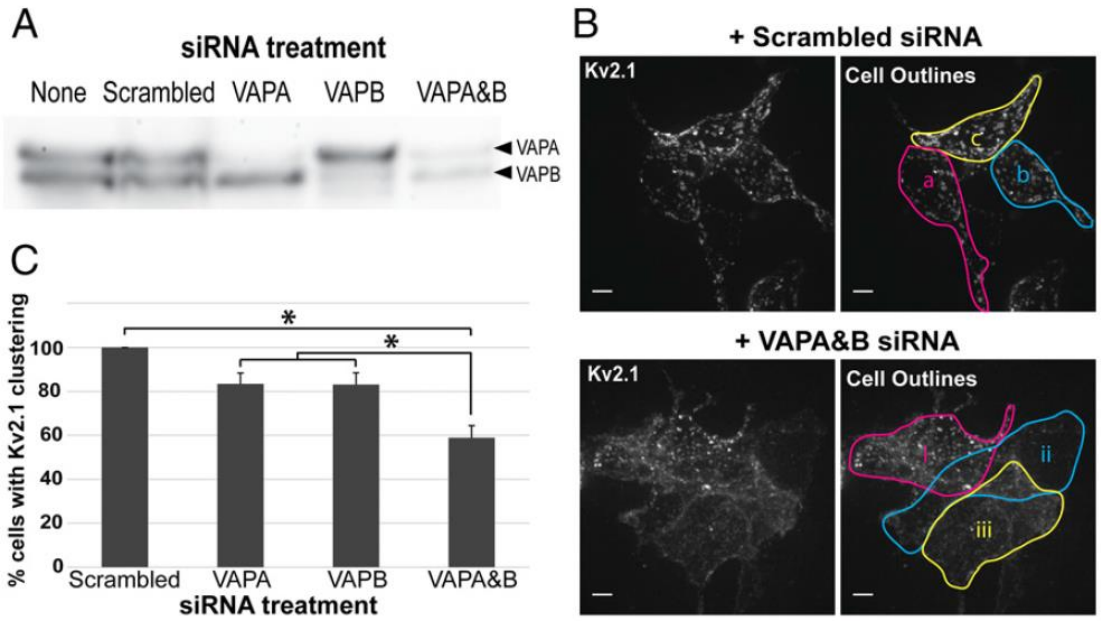

Figure 2.4. Effect of siRNA-mediated knockdown of VAPA and VAPB on Kv2.1 clustering. (A) Western blot demonstrating efficacy of VAPA and VAPB siRNA. Protein blot was probed with anti-VAPB antibody which cross-reacts with VAPA. (B) Representative image of GFP-Kv2.1-loopBAD clustering in the presence of scrambled or VAPA and VAPB siRNA taken via spinning-disk microscopy. z-stack maximum intensity projections are shown. In Upper Right image all three cells (a–c) were scored as having clustered Kv2.1. In the Lower Right image only cell i was scored as having clusters. Note that this image is presented simply to illustrate how clustering was defined as opposed to being quantitative with respect to the effect of the siRNA treatment. (Scale bars: 5 μm.) (C) Quantification of the percentage of cells displaying Kv2.1 clustering after various siRNA treatments. Eighty-six cells receiving the scrambled siRNA, 90 cells receiving VAPA siRNA, 61 cells receiving VAPB siRNA, and 144 cells receiving both VAPA and VAPB siRNA were examined within 26, 27, 21, and 41 images, respectively. Error bars represent SEM. For analysis, a one-way ANOVA was performed, $F(3, 111) = 13.61$, $P = 1.27 \times 10{-}7$, with post hoc Tukey's tests. *$P < 0.01$ significance.

siRNA specific for either VAPA or VAPB independently reduced the levels of these two proteins. Combining both siRNAs greatly reduced both VAPA and VAPB. We next examined the effect of VAP knockdown on Kv2.1 clustering as illustrated in Fig. 2.4B and summarized in Fig. 2.4C. As shown in Fig. 2.4B, knocking down both VAPA and VAPB visually decreased the extent of GFP-Kv2.1-loopBAD clustering as imaged with CF640-SA binding to the biotinylated channels on the cell surface. Since Kv2.1 cluster size and intensity are dependent on the Kv2.1 expression levels, we quantitated the effect of VAP knockdown by simply comparing the percentage of cells with

clusters observed under the different siRNA treatments. For a cell to be classified as Kv2.1 cluster-free it had to have the homogeneous surface distribution illustrated by the two cells (ii and iii) in the lower right-hand panel of Fig. 2.4B. The cell shown in the top left (i) was classified as possessing clustered Kv2.1. Using this quantitation approach the effects of reducing VAPA or VAPB levels are summarized in Fig. 2.4C (83.4 and 83.1%, *NS*, as compared to the scrambled siRNA control). Combining both siRNAs had the greatest effect on Kv2.1 clustering percentage, reducing clustering from 100% to 58.9% ($p = 6.26 \times 10^{-8}$) as compared to the scrambled siRNA control. In summary, the results presented in Fig. 2.4 indicate both VAP isoforms are involved in Kv2.1 clustering, i.e. binding to the cortical ER, in HEK cells. While not apparent in Fig. 4, VAP siRNA, relative to the scrambled siRNA control, decreased the total surface Kv2.1 to 41% of control and decreased the intensity of Kv2.1 clusters to 40%. GFP intensity was reduced to 55% of control. Thus, VAP knockdown suppressed Kv2.1 surface levels to a somewhat greater extent than the overall Kv2.1 expression. Whether VAP levels are specifically linked to Kv2.1 biosynthesis, trafficking or stability remains an open question.

VAP resident time at Kv2.1-induced ER/PM junctions is long lived

Our previous analysis of Kv2.1 behavior at the single molecule level revealed that individual Kv2.1 channels can reside within a cluster for > 25 min (173), suggesting a very stable interaction between the Kv2.1 C-terminus and their ER binding partner. To examine the stability of Kv2.1 VAP binding we measured the dissociation kinetics of photoactivatable GFP (paGFP) tagged VAPA at Kv2.1 clusters following photoactivation. We selectively activated and quantitated VAP-paGFP fluorescence solely within the TIRF field to avoid activating fluorescence removed from the PM as demonstrated in Fig. 2.5A. Activating the paGFP and then measuring its

loss due to diffusion into the cytoplasmic ER allowed us to measure the relative stability of the VAP-Kv2.1 interaction (see Fig. 2.5B). We found that VAPs were demonstrably more stable at

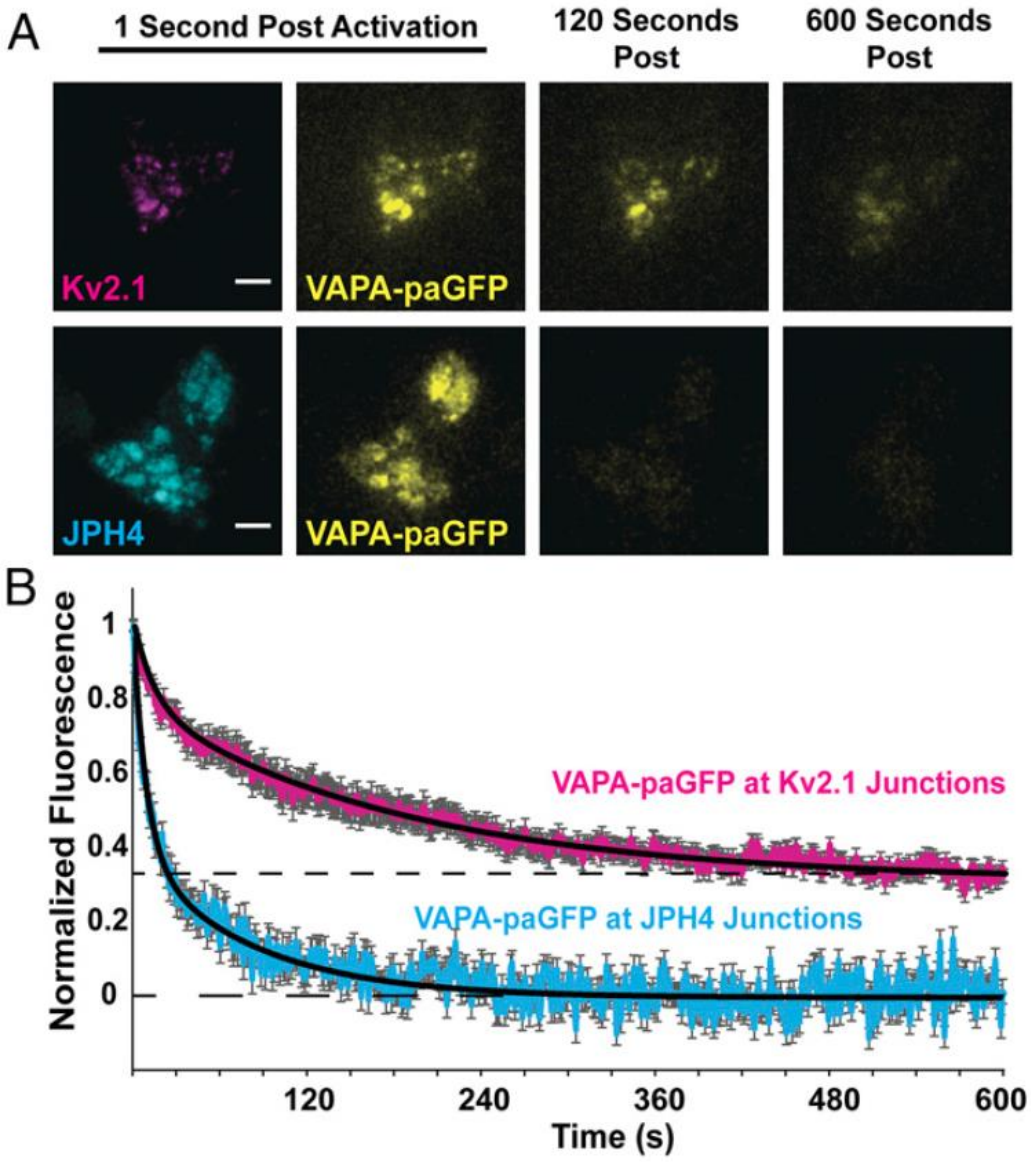

Figure 2.5. Photoactivatable-GFP (paGFP)-based analysis of VAPA stability at Kv2.1induced ER/PM junctions. (A) Representative TIRF microscopy images of VAPApaGFP at either Kv2.1- or JPH4-induced ER/PM junctions 1 s, 120 s, and 600 s after 405-nm induced photoactivation in TIRF. (Scale bars: 5 μm.) (B) Time course of paGFP-fluorescence loss. Normalized fluorescence measurements were fitted with a two-exponential decay, black lines ($y = y0 + A1e^{-(x-x0)/t1} + A2e^{-(x-x0)/t2}$). VAPA was significantly less stable at JPH4-induced ER/PM junctions ($\tau1 = 9.1$, $\tau2 = 80.5$) than at Kv2.1 junctions ($\tau1 = 13.9$, $\tau2 = 186.3$), $P = 0.0395$ at 600 s. Error bars represent SEM. Twenty-five ROIs from 5 Kv2.1-expressing cells and 20 ROIs from 20 JPH4-expressing cells were used.

Kv2.1 junctions than at JPH4-induced junctions, as expected if Kv2.1 channels and VAPs are interacting to form this junction. As indicated in Fig. 2.2, though VAPs are not concentrated to these areas, VAPs are present at the JPH4 membrane junctions solely because they exist throughout the ER. The paGFP fluorescence decayed to baseline with the JPH4 induced junctions while in the presence of Kv2.1 approximately one-third of the original paGFP-VAPA was stably retained, suggesting a stable Kv2.1-VAP interaction lasting longer than 10 min. If VAPs do indeed function as scaffolding proteins at ER/PM contacts this stability allows for the existence of long-lived complexes. A two-exponential decay was required to fit the data, indicating time constants of 9.1s and 80.5s for the JPH4 membrane junctions as compared to 13.9s and 186.3s for the Kv2.1-induced ER/PM contacts. These time constants are likely the result of VAP diffusion into the deeper ER that is removed from the PM. The time constant increases observed in the presence of Kv2.1 could be due to increased molecular crowding in the presence of Kv2.1 as compared to JPH4.

Interaction with VAPs is mediated by the Kv2.1 and Kv2.2 C-terminus

VAPs bind a loosely defined FFAT motif (two phenylalanines within an acidic tract) contained within their binding partners. Kv2.1 clustering requires a previously defined motif within the channel C-terminus as highlighted in Fig. 1A (29), with the underlined serines likely representing phosphorylated amino acids involved in Kv2.1 clustering over the ER (29, 46). However, obvious VAP binding FFAT motifs, which have a consensus sequence of EFFDAxE, (110) are lacking within both the Kv2.1 and 2.2 C-terminus (compared in Fig. 2.6A). As a first step towards identifying the sequences within Kv2 channels that are involved in VAP binding we appended amino acids 445-609 of Kv2.1, and amino acids 552-911 of Kv2.2, to the single pass

transmembrane protein CD4 as diagrammed in Fig. 2.6B. These amino acids were selected so as to keep the total amino acid length from the PM to the regions known to be required for clustering as close to WT Kv2.1 as possible, as there is reason to believe that ER-PM membrane distance can have a profound effect on protein localization to ER/PM junctions (117). CD4 was chosen because wild-type CD4 shows a homogenous cell surface distribution in both transfected rat hippocampal neurons and HEK cells. Thus, any clustering or concentration over the cortical ER is readily detected. Since structural studies indicate CD4 forms a dimer (187) we assume each of these chimeric constructs contains two Kv C-terminal domains. The CD4/Kv2 chimeras were then co-expressed with VAPA-GFP in HEK cells and the CD4 localized using CF640-conjugated anti-CD4 monoclonal antibody directed against an extracellular epitope. As shown in Fig. 2.6C the CD4/Kv2.1 C-terminus chimera clustered on the cell surface and concentrated VAPA similar to the full-length Kv2.1 in Fig. 2B. The same clustering and VAPA redistribution was observed with the CD4/Kv2.2C-terminal chimera (Fig. 2.6D). Thus, a non-canonical VAP-binding motif is likely present within these C-terminal sequences.

Since phosphorylation is believed to regulate the Kv2.1-ER interaction, and the resulting channel clustering phenotype, we next mutated the underlined serines highlighted in Fig. 6A to either alanines incapable of phosphorylation or aspartic acids in order to create phosphomimetics. CD4/Kv2.1 C-terminus chimeras containing these substitutions within appended 445-609 amino acids of Kv2.1 were then co-expressed with VAPA-GFP and VAPA redistribution assessed. As illustrated in Fig. 6E alanine substitution prevented both the chimera clustering and the VAPA redistribution while Fig. 6F shows robust clustering and VAPA redistribution with the phosphomimetic substitutions. These data further support the idea that Kv2.1-VAP interaction is regulated by phosphorylation within a small section of the channel C-terminus.

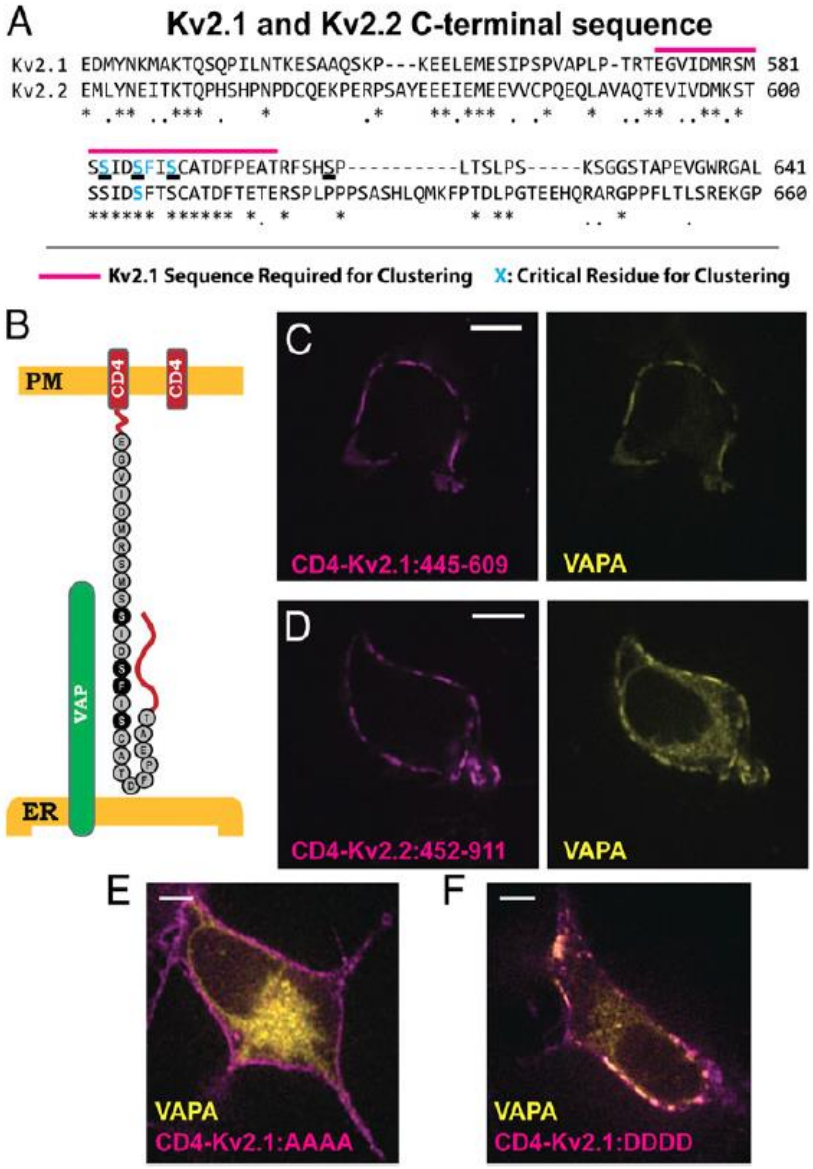

Figure 2.6. Kv2 channel C terminus is sufficient to form ER/PM junctions through VAP interaction. (A) Sequence comparison of Kv2.1 and Kv2.2 C termini. Note the high degree of conservation in the area required for clustering, but lack thereof elsewhere. Known sequence required for clustering in Kv2.1 is indicated by the magenta line. Known amino acids required for clustering are highlighted in cyan. (B) Schematic of WT CD4, on right, and the CD4Kv2.1:445–609 construct, on left. Critical amino acids for Kv2.1 clustering are included in black. (C) Appending amino acids 445–609 of Kv2.1ontothe CD4 C terminus results in ER/PM junctions that concentrated VAPA at the PM. (D) The C terminus of Kv2.2 attached to CD4 also results in a construct that clusters and interacts with VAPs. (E) Expression of VAPA-GFP with the CD4-Kv2.1:445– 609 construct in which the serines underlined in A were mutated to alanines. (F) Expression of VAPA-GFP with the CD4-Kv2.1:445–609 construct in which the serines underlined in A were mutated to aspartic acids. (Scale bars: 5 μm.)

Kv2.1 forms ER/PM junctions through interaction with VAPs via a non-canonical FFAT motif

In order to identify the exact Kv2.1 C-terminal sequence involved in VAP binding we generated a series of CD4 chimeras containing varying amounts of Kv2.1 C-terminal sequence (summarized in Fig. 2.7D). In order to provide enough cytoplasmic depth to contact the cortical ER we added β2-microglobulin between the CD4 and channel sequence to create a rigid linker.

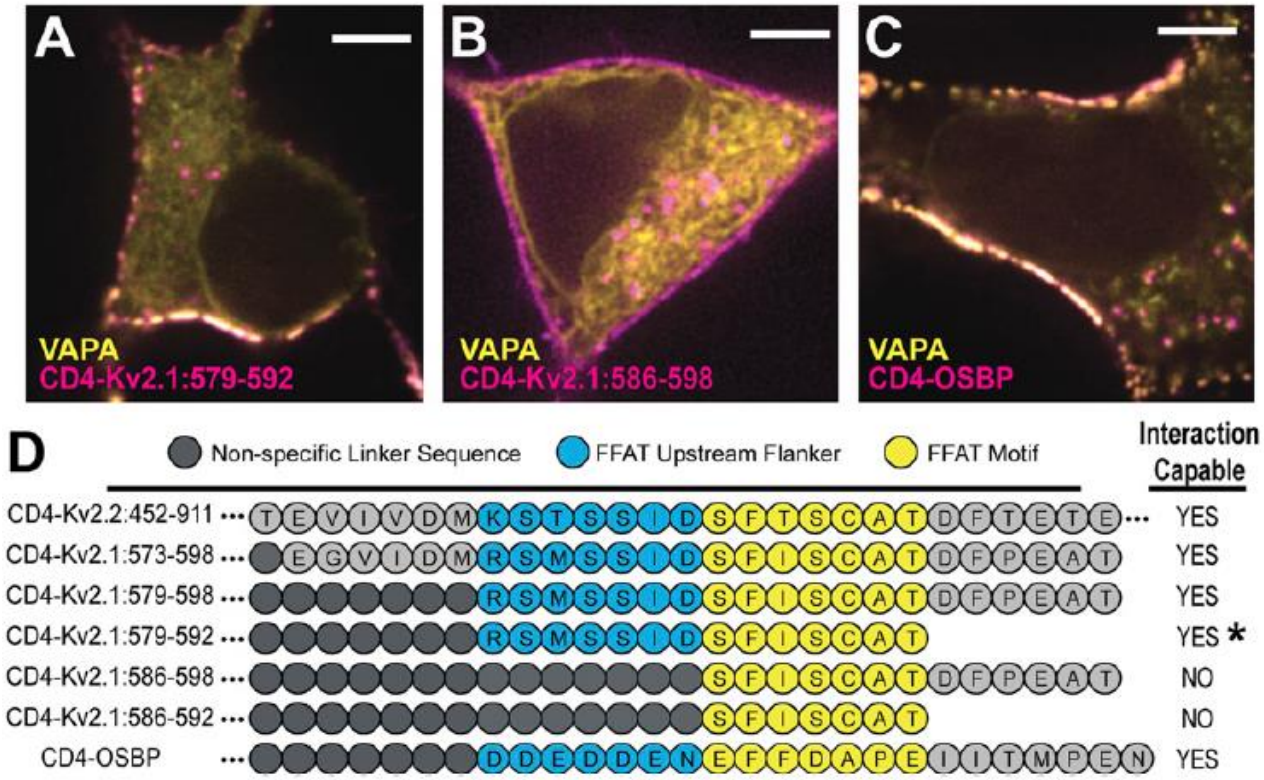

Figure 2.7. Defining the minimum domain necessary for Kv2.1–VAP interaction. (A) CD4-Kv2.1:579–592 forming ER/PM junctions in HEK cells via VAP interaction. This construct represented the minimal sequence of amino acids we observed capable of this behavior (however, see asterisk in D). (B) CD4-Kv2.1:586–598 was not capable of forming ER/PM junctions through VAP interaction. (C) CD4-OSBP construct demonstrating that ER/PM formation and VAP concentration occur in the presence of a classic FFAT motif containing protein on the PM. (Scale bars: 5 μm.) (D) Schematic displaying amino acid identity and relative position of Kv2.1 sequence fragments appended to the CD4 backbone. Right-hand side indicates which chimeras formed clusters on the membrane with concomitant VAP relocalizationto these sites. *, CD4-Kv2.1:579–592 was capable of forming ER/PM junctions if VAP was coexpressed but did not form these microdomains with only the endogenous VAP levels.

Variable length flexible linkers were also inserted between the microglobulin and lengths of short Kv2.1 sequence in an effort to maintain constant spacing between the ER and PM. As a positive control, we also appended the classic FFAT sequence of oxysterol binding protein (OSBP) with both upstream and downstream flankers (see Methods for additional details). OSBP is a lipid transfer protein that is a known VAP interactor and has a well characterized FFAT motif (99, 110, 167). We began by confirming that the amino acid sequence already known to be responsible for the clustering behavior of Kv2.1 channels (amino acids 573-598 (29)) was also responsible for VAP interaction. As shown in Fig. 2.7A a CD4/Kv2.1 C-terminus chimera containing only amino acids 579-592 of Kv2.1 both clustered and concentrated VAPA at the ER/PM junction. In contrast, the chimera with amino acids 586-598 failed to both cluster and redistribute the VAP as illustrated in Fig. 2.7B. Fig. 2.7C shows the VAP interaction observed with the CD4-OSBP FFAT motif positive control. The sequence and behavior of these and other constructs is summarized in Fig. 2.7D. For comparison the Kv2.2 C-terminal sequence used in Fig. 2.6D is included. The comparisons shown in Fig. 2.7D suggest that there is a non-canonical FFAT motif present in both the Kv2.1 and 2.2 C-termini. The seven amino acids in yellow represent the core motif where the first expected phenylalanine is absent. The upstream amino acids in blue likely substitute for the upstream acidic tract obvious in the OSBP sequence. In Kv2.1 serine phosphorylation likely provides the negative charge required to guide the Kv2-VAP interaction, similar to other studied FFAT-containing proteins which are known to interact with the VAPs (110). This required phosphorylation explains the calcineurin-induced declustering of Kv2.1 that occurs in response to excitotoxicity or neuronal insult (31, 32, 176). Note that the 579-592 construct clusters only when VAPs are co-transfected suggesting that the lack of downstream sequence reduces VAP affinity. We cannot say if these specific amino acids are increasing affinity of interaction, or if any random

sequence after the FFAT motif would serve this purpose; to our knowledge no FFAT motif has ever been described that is localized at the very end of any protein as is the case with this CD4-chimera.

Interestingly, three of the four amino acids already found to be critical for the clustering of Kv2.1 (S586, F587, S589) reside directly within the FFAT motif (29, 46). A fourth critical residue (S583) is located just three amino acids upstream and within the FFAT motif flanker region known to be important for VAP interaction (110). The serine at 586 is a known phosphorylation site (176).

Kv2.1 and Kv2.2 interact with and regulate the localization of VAPA and VAPB in rat hippocampal neurons

In order to confirm that the Kv2 VAP interactions also occur in hippocampal neurons Kv2.1-loopBAD was co-expressed with VAPA-GFP in DIV 7 rat hippocampal neurons as illustrated in Fig. 2.8A. Again, VAPA concentrated at the Kv2.1-induced ER/PM junctions. Fig. 8B shows a similar result when GFP-Kv2.2 and VAPB-mRuby2 were co-expressed. Kv2 channels also form ER/PM junctions within the axon initial segment (AIS) (188, 189) and Figs. 2.8C and D illustrate VAP concentration here in the presence of Kv2.1 and Kv2.2, respectively. Fig. 8E illustrates the interaction of the CD4-Kv2.1: 573-589 chimera with VAPA within the AIS. Recent work indicates that Kv2.1 likely contains two independent AIS localization signals within the C-terminus, one is contained within the sequence shown in Fig. 2.6A and the other is located distally at amino acids 720-745(190). The CD4 chimera lacks this secondary AIS localization signal, thus demonstrating that VAP binding alone can localize Kv2.1 to the AIS. Quantitation of Kv2-VAP interaction is summarized in Fig. 2.8F. Here the percentage of transfected neurons concentrating either VAPA or VAPB to the Kv2 induced ER/PM junctions is indicated. The CD4 chimeras that

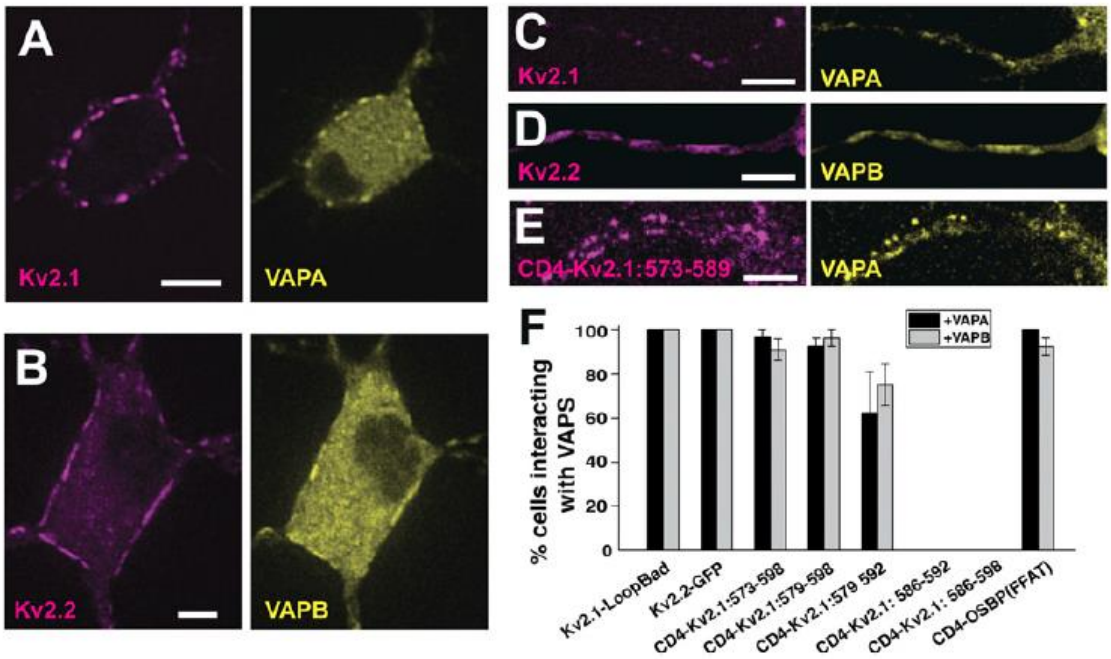

Figure 2.8. Kv2 interaction with VAPs in rat hippocampal neurons. (A) Coexpression of Kv2.1-loopBAD and VAPA-GFP. Surface Kv2.1-loopBAD was visualized with CF640-conjugated streptavidin. (B) Coexpression of GFP-Kv2.2 and VAPB-mRuby2. (C–E) Colocalization ofKv2.1-loopBAD,GFP-Kv2.2,and theCD4-Kv2.1:573– 589 chimera with VAPA-GFP, VAPB-mRuby2, and VAPA-GFP, respectively, within the AIS. The AIS was confirmed with anti-neurofascin antibody staining as illustrated in Appendix II (Scale bars: 5µm.) (F) Summary of the percentage of neurons concentrating VAPs at induced ER/PM junctions. Error bars indicate SEM. P values comparing the interaction of the first three CD4-Kv2.1 chimeras with either VAPA or VAPB to WT Kv2.1 were not significant, with Kruskal–Wallis ANOVA values of $p = 0.37$ and $p = 0.1$, respectively.

failed to interact with VAPs in HEK cells (Fig. 2.7) also failed to bind VAPs in neurons. These data indicate that Kv2-VAP interaction is similar between HEK cells and rat hippocampal neurons, which is not surprising given that HEK cells are of neuronal origin (191) and the calcineurin-dependent regulation of Kv2.1 clustering is conserved between these two cell types (192).

Discussion

Our data demonstrate that a Kv2 channel-VAP interaction links the PM to cortical ER as summarized in Fig. 2.9. The formation of this membrane contact site gives rise to Kv2 channel

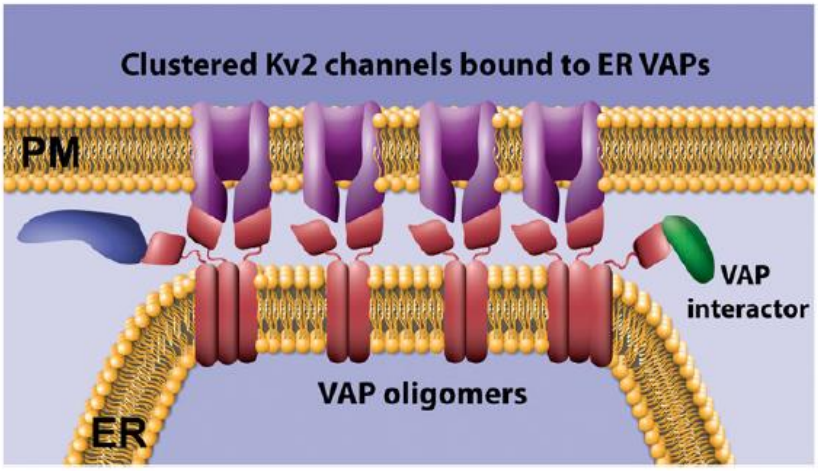

Figure 2.9. Working model of the Kv2.1-VAP junction. Kv2 channels concentrate ER VAPs by both direct binding via the C-terminal noncanonical FFAT motif and VAP oligomerization via the VAP transmembrane domain.

clusters on the neuronal surface. VAPA and VAPB are abundantly expressed in hippocampal, cortical and motor neurons based on both western blot and immuno-staining approaches and these neuronal types display prominent Kv2.1 clusters on the somatic surface (102). However, no concentration of VAPs into plasma membrane associated clusters has been previously reported, perhaps because the available antibodies target VAP domains associated with FFAT motif binding, thus preventing immune-labeling of VAPs within an assembled complex. While we previously proposed that individual Kv2 channels within these microdomains must be corralled behind a cytoskeletal fence due to their high lateral mobility within the PM (173), both the mobility and clustering are now best explained by the binding to freely diffusing VAPs within the ER. The FRET experiments presented in Fig. 3 indicate Kv2.1 and VAPs reside within 1-10 nm of each other (193), suggesting they are in direct contact. The fluorescence loss kinetics after VAP-paGFP photoactivation (Fig. 2.5) suggest this interaction is relatively long-lived (>10 min), which agrees

with our previous studies indicating that individual Kv2.1 channels can remain within a cluster for 25 min or more under resting conditions (173). The siRNA VAP knockdown experiments (Fig. 2.4) support the idea that VAPs are required for the Kv2.1 clustering and indicate that both VAPA and VAPB participate in this process. However, Kv2.1 expression was depressed by 60% upon knockdown of both VAPA and VAPB. Whether this result means VAPs are specifically involved in Kv2.1 biosynthesis, trafficking or stability remains an open question. However, Kv2.1 channels are delivered to the cell surface at Kv2.1-induced ER/PM junctions, making it likely that disruption of this membrane contact site will affect Kv2.1 delivery. Note that when Kv2.1 is first synthesized in a transfected HEK cell it is delivered to the cell surface at the small and dynamic ER/PM contacts that exist in the absence of Kv2.1 (44). As Kv2.1 accumulates on the surface it begins to bind ER VAPs and form the large and stable membrane junctions.

VAPs bind FFAT motifs via a positively charged surface located in their major sperm protein-like domain (110). The FFAT motif core is a sequence of seven amino acids that are extended, typically upstream, by an acidic tract. VAP-FFAT motif interaction is initiated through the non-specific negatively-charged amino acids upstream of the core motif, as illustrated in Fig. 2.7 by the classic FFAT motif of our CD4-OSBP(FFAT) construct. While the originally defined sequence for FFAT domains is EFFDAxE, this motif can tolerate a high degree of variability. For example, the two phenylalanines are not present in all VAP-binding sequences, for instance protrudin has an FFAT-like motif with a lysine at position 3 (as compared to isoleucine in Kv2.1) (110). The Kv2.1 and 2.2 VAP-binding domains identified in our present work, SFISCAT and SFTSCAT respectively, again demonstrate that the two phenylalanines are not essential for binding, and that phosphorylated serines likely can substitute for acidic residues. Importantly, the Kv2 sequences adhere to a minimal requirement for FFAT-like motifs: F/Y at position 2, negative

residue at position 4, small residue at position 5, and negative flank. Nevertheless, criteria suggested for finding FFAT motifs would place the Kv2 sequences below the established threshold (110). The feature that made these motifs detectable is the previous precise mapping across Kv2.1's C-terminus (29).

Clustering of Kv2.1, and to a lesser extent Kv2.2, is regulated by phosphorylation (7, 31, 40) and phosphorylation of serine residue 586 at the beginning of the non-canonical FFAT motif, confirmed by mass spectrometry and phospho-specific antibody binding (40, 176), likely generates negative charge necessary to facilitate VAP interaction. Phosphorylation of residues surrounding FFAT motifs to facilitate binding is already known to occur in other VAP interactors (110). It is currently unknown whether serine 583 within the upstream linker, required for Kv2.1 clustering (29), or serine 589, a critical FFAT motif residue, are phosphorylated. What is known is that neuronal insults, such as ischemia, and neuronal activity result in calcineurin-dependent dephosphorylation of the channel, dispersal of channel clusters, and retraction of the cortical ER (31, 32, 46, 194). How calcineurin accesses the phosphorylated serines involved in VAP binding is unclear. Perhaps the individual FFAT motif-VAP interactions are dynamic enough to allow calcineurin access over the 2 min period required for significant glutamate-induced declustering and ER retraction (46). It is important to note that Kv2 channels are tetrameric. This current study has not investigated the stoichiometry involved in Kv2-VAP interaction but it is likely that one Kv2 tetramer can bind up to four VAPs. Individual VAPs unbinding and quickly rebinding different α-subunits both within a single channel and across channels could explain transient calcineurin FFAT access and would still be consistent with the general long-term stability of proteins within these domains. Clearly, future research is required to address the exact mechanisms underlying the phosphorylation-dependent VAP interaction.

Data presented in Figs. 2 and 3 suggest the VAPA(K87D/M89D) mutant, which is unable to bind FFAT motifs, still localizes to Kv2 channel-induced ER/PM junctions, although to a reduced extent relative to wild-type VAPA. Since VAPs can form homomeric and heteromeric oligomers, possibly through a transmembrane GxxxG motif (186), the mutant GFP-tagged VAPA may be assembling into oligomers with endogenous wildtype VAPs that are bound to Kv2 channels at junctions. Such a mechanism would allow for the localization of VAPs to these microdomains which possess FFAT binding motifs available to interact with additional partners apart from Kv2 channels (see Fig. 2.9 for depiction). VAPs have a growing list of interactors, including AKAPs, protein kinases, kinase regulators, kinesins, transcription factors, Rabs, and lipid transfer proteins (99, 110, 169) and any concentration of these proteins to ER/PM contact sites should be physiologically significant. Given that the Kv2-VAP interaction is likely directly regulated by phosphorylation within, and adjacent to, the Kv2 C-terminal FFAT motif, it is possible that the kinases and phosphatases involved are VAP tethered. However, to the best of our knowledge, known Kv2.1 modifying kinases (cdK5, p38 MAPK, src) (21, 22, 195) and phosphatases (calcineurin) (31, 32) have not been confirmed to be part of the VAP interactome (169). However, FFAT motif containing proteins are involved in the non-vesicular transfer of ceramide, cholesterol and phosphotidylinositols between the ER and late secretory organelles including TGN and PM. Kv2 channels may establish an ER/PM junction where the concentrated VAPs function as a scaffolding hub, making these membrane contact sites not only functionally distinct from ER/PM contacts such as those induced by STIM1 or the extended synaptotagmins (167), but also one which is regulated by neuronal activity and sensitive to insult. In addition, it is possible that the converse is true, where the VAP-mediated concentration of Kv2 channels imparts specific functions onto the ER/PM junction due to domains contained within the channel itself.

Kv2.1 contains a syntaxin binding region (41, 42), an ion pore and a voltage-sensing domain that, even in the non-conducting channel, responds to membrane potential (36). In addition to localized SNARE protein binding or K^+ conductance, perhaps Kv2.1 communicates neuronal electrical activity to functions occurring at the ER/PM contacts.

ER/PM contact sites represent approximately 12% of the somatic surface *in vivo* but not all junctions are created equal (51). Junctions can be formed by extended synaptotagmins, STIM proteins, junctophilins, and other proteins in addition to Kv2 channels and an obvious question deals with the dynamic composition of these membrane contacts at any particular time. It's likely that multiple junction forming proteins can be present and that these components will differentially recruit specific interactors as proposed here for the Kv2 recruitment of VAPs. Given that different membrane bridging systems will have optimal ER/PM distance requirements it is likely that neuronal ER/PM contacts will be segregated into distinct domains with distinct functional properties. Kv2.1 and Kv2.2 are differentially expressed in cell types throughout the brain and exhibit different functional properties, including response to stimuli such as acute hypoxia, with Kv2.2 being less responsive (Hermanstyne et al. 2010; Bishop et al. 2015). It seems probable that these differences in junction location and stability as well as functionality are significant with respect to different cell types. In addition to this, Kv2.1 exhibits different behavior depending on the subcellular compartment it is located in. Kv2.1 channels on the AIS are more resistant to glutamate-induced declustering as compared to channels on the soma (190, 196). While our data indicates VAP-based tethering occurs in both compartments, there is a domain downstream of the FFAT motif (amino acids 720-745) that is sufficient for AIS-specific localization (190). Perhaps during evolution the addition of a second ER targeting motif ensured that neuronal activity does not alter Kv2.1-ER contacts within the AIS.

As with many ion channels, mutations in Kv2.1 that alter conductance are linked to human disease, with mutations that alter ion selectivity and voltage-sensing being associated with epilepsy and developmental delay (23, 24). However, three recently described Kv2.1 mutations result in premature stop codons that are predicted to not alter Kv2.1 conductance (197). These mutations occur downstream of the conserved channel domains, falling between the last transmembrane domain and the non-canonical FFAT motif identified in the present work. One of these mutations truncates Kv2.1 at the arginine residue immediately upstream from the FFAT motif flanker region (R571). All three mutations result in developmental delay and all three are expected to abolish the ER/PM junctions formed by Kv2.1. Thus, mutations that specifically interfere with Kv2.1-VAP binding are likely to be involved in human disease.

Chapter Three: Dynamic Composition of the Kv2-VAP Endoplasmic Reticulum / Plasma Membrane Microdomain

Chapter Overview

Endoplasmic reticulum / plasma membrane junctions contain a rapidly growing assortment of known resident proteins whose location at these sites is dynamically regulated through an assortment of stimuli and cellular states. Here we explore protein residents of Kv2-VAP junctions. We show that VAP proteins concentrated at ER/PM junctions are capable of binding additional partners as we had previously hypothesized. While we fail to observe concentration of other VAP-binding proteins to Kv2-VAP junctions as a direct consequence of this scaffolding, we do observe stimulus-induced translocation of a number of proteins to these sites, e.g. Nir2 concentration during angiotensin II treatment and STIM1 concentration during store depletion via thapsigargin application. In a novel finding, we report that Nir2 translocation to ER/PM junctions displaces junctophilin-4 from these sites. We also observe MOSPD3 concentration due to Kv2-induction of ER/PM contacts, suggesting that this protein may be acting in a similar manner as the VAPs and interacting with the Kv2 channels from its location in the ER membrane. Lastly, we find that ER calcium store recovery is enhanced in the presence of Kv2.1 and this enhancement is likely due to multiple facets of the channel complex, not just its action as an ER/PM tether.

Introduction

Endoplasmic reticulum / plasma membrane (ER/PM) junctions are complex and dynamic organelles that represent up to 12% of the neuronal soma in addition to being present in both the axon and dendritic arbor (51). ER/PM junctions regulate calcium and lipid homeostasis (72, 198-

202), are involved in endo- and exocytosis (14, 44, 75, 203, 204), and coordinate a variety of cell signaling cascades (54). In the intact brain, these contact sites contain multiple components: junctophilins, STIM proteins, lipid transfer proteins, extended synaptotagmins, etc. These contact sites are regulated in time and space to fulfill cellular requirements (88). The protein composition of junctions is known to be influenced by the calcium concentration of the ER (90), the calcium concentration of the cytosol (91, 92), the activity of the excitable cell (93, 94), and the lipid composition of the PM (72). The full range of protein residents, how the functional specificity of junctions changes as a consequence of internal composition, and how proteins within these spaces effect the function of other residents is of high current interest (50).

In Chapter 2 of this dissertation we described the Kv2-VAP interaction that induces the formation of stable ER/PM junctions. In this chapter we further explore this location by examining other possible protein residents at these contacts and how these residents may come together to regulate the functionality of these sites. We begin by testing the hypothesis that VAP proteins concentrated at Kv2-induced junctions are free to bind additional interactors. We then test other known VAP interactors and their localization to these sites. VAP has a growing list of proteins it may bind to, and a number of these have already been found to localize to membrane-membrane contact sites (97, 108, 110). Determining which of these proteins, if any, colocalize with Kv2/VAP at ER/PM junctions would be incredibly beneficial for determining functionality of these microdomains.

Methods & Materials

DNA Constructs GFP-Nir2 and GFP-Nir2(F350,351A) were gifts from Tamás Balla. MOSPD3 was a gift from Eric Schirmer (Addgene plasmid #62011). Cerulean3-Orai1 and YFP-STIM1 were

gifts from Albert Gonzales. Plasmids encoding fluorescent protein- and biotin acceptor domain-tagged Kv2.1 have been described previously (35, 172, 173). mRuby-FFAT was created using standard molecular cloning techniques and uses the FFAT motif of OSPB plus flanker regions (DDEDDENEFFDAPEIITMPEN) with a single serine residue in the upstream flanker mutated to aspartic acid to avoid any possible phosphorylation effects. The luminal ER marker dsRedER has been previously described (39, 46). mCherry-JPH4 was provided by Yousang Gwack (Addgene 79599).

Cell culture, transfection, and surface Kv2.1 labeling Transfection of HEK 293 cells [American Type Culture Collection (ATCC), passage 45-48] was performed via electroporation prior to plating cells onto Matrigel-coated 35 mm glass bottom coverslip dishes (Matsunami Glass Corporation. HEK-AT1 cells, a cell line stably expressing angiotensin receptors, were a kind gift from Tamás Balla and were treated identically as normal HEK293 cells. Imaging was performed 24 hours after transfection. Kv2.1-BAD constructs were co-transfected with BirA to biotinylate the biotin acceptor domain. Labeling biotinylated BAD residues was accomplished using a 1:1000 dilution of CF640-conjugated streptavidin (CF640-SA; Biotium) in HEK imaging saline (146 mM NaCl, 4.7 mM KCl, 2.5 mM $CaCl_2$, 0.6 mM $MgSO_4$, 1.6 mM $NaHCO_3$, 0.15 mM NaH_2PO_4, 0.1 mM ascorbic acid, 8 mM glucose, and 20 mM 4-(2-hydroxyethyl)-1-piperazineethanesulfonic acid (HEPES), pH of 7.4) for 10 mins. Washes were then applied to remove unbound fluorescent streptavidin.

To isolate hippocampal neurons, embryonic rats were anesthetized using isoflurane as per an Institutional Animal Care and Use Committee of Colorado State University approved protocol (Protocol ID: 15-6130A). A mixed population of male and female cells were used as embryos of both sexes were collected. Dissociation of the neurons was performed as previously described

(175). Cells were plated on glass bottom dishes that had been coated with a 1:2 mixture of poly-L-Lysine (P4707, Sigma) and 0.15 borate buffer pH 8.4. This plating solution was washed off with 2x washes of sterile water and $5x10^5$ cells were plated per dish. Cells were fed with Neurobasal media (Gibco by Life Technologies, REF# 21163-049) that had been supplemented with 1:100 GlutaMAX Gibco by Life Technologies, REF# 35050-061), Pen-Strep (HyClone, CAT# SV30010, 100 units/mL, 100 µg/ml respectively) and 1:500 NeuroCult SM1 (Stem Cell Technologies, CAT# 05711). DIV5 rHN cultures were transfected using 2µl of Lipofectamine 2000 mixed with appropriate amounts of construct plasmid DNA.

Previously transfected DIV7 rHN cultures were washed in neuronal imaging saline (126 mM NaCl, 4.7 mM KCl, 2.5 $CaCl_2$, 0.6 mM $MgSO_4$, 0.15 mM NaH_2PO_4, 0.1 mM ascorbic acid, 8 mM glucose, and 20 mM HEPES, pH 7.4) prior to labeling for 10 minutes with 1:1000 CF640-conjugated streptavidin and then washed again.

Microscopy For spinning disk confocal microscopy, a Yokogawa-based CSUX1 system combined with an Olympus IX83 inverted stand and an Andor laser launch (100-150 mW 405, 488, 561, and 637 nm diode lasers) was used. Image collection occurred through a 100X Plan Apo, 1.4 NA objective and an Andor iXon EMCCD camera (DU-897). Imaging software by Metamorph runs the system. The spinning disk microscope is equipped with ZDC constant focus system and a Tokai Hit chamber and objective heater. TIRF microscopy was performed using a Nikon Eclipse Ti fluorescence microscope. This system is equipped with 100 mW 405, 488, 561, and 633 nm diode lasers split between TIRF and photoactivation pathways. Images were collected on an Andor iXon emccd DU-897 camera using a Plan Apo 100x, NA 1.49 TIRF objective. This system is run on NIS AR software. Both objective and dish are temperature controlled and the Nikon Perfect-Focus was used to control z-drift. Spectral detectors, sequential excitation, dichroics, and bandpass

filters were used to separate fluorophores. Additional information can be found in our previous publications (47, 175).

Image processing and analysis ImageJ was used for image processing. Images were pseudo-colored, cropped, and contrast adjusted. Analysis was performed using ImageJ. Experimental specifics can be found in either the results section or in figure legends. Single z-slices are presented unless otherwise noted.

Experimental Design and Statistical Analysis HEK 293 cells were used unless otherwise noted as they are an ideal model system for imaging interactions that occur in ER/PM junctions. In both HEK cells and rHNs, are primary concern was expression levels of the various DNA constructs we used. Our aim throughout was to express just enough protein in order to be able to visualize location. Our high sensitivity microscopes, which allow for imaging of single molecules, allow for minimal expression levels.

For statistical analysis, unless otherwise noted in the manuscript or within figure legends, student's t-tests were performed to generate p-values.

Results

Additional VAP interactors are capable of localizing at Kv2.1-induced VAP scaffolds

To examine if a VAP scaffold exists, we tested the location of a new construct, mRuby-FFAT. This construct has the concensus FFAT motif of the known VAP interactor, OSBP, attached to the fluorescent protein mRuby via a short linker. As shown in Figure 3.1, mRuby-FFAT is a soluble protein (see internal z-stack image) that concentrates at Kv2.1 clusters when coexpressed with VAPA. We did not witness this level of mRuby-FFAT concentration to junctions when we did not coexpress VAP, possibly because the levels of mRuby-FFAT localized to junctions without

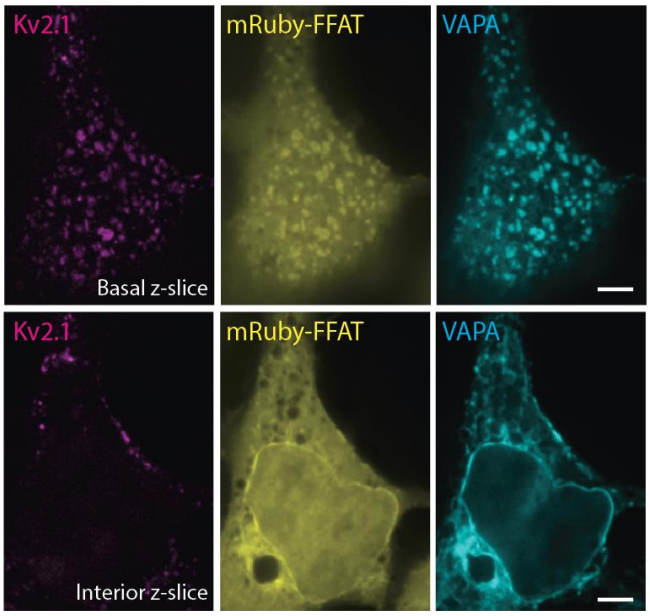

Figure 3.1 VAP platforms at Kv2.1-induced ER/PM junctions are capable of binding additional partners (A) mRuby-FFAT concentrates at ER/PM junctions formed by Kv2.1loopBAD and GFP-VAPA interaction. Scale bars represent 5 µm.

VAP coexpression was low enough to be obscured by the cytosolic signal. This served as a proof of principal that concentrated VAPs at ER/PM junctions are free to bind multiple interactors at high expression levels.

CERT, Syntaxin1A, and Occludin do not robustly concentrate at Kv2/VAP junctions

We began by examining known VAP interactors that have been previously found to reside at ER/PM junctions. CERT is a transfer protein that trafficks ceramide in a non-vesicular manner (205). It contains an FFAT motif and is a known VAP interactor (206). As demonstrated in Figure 3.2A, we did not observe any robust concentration of CERT to Kv2.1-induced ER/PM junctions. The Kv2.1 C-terminus also contains a Syntaxin-1 binding domain (207, 208). If Kv2.1 was binding syntaxin, that could possibly explain the role in endo- and exocytosis Kv2.1 has at sites of ER/PM

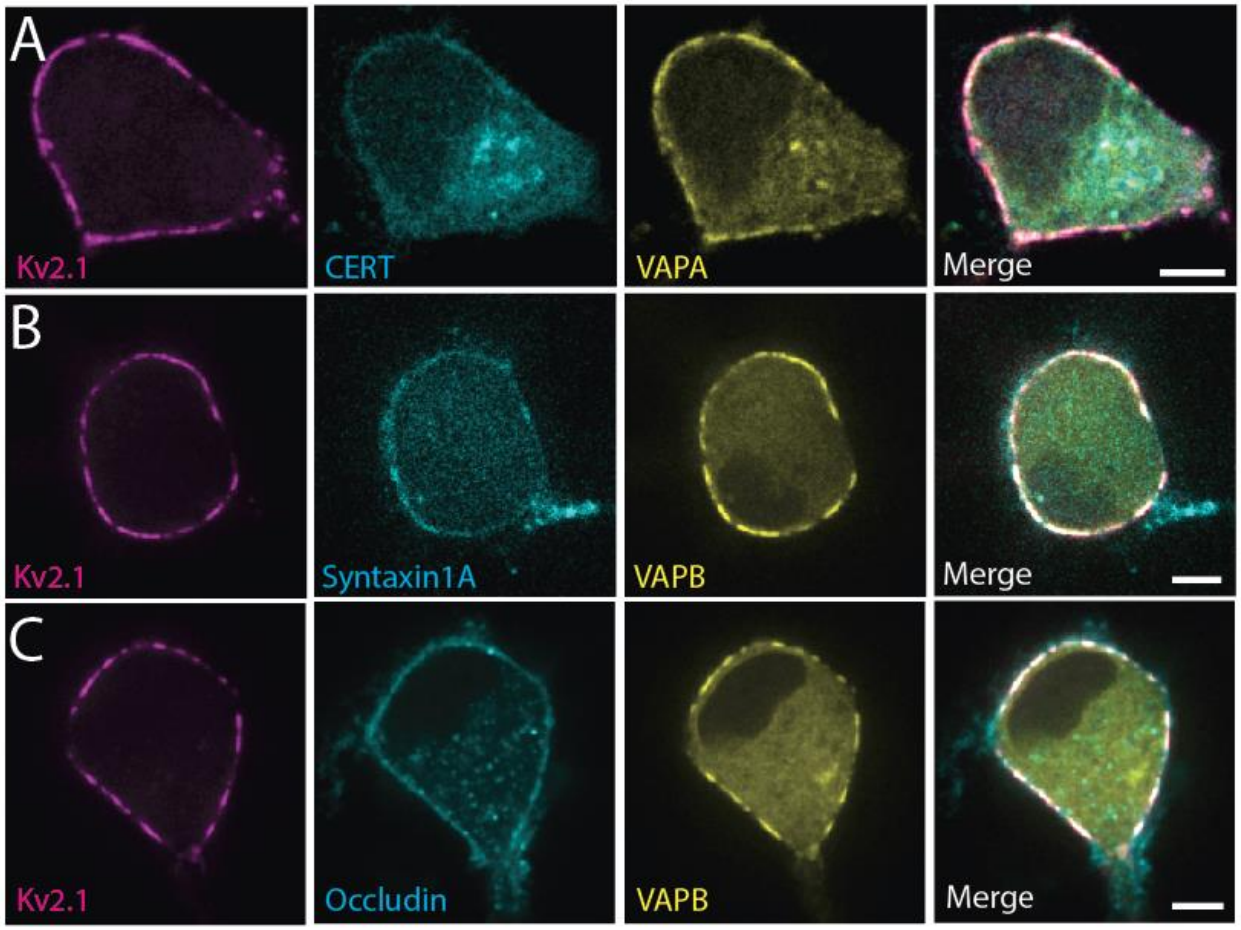

Figure 3.2. Lack of colocalization to Kv2.1-induced ER/PM junctions in rat hippocampal neurons. (A) CERT-mRuby does not concentrate at ER/PM junctions formed by Kv2.1loopBAD/GFP-VAPA interaction. (B) GFP-Syntaxin1A does not concentrate at ER/PM junctions formed by Kv2.1loopBAD/mRuby-VAPB interaction. (C) mEmerald-Occludin does not concentrate at ER/PM junctions formed by Kv2.1loopBAD/mRuby-VAPB interaction. Scale bars represent 5 µm.

junctions (14, 15, 18, 44). However, we also did not observe concentration of Syntaxin1A to Kv2.1-induced ER/PM junctions (see Figure 3.2B). Occludin is another known VAP interactor and along with ZO-1 is a component of tight junctions (209-211). While we did observe occasional colocazation between occludin clusters on the cell membrane and Kv2.1 junctions, the majoriy of Kv2-induced ER/PM junctions did not have substantial levels of occludin localized to these sites (see Figure 3.2C).

Kv2.1 may also interact with MOSPD3 to form ER/PM junctions

We next tested the location of MOSPD3. The MOSPDs are structurally similar to the VAPs and are thought to be playing functionally similar roles (212). Both VAP proteins and the MOSPDs are capable of binding FFAT motifs via a major sperm protein (MSP) domain (97, 212). Given this, it is possible that the Kv2 channels could also bind the MOSPDs and form ER/PM junctions in this manner.

We found significant concentration of MOSPD3 to Kv2.1-induced ER/PM junctions, suggesting that it can also function as an interactor (see Figure 3.3). Compared to the ER marker CP450, we found that MOSPD was significantly more concentrated ($p = 0.000183637$). MOSPD3 was also significantly more concentrated at Kv2-induced junctions than junctions created using junctophilin-4 (JPH4), suggesting that this concentration is Kv2.1 specific ($p = 0.000618526$). Despite this significant redistribution, the level of concentration of MOSPD3 is far below that of VAP levels and when MOSPD3 is coexpressed with exogenous VAPB this MOSPD3 concentration to Kv2-induced junctions is lost ($p = 0.996059086$, MOSPD3 withVAPB at Kv2.1 clusters versus CP450 at Kv2.1 clusters). A greater binding affinity for VAP would explain the significantly lower concentration of MOSPD3 to Kv2.1 clusters compared to the concentration of VAPs at these sites, and would also explain how coexpression of exogenous VAP could disrupt this redistribution as VAP outcompetes MOSPD3 for the FFAT motif of Kv2.1.

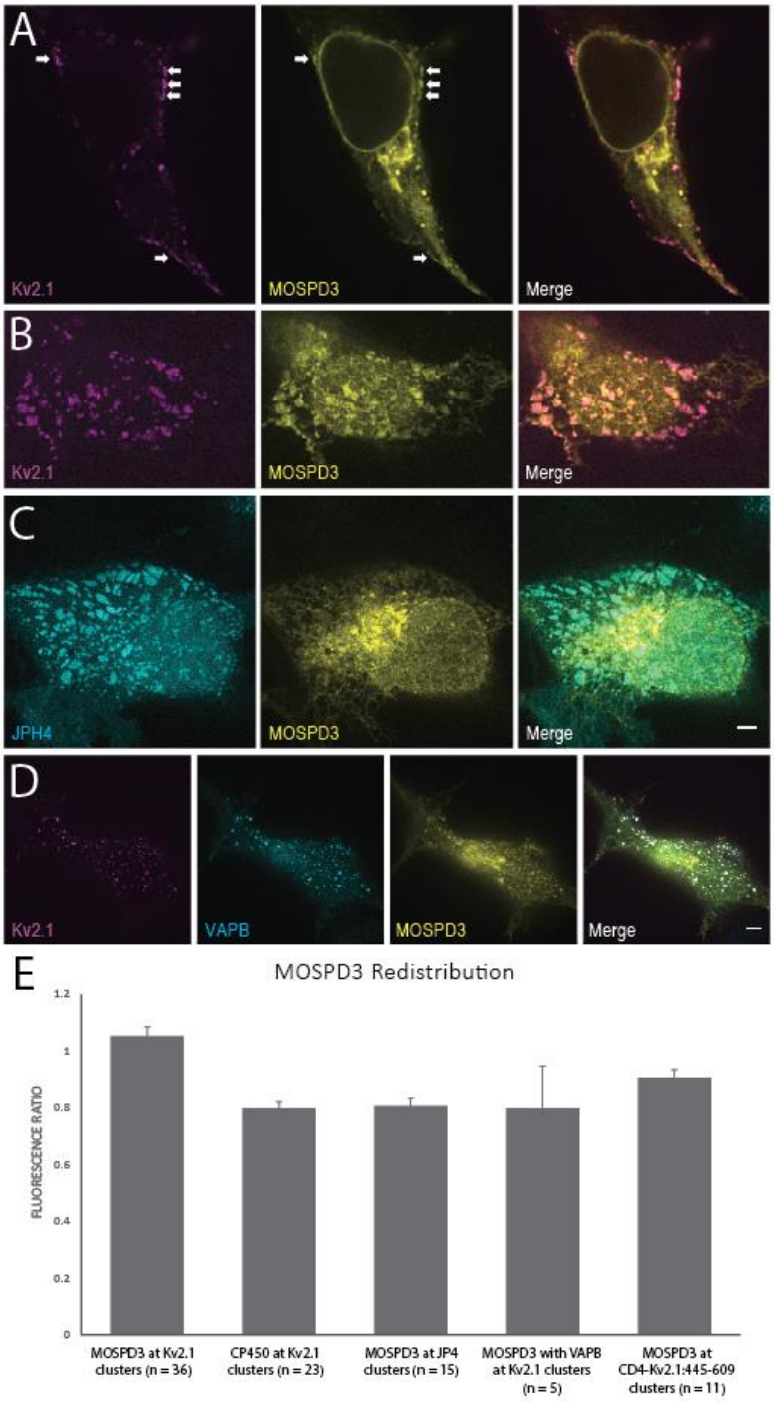

Figure 3.3. MOSPD3 concentrates at Kv2.1-induced ER/PM junctions. (A) Cross sectional spinning disk z stack image of MOSPD3 concentration at Kv2.1loopBAD-induced ER/PM junctions in HEK293 cells. (B) Basal surface showing concentration of MOSPD3. (C) Basal surface of MOSPD3 in the ER at sites of JPH4-induced ER/PM junctions. Note the enhanced concentration of MOSPD3 at junctions in B compared to C. (D) MOSPD3 concentration to Kv2.1loopBAD-induced junctions decreases when coexpressed with VAPB. (E) Bar graph of the MOSPD3 junction/internal fluorescence ratio at junctions created by various tethers. Scale bars represent 5 µm. Error bars indicate S.E.M.

Nir2 redistributes to Kv2.1-induced ER/PM junctions during angiotensin treatment and displaces JPH4 from these locations

Nir2 coordinates phosphatidylinositol-phosphatidic acid exchange at ER/PM junctions and can be recruited to these sites by angiotensin application in a PKC-mediated pathway (70, 71). Under resting conditions Nir2 is freely diffusive within the cellular cytosol (see Fig. 3.4, upper panels), however when activated via 100 nM angiotensin II stimulation, Nir2 redistributes to Kv2.1-induced ER/PM junctions (see Fig. 3.4, lower panels).

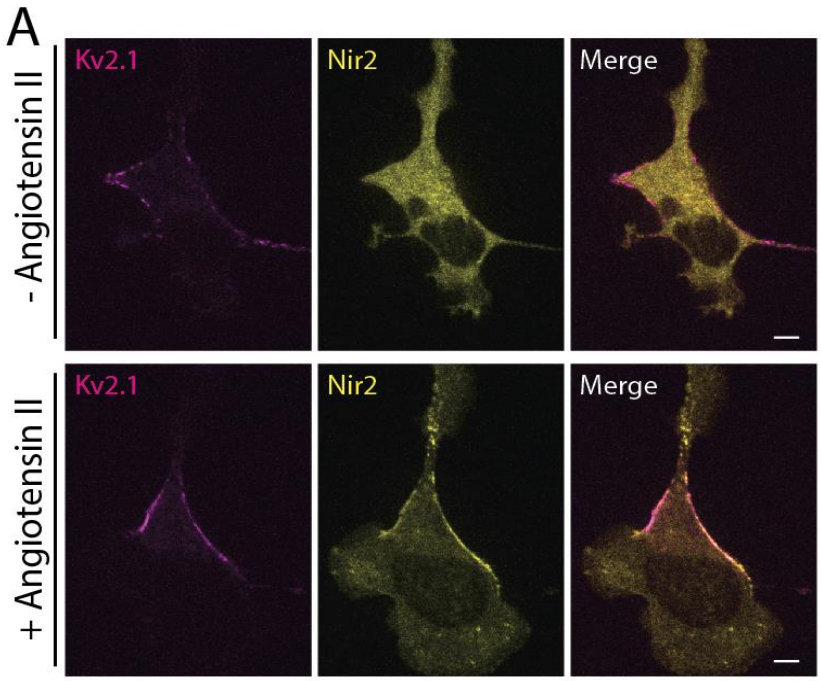

Figure 3.4. Angiotensin activated Nir2 translocates to Kv2.1-induced ER/PM junctions. A) Prior to angiotensin II treatment, GFP-Nir2 is fully diffuse throughout the cytosol of HEK-AT1 cells. Upon 100 nM angiotensin II treatment, GFP-Nir2 concentrates to Kv2.1loopBAD-induced ER/PM junctions. The same cell is pictured in both upper and lower panels. Spinning dick microscopy was used to image internal dynamics during treatment. Scale bars represent 5 µm.

We also investigated changes in the JPH4 junction during this concentration of Nir2 protein. We found that concentration of Nir2 at JPH4 junctions through angiotensin II activation

resulted in JPH4 loss from these sites, being replaced at the ER/PM contact by Nir2 in HEK-AT1 cells (see Fig. 3.5).

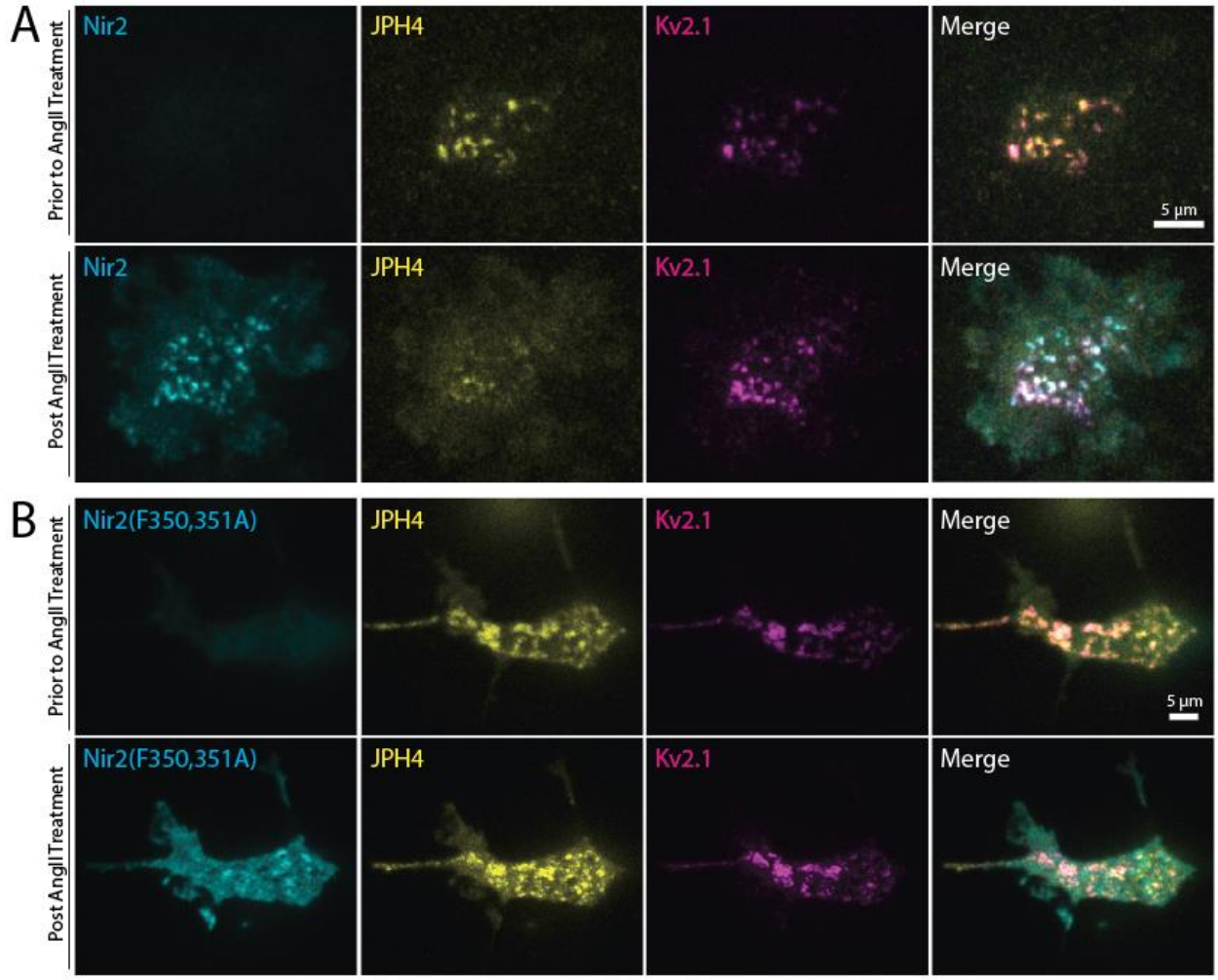

Figure 3.5 Angiotensin activation of Nir2 results in JPH4 disruption. A) Prior to angiotensin treatment, GFP-Nir2 fluorescence is weak at the PM as imaged by TIRF microscopy. JPH4-mCherry and Kv2.1loopBAD colocalize. After angiotensin treatment, GFP-Nir2 concentrates at ER/PM junctions, resulting in mCherry-JPH4 loss from these locations. Kv2.1loopBAD is uneffected. (B) Angiotensin activation of the GFP-Nir2(F350,351A) mutant results in it binding lipid on the PM, but not being recruited to ER/PM junctions. Both JPH4 and Kv2.1 are not displaced under these conditions. Scale bars are 5 µM.

When junctions contained both Kv2.1 channels and JPH4, Nir2 activation resulted in loss of JPH4, but Kv2.1 remained in residence. A Nir2 FFAT mutant, Nir2(F350,351A), which binds lipid on the cellular membrane but is unable to interact with VAPs in the ER, failed to disrupt

JPH4 localization to ER/PM junctions (Fig. 3.5B). In fact, Nir2(F350,351A) appeared to be partially excluded from junctions containing Kv2.1 and JPH4. This could be due to either the lipid composition of these domains or to steric hindrance, but as the wildtype Nir2 seems to have little problem binding lipids at these locations the latter hypothesis appears more likely. To our knowledge, this is the first example found of a junction resident protein completely displacing another tether at these locations.

Kv2.1 enhances ER calcium recovery after store depletion

STIM1 interacts with Orai at junctions to generate store operated calcium entry. We previously showed that in cells with junctions formed by Kv2.1, STIM will preferentially relocate to these sites, concentrating Orai on the PM to these locations as well (46). In Figure 3.6, STIM is

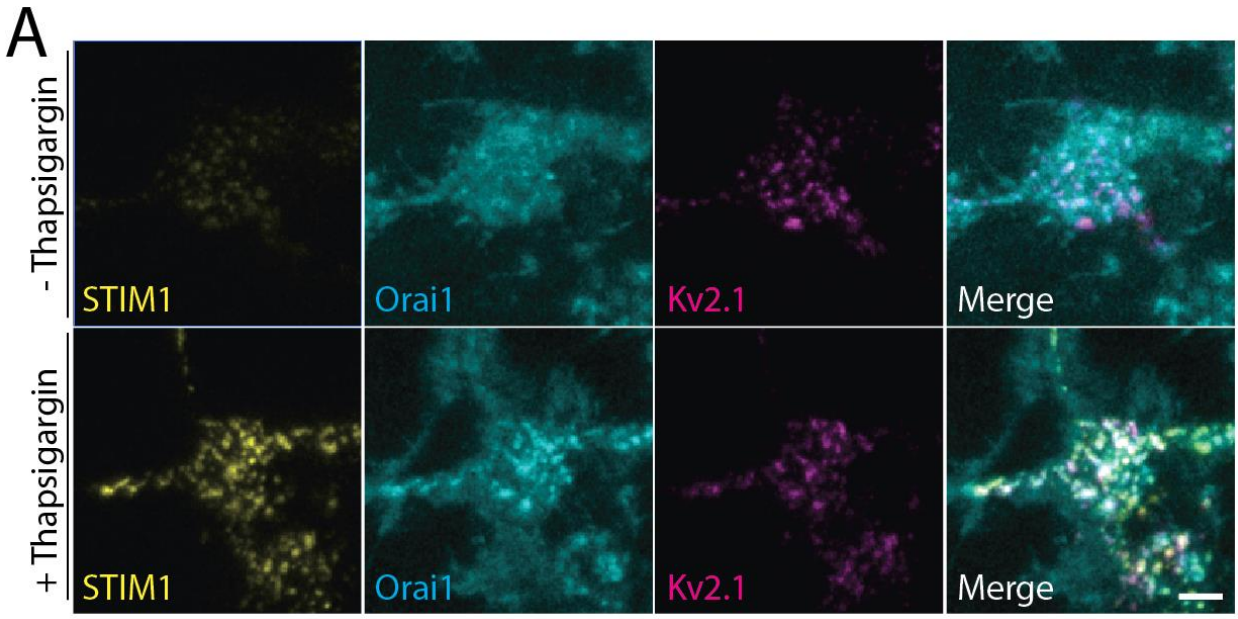

Figure 3.6. STIM1, Orai1, and Kv2.1 localization pre and post thapsigargin treatment. (A, upper panels) Before thapsigargin treatment, YFP-STIM1 fluorescence is weak and confined to the ER beneath Kv2.1 clusters. Cerulean3-Orai is localized diffusely across the PM. After thapsigargin treatment (lower panels) YFP-STIM1 concentrates to Kv2.1loopBAD-induced ER/PM junctions. Cerulean3-Orai relocalizes to sites of STIM1 concentration. Representative TIRF images. Scale bar represents 5 µm.

observed as a weak signal located to the ER beneath Kv2.1 clusters and Orai is fully diffuse on the PM (upper panels). Upon ER calcium store depletion via thapsigargin treatment, STIM concentrates at Kv2.1 clusters and Orai is redistributed to these sites on the PM (lower panels). The STIM-Orai interaction is fully capable of forming ER/PM junctions independently of other tethers, however, calcium refilling can be influenced by the protein make-up of junctions (150). We examined here if the presence of Kv2.1 at these sites effected ER store recovery. Using CEPIAer as an indicator of ER calcium, we depleted ER calcium levels using a zero calcium imaging solution. Exchange with a new solution containing 2.5 mM calcium allowed for the observation of store refilling (Fig. 3.7A). ER calcium replenishment occurred at a significantly increased rate in cells expressing Kv2.1 (Fig. 3.7B). Interestingly, cells expressing a CD4-Kv2.1:445-609 chimera displayed an intermediate recovery rate. This chimeric protein, while containing a large portion of the channel C-terminus including the Kv2.1 FFAT motif allowing for VAP interaction and the formation of ER/PM junctions, lacks the entire channel n-terminus and transmembrane domains including the S4 voltage sensor and pore region.

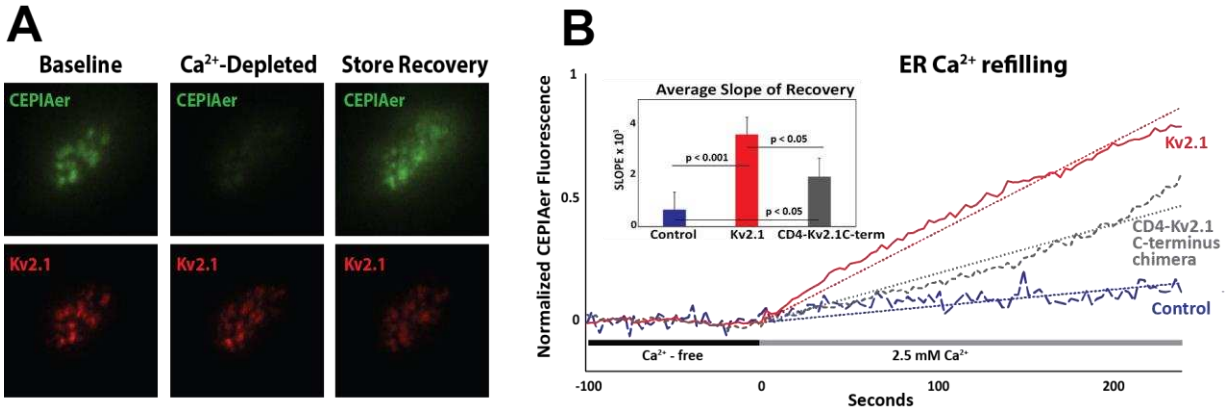

Figure 3.7. Calcium store recovery is enhanced in the presence of Kv2.1. (A) CEPIAer fluorescence showing calcium concentration before calcium depletion, during depletion, and after store recovery. Kv2.1 junctions remain constant throughout treatment. (B). Rates of store recovery in untransfected control cells, cells with ER/PM junctions made with Kv2.1, and cells with ER/PM junctions created with CD4-Kv2.1:445-609. All three conditions have significantly different rates of refilling, see inset.

Discussion

While we did not observe colocalization between Kv2.1 and CERT, Syntaxin1A, or Occludin, there are a number of caveats to these findings. The attachment of fluorescent proteins may have interfered with the proteins' localization to these ER/PM junction domains either through steric hindrance or by masking domains necessary for this localization. For the case of cytosolic proteins, fluorescence background from the cytosol may have been obscuring signal from proteins truly located to these areas. Some investigators will treat cells with saponin in order to release the cytosolic portion of protein in order to better visualize that fraction of protein that resides within these ER/PM junctions (70, 71). We did not do this here. There is also the possibility that localization of proteins to these domains is regulated, and the correct stimuli was lacking in our experimental procedures. Colocalization in cell types beyond HEK cells and rat hippocampal neurons were not investigated in the current findings.

It was somewhat surprising that mRuby-FFAT localized to junctions rather than break them apart by saturating available VAPs in the ER, leaving them unavailable to bind Kv2.1. This is what occurs when a soluble FFAT motif is expressed in cells (38). Our best hypothesis on why this occurs is that the fluorescent protein attached to the FFAT concensus sequence allows binding of a single mRuby-FFAT protein to a VAP dimer or oligermerized complex. The FFAT motif of Kv2.1, being more disordered, would then be free to bind the other FFAT binding motifs available. It could also be the case that the Kv2.1 FFAT motif out-competes the FFAT motif of OSBP. Analysis of binding affinity was not performed in the current study.

Kv2-VAP junctions acting as a hub for the concentration of additional ER/PM junction residents fits with what the field already knows about these sites. E-Syt1 inhances Nir2 recruitment to ER/PM junctions (92), could the Kv2 channels be acting in a similar manner? The concentration

of lipid transfering proteins to ER/PM junctions formed by a potassium ion channel is particularly interesting, as lipids are known to influence ion channel behavior (213-215) including that of Kv2.1 (216). Could the local lipid environment, particularly the concentration of $PI(4,5)P_2$, of the ER/PM junction created by Nir2 or other lipid transfer proteins be effecting the behavior of Kv2 channels forming this contact zone? Future research is required.

With regards to ER store refilling, the intermediate phenotype observed for the CD4-Kv2.1:445-609 chimera suggests that Kv2.1 is not serving simply as a tether. It suggests that additional domains beyond 445-609 may be contributing to the rate of calcium store refilling. What those domains may be, however, will have to be left for future investigation.

Chapter Four: Domain Architecture and Nanostructure of the Kv2-VAP Endoplasmic Reticulum / Plasma Membrane Junction

Chapter Overview

The endoplasmic reticulum adopts a wide variety of structures and is highly dynamic. These behaviors hold true at sites of ER-membrane contact, such as at sites of ER/PM junctions. This structural rearrangement is predicted to hold functional significance. Using both stochastic optical reconstruction microscopy (STORM) and super-resolution radial fluctuations (SRRF) super-resolution techniques, we image actin and ER dynamics at Kv2-VAP ER/PM junctions. We describe actin filament adjacency and interplay with cortical ER at these sites, and observe ER dynamics within these spaces. ER/PM junctions forming 'donut-like' structures has been reported in the literature. We find this same structure present in our hippocampal neurons and are able to induce this structure in HEK293 cells by activating STIM1.

Introduction

Endoplasmic reticulum / plasma membrane (ER/PM) junctions are sites of dynamic contact between membranes (217). Accumulating evidence suggests ER/PM junctions are not homogeneous, but that within these microdomains there exists nanodomain heterogeneity. For example, different proteins capable of forming ER/PM junctions require different spacing between the PM and ER membrane. This requirement, as has been demonstrated by the Balla group, can cause exclusion of certain proteins from specific contact site regions based on size (117). It is possible that within intact brain tissue a singular ER/PM junction is subdivided into various nanodomains which perform different functions (refer back to Figure 1.4). This may account for

the ‘donut-like’ localization pattern of some ER/PM junction resident proteins; the proteins which require less distance between membranes are forced to the center of the junction and those that require more distance between membranes are forced to the periphery (117). Endogenous Kv2.1 clusters in neurons are sometimes reported to have a ‘donut-like’ pattern with neuregulin-2 and vesicular acetylcholine transporters occupying the center space (218, 219). Both the extended synaptotagmins (136) and STIM1 (137) are known to rearrange the cortical ER at contact sites.

There is also the question of actin surrounding these spaces. Cortical actin is known to contribute to the organization of ER/PM contact sites (220, 221) and these are areas of the cell that are sensitive to actin disruption in HEK cells and cultured hippocampal neurons (35, 173, 222).

With super-resolution techniques now becoming increasingly common to perform (147), investigating the local membranous and cytoskeletal structure at sites of ER/PM contact becomes not only accessible, but given the structure-function relationship being found at these sites (77, 78), these type of investigations become increasingly important. In this Chapter we delve into the nanoarchitecture of ER/PM junctions, using both STORM and SRRF approaches. While this chapter is primarily observational and descriptive, it provides a great deal of insight into the molecular environment of Kv2-VAP junctions.

Materials and Methods

DNA Constructs YFP-STIM1 was a gift from Albert Gonzales. Plasmids encoding fluorescent protein- and biotin acceptor domain- tagged Kv2.1 have been described previously (35, 172, 173). In order to ensure robust biotinylation, this construct was always coexpressed with birA. CD4-Kv2.1:445-609 has been previously described (47). The ER luminal marker, dsredER, has been previously described (47). Syn-AMIGO-GFP was a kind gift from Ashley Leek. In this construct AMIGO-GFP is driven behind the Syn promoter and is thus neuronal specific in expression.

Cell culture, transfection, and surface labeling of proteins Passage 45-48 HEK 293 cells [American Type Culture Collection (ATCC)] were used in these experiments. Cells were cultured in FBS supplemented DMEM media and transfected with noted DNA via electroporation. For Kv2.1BAD transfection, BirA contransfection was performed to ensure robust biotinylation on the biotin acceptor domain. Post transfection cells were plated on 35 mm glass bottom coverslip dishes (Matsunami Glass Corporation) that had been coated in Matrigel. Imaging was performed 24 hours post transfection. To label surface Kv2.1loopBAD and surface CD4-Kv2.1:445-609, cells were incubated with a 1:100 dilution of either CF640-conjugated streptavidin (CF640-SA, Biotium) or 1:1000 dilution CF640-conjugated anti-CD4 antibody for 10 minutes in HEK physiological imaging saline (146 mM NaCl, 4.7 mM KCl, 2.5 mM $CaCl_2$, 0.6 mM $MgSO_4$, 1.6 mM $NaHCO_3$, 0.15 mM NaH_2PO_4, 0.1 mM ascorbic acid, 8 mM glucose, and 20 mM 4-(2-hydroxyethyl)-1-piperazineethanesulfonic acid (HEPES), pH of 7.4). Excess label was washed off.

Hippocampal neurons were taken from embryonic (E18) rats that had been anesthetized with isoflurane in accordance with a protocol approved by the Institutional Animal Care and Use committee of Colorado State University (Protocol ID: 15-6130A). Cultures were a mix of both sexes. Dissociation of neurons was performed as previously described (46, 174, 175). Post dissociation cells were plated onto glass bottom coverslip dishes that had been coated for 1 hr with poly-L-Lysine (P4707) diluted 1:2 in 0.15 M borate buffer, pH 8.4 and washed with water. Cells were seeded at a density of $5x10^5$ per dish and fed with Neurobasal media (Gibco by Life Technologies, REF# 21163-049) supplemented with 1:100 GlutaMAX(100X) (Gibco by Life Technologies, REF# 35050-061), Pen-Strep (HyClone CAT# SV30010, 100 units/ml, 100 µg/ml respectively) and 1:500 NeuronCult SM1 (Stem Cell Technologies, CAT# 05711). rHN cultures were transfected on DIV5 using 2 µl Lipofectamine 2000 and the appropropriate amounts of DNA.

On DIV14 dishes were washed with neuronal imaging saline (126 mM NaCl, 4.7 mM KCl, 2.5 $CaCl_2$, 0.6 mM $MgSO_4$, 0.15 mM NaH_2PO_4, 0.1 mM ascorbic acid, 8 mM glucose, and 20 mM HEPES, pH 7.4) and imaged.

Microscopy A Yokogawa-based CSUX1 system built around an Olympus IX83 inverted stand with an Andor laser launch was used for spinning disk confocal microscopy. The laser launch on this system contains 100-150 mW 405, 488, 561, and 637 nm diode lasers. An Anodor iXon EMCCD camera (DU-897) was used to collect images through a 100X Plan Apo, 1.4 NA objective. Stage and objective were maintained at 37°C using an objective heater and a Tokai Hit chamber. Focus was maintained using the ZDC constant focus system. This system is controlled by Metamorph imaging software. For TIRF microscopy, a Nikon Eclipse Ti fluorescence miscrope was used equipped with 100 mW 405, 488, 561, and 633 nm diode lasers split evenly between TIRF and photoactivation pathways. Images were collected on an Andor iXon EMCCD camera (DU-897) through a Plan Apo 100x, NA 1.49 TIRF objective. Nikon Perfect-Focus was used to maintain focus. Objective and stage were temperature controlled and held at 37°C. This system runs on NIS AR software.

The appropriate spectral detectors, sequential excitation, dichoroics, and bandpass filters were used to separate fluorophores. For more information on our microscopes, see (46, 175).

Image processing and analysis ImageJ was used for both image analysis and processing. Images were cropped, adjusted for contrast, and pseudo-colored. Details specific to each experiment are presented in the Results section or individual Figure legends.

STORM and SRRF processing Cells transfected with paGFP-actin and fluorophores converted from a nonfluorescent state to a fluorescent state using 405 nm laser. Exposure to low levels of 405 nm laser photoconverted a small subpopulation of the actin molecules before photobleaching

with 488 laser. Super-resolution images were reconstructed using the ImageJ ThunderSTORM plugin Ovesný et al., 2014 (223). TetraSpeck beads were used to correct for drift. SRRF processing was performed in ImageJ via the SRRF plugin generously published by the Henriques lab (147). Prior to SRRF processing, images acquired during TIRF or spinning disk microscopy were subjected to background subtraction and weak Gaussian blur filtering (0.65 sigma). SRRF was performed using temporal radiality pairwise product mean with a ring radius of 0.45, radiality magnification of 8, 8 axes per ring and 10 frames per time point. Positivity constraint was removed, images were renormalized, intensity weighting was performed, and SRRF patterning was minimized.

Results

Actin filaments border Kv2.1 junctions as observed in STORM imaging

It has already been reported that actin surrounds Kv2-VAP ER/PM junctions (35, 173, 224). In Figure 4.1, to better observe this relationship we used STORM imaging of actin filaments

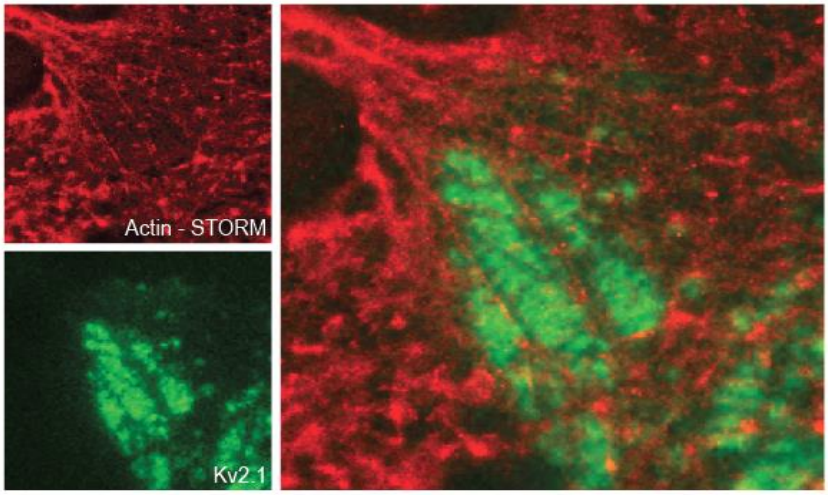

Figure 4.1. STORM imaging of actin adjacent to Kv2.1 ER/PM junctions. STORM reconstruction of photoactivatable-actin in the top left panel. Normal fluorescence image of GFP-Kv2.1 in bottom left. Merge on left.

in HEK cells expressing Kv2.1. This junction-actin relationship is readily apparent. From the normal fluorescence GFP-Kv2.1 image, these ER/PM junctions have clearly defined borders. These borders are occupied by filamentous actin, as imaged by STORM reconstruction.

SRRF reconstruction demonstrates ER-actin dynamics

We next turned to SRRF super-resolution approaches in order to better study the junction-actin dynamics in live cells. We created ER/PM junctions in HEK cells using our CD4-Kv2.1:445-609 construct and imaged a GFP-actin construct when coexpressed (see Figure 4.2).

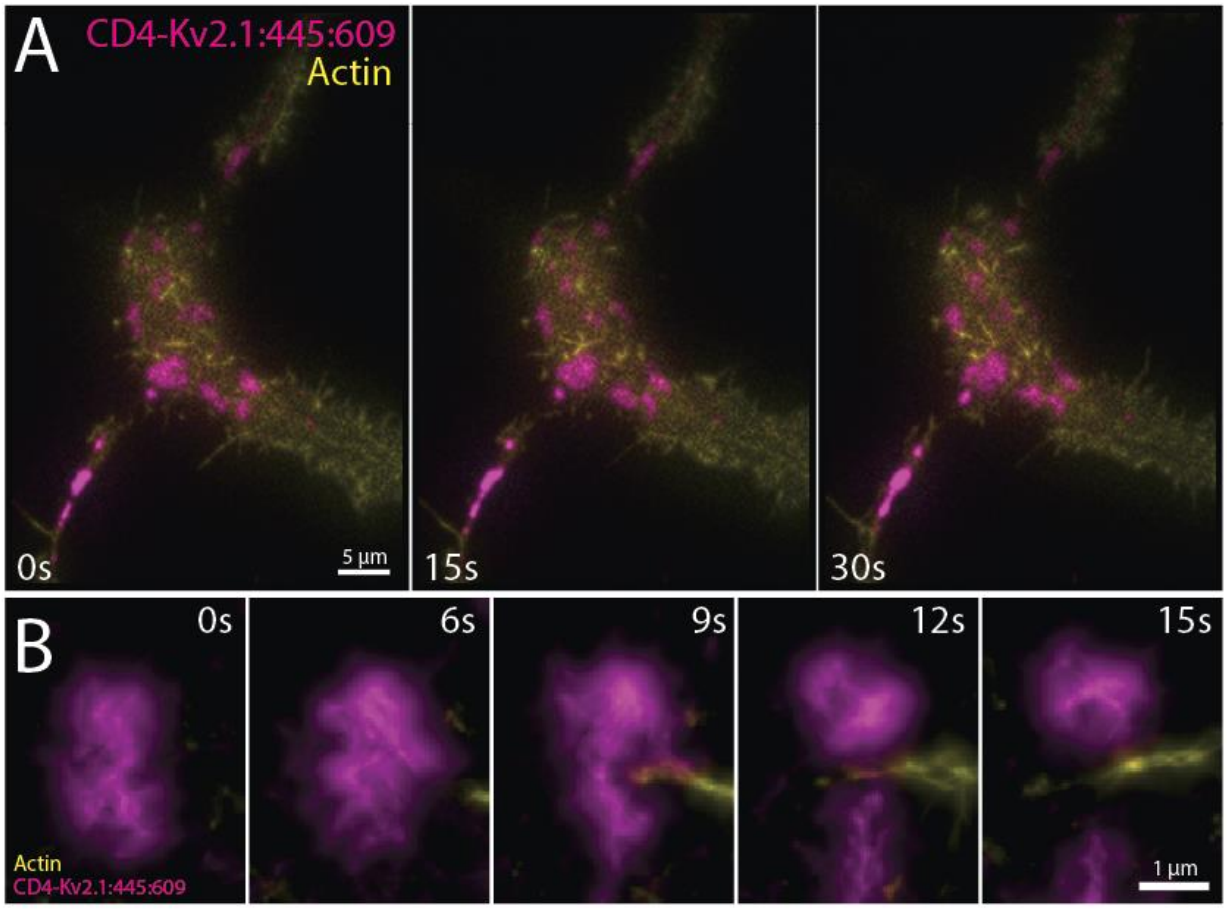

Figure 4.2. SRRF reconstruction of actin dynamics adjacent to ER/PM junctions in HEK293 cells. (A) GFP-actin was imaged adjacent to ER/PM junctions formed by CD4-Kv2.1:445:609. Filament growth can be seen over the 30s timecourse. (B) Time course close-up of an ER/PM junction splitting into two domains as an actin filament grows between. Images taken using TIRF microscopy.

We observed actin filament growth adjacent to the PM throughout the cell during the 30s time course (Figure 4.2A). Often this growth stemmed from common points of nucleation. We also observed junctions splitting into two separate domains as actin grew between these two newly defined areas. We cannot state if actin growth was the driving force behind junction fragmentation, or if actin was simply growing into this newly created space.

SRRF reconstruction reveals dynamic ER structural rearrangement within the ER/PM microdomain

We next turned to SRRF reconstruction to examine the dynamics of the ER at the sites of junctions. This reconstruction allows us to gain resolutions of between 100-150 nm, not amazing but certainly helpful. We expressed CD4-Kv2.1:445-609 to create ER/PM contact sites in HEK cells (see Figure 4.3A). Using the ER volume marker, dsredER, allowed us to visualize the ER at these sites. We then processed these movies using SRRF reconstruction analysis to generate super-resolution images of the ER. We found increased dsredER signal, and therefore more voluminous ER, at the junction border (Figure 4.3B). This is consistent with EM analysis of Kv2.1 contact sites performed by other investigators (8). We also found a great deal of internal structural rearrangement within the junction itself, observing punctate spots of greater ER volume form and move throughout the junction perimeter (Figure 4.3B, green arrowheads). In addition to these puncta were larger areas of more volumous ER that formed within the junction before dispersing (Figure 4.3B, cyan arrows). All this occurred over a period of ~100s, suggesting that even though Kv2.1-induced ER/PM junctions are fairly stable structures overall, there is a great deal of internal ER rearrangement.

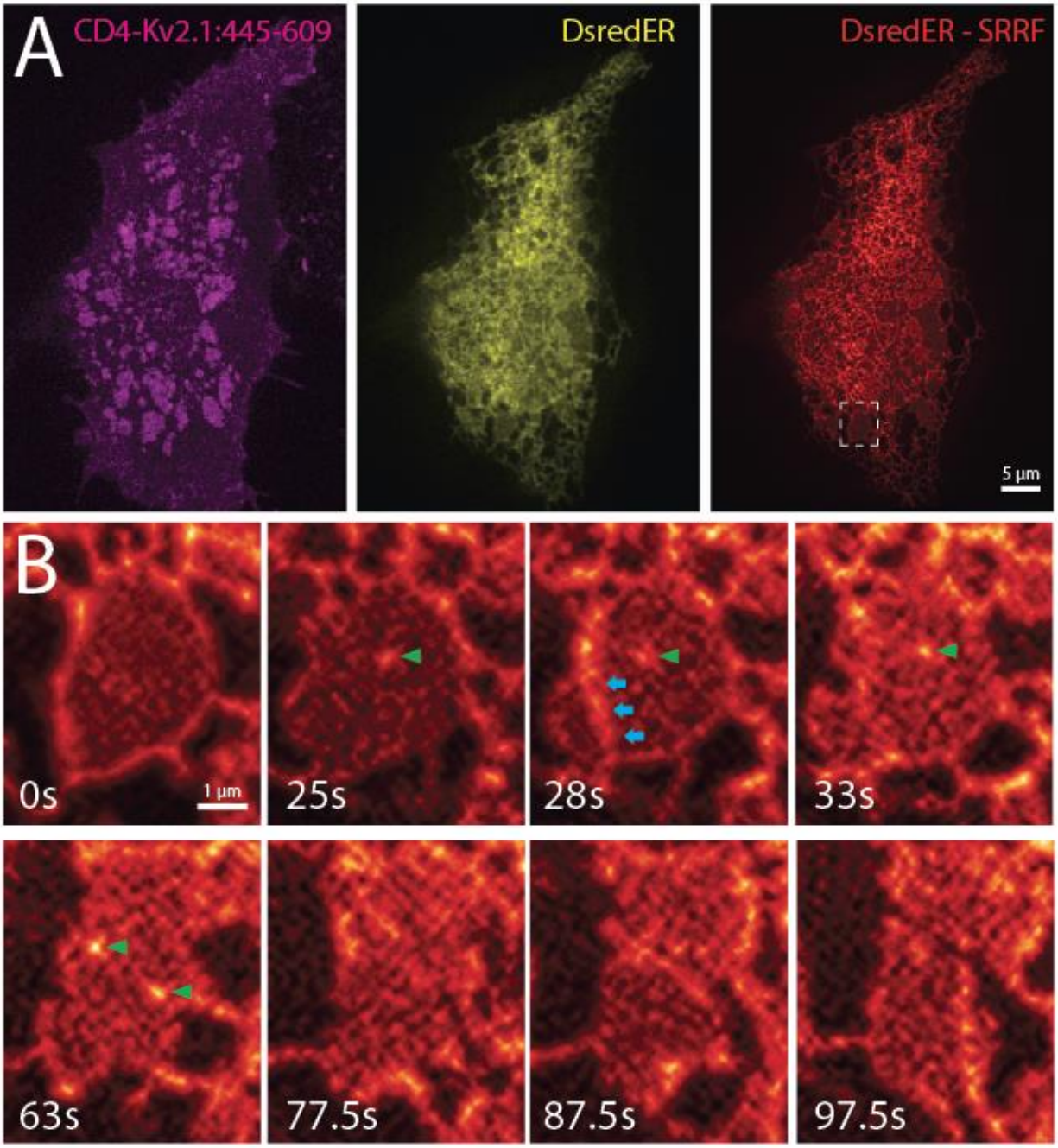

Figure 4.3. SRRF image of ER/PM junctions in HEK cell (A) CD4-Kv2.1:445-609 inducing ER/PM junctions in HEK cells. Normal fluorescence spinning disk images of CD4-Kv2.1:445-609 and dsredER are shown next to SRRF reconstruction of the dsreER. (B) Enlarged time course of the box pictured in (A). Note the increased volume (dsredER signal) at the junction border. Green arrowheads indicate punctate areas of increased dsredER fluorescence within the junctions. Blue arrows point towards a filamentous area of increased volume that grew across the face of the junction before dispersing. Beginning at second 87.5, the junction separates, possibly due to actin filament growth, and by second 97.5 two distinct junctions are present.

While the distribution of fluorescence within the contact site would seem to suggest that the entire domain is composed of small dynamic tubules, as has been reported with other sheet-like ER structures (53), we are unwilling to confirm or refute this with our data. SRRF reconstruction can artificially induce such patterning and though our protocols have been optimized to eliminate such patterning, at that minute a resolution we are still unwilling to state anything with confidence. The matter of these junctions being sheets or an assembly of small dynamic tubules requires further investigation.

Endogenous Kv2 junctions are 'donut-shaped' in hippocampal neurons

There are reports in the literature that Kv2.1-induced ER/PM junctions can adopt 'donut-like' structures on the surface of some cell types and that neuregulin2 receptors and vesicular acetylcholine transporters reside within the center of this domain (218, 219). Using SRRF reconstruction we are able to confirm that these types of structures exist in our DIV14 rat hippocampal neurons (see Figure 4.4). Here we used AMIGO-GFP behind a syn promotor to drive expression of the Kv2.1 beta-subunit in hippocampal cells. As AMIGO is normally freely diffuse but localizes to ER/PM junctions when Kv2.1 is present (184), it acts as a marker for the endogenous channel. In Figure 4.4A donut-like structures are observable after SRRF reconstruction. These structures are noticeable in normal fluorescence images, but to a lesser degree. Figure 4.4B shows an enlarged image of these sites.

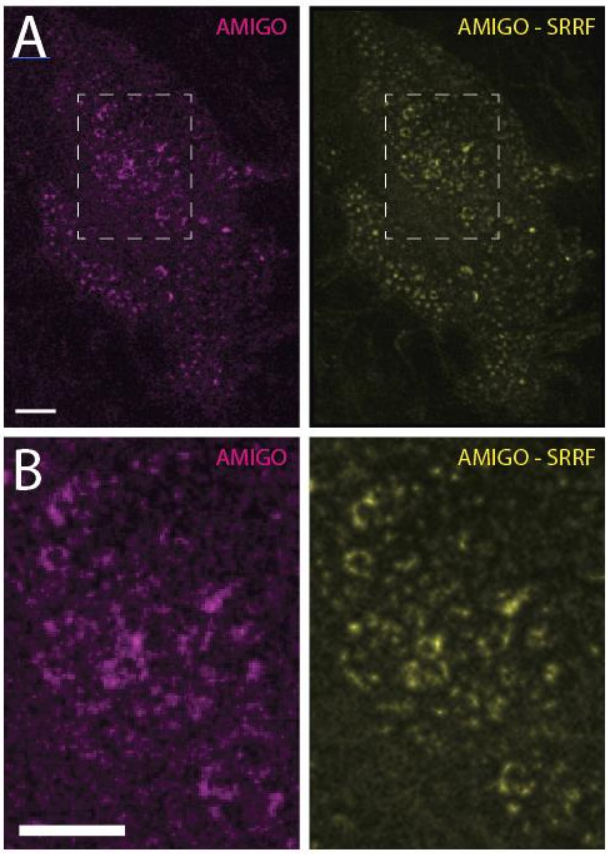

Figure 4.4. SRRF reconstruction of Kv2-induced ER/PM junctions in DIV14 rHNs reveals presence of 'donut' shapes. (A) Using AMIGO-YFP to mark endogenous Kv2-induced ER/PM junctions, SRRF reconstruction reveals a 'donut-like' structure. (B) Enlarged image of boxed region in A. Scale bars represent 5 µm.

Kv2 ER/PM junctions structurally rearrange during STIM activation

During STIM recruitment to ER/PM junctions, this protein will concentrate at Kv2.1-induced ER/PM junctions (46). Wanting to investigate the structural rearrangements that occur during a concentration of an additional protein to these sites, we coexpressed Kv2.1 in HEK cells alongside STIM1 and depleted ER stores using thapsigargin treatment to cause STIM1 to relocalize to ER/PM junctions then used SRRF analysis (see Figure 4.5).

We observed a drastic alteration in domain structure coincident with STIM1 concentration (Figure 4.5A). Kv2.1 repositioned itself from being located throughout the ER/PM junction to

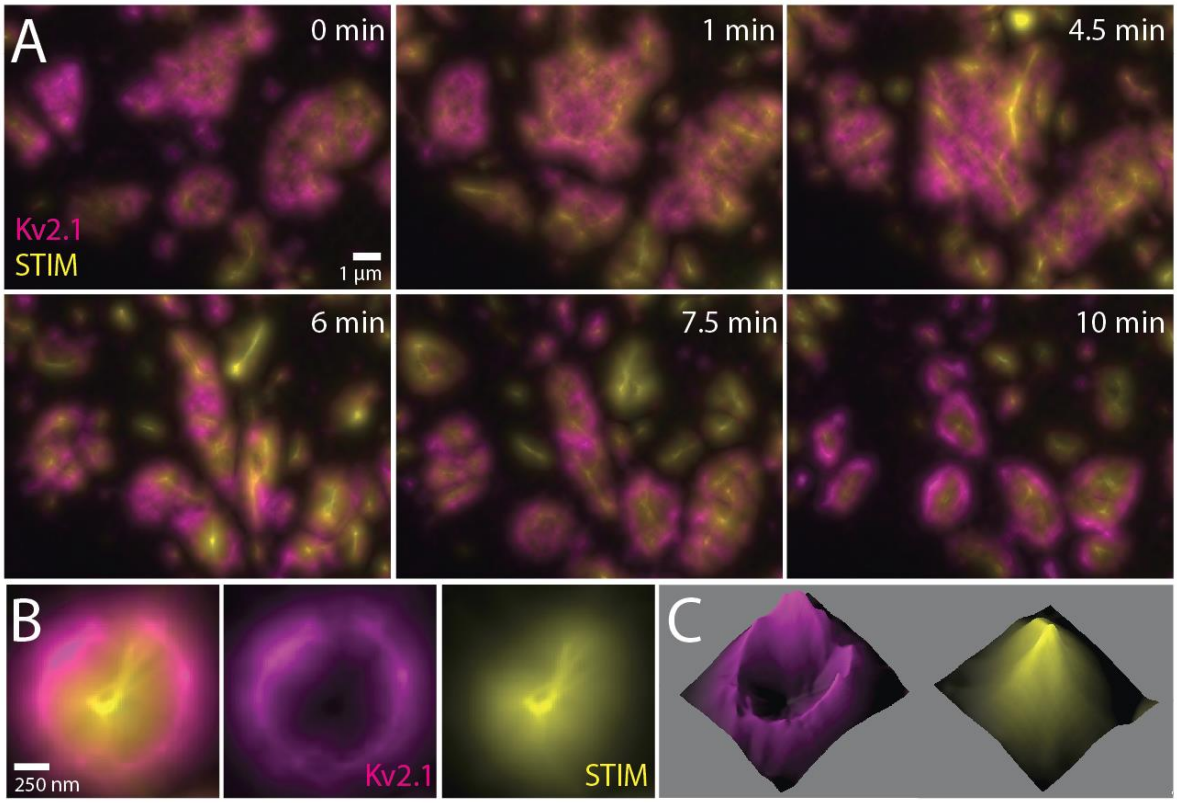

Figure 4.5. STIM activation causes structural rearrangement of the Kv2 ER/PM junction. (A) Time course of thapsigargin treatment. YFP-STIM1 goes from being distributed throughout the Kv2.1loopBAD-induced ER/PM junction to being concentrated at the center of the contact site, with Kv2.1loopBAD relocalizing to the periphery. (B) Close-up of a Kv2.1-STIM 'donut'. (C) Fluorescence intensity 3D map of the image in B. SRRF reconstruction and 3D fluorescence plotting were performed in ImageJ.

being located on the periphery. STIM1 concentrated within this center space (Figure 4.5B&C). This is the first time such a Kv2.1-created ER/PM junction structure has been induced.

Discussion

Super-resolution imaging of actin-ER/PM dynamics offers clear benefits for understanding this relationship. The work above represents a small first step towards this end, but clearly more work needs to be accomplished and pressing questions remain unanswered. Depolymerizing actin has a clear effect on junctions (35, 173), but does actin filament growth push aside ER, carving a

path through the junction? Or does actin merely fill the empty space created as the ER rearranges itself? Does cortical ER actively 'burn' a whole through the actin meshwork to reach the PM or is actin rearrangement allowing for these spaces to occur?

There are a number of proteins that can alter ER morphology (62, 225, 226) and STIM1 is known to alter ER/PM structure during activation (137). It's association with end-binding protein 1 (EB1) may be involved in this structural rearrangement (137, 227). The purpose of such a redistribution is still open to conjecture, but it is easy to imagine how such architecture could aid cells in the establishment of signaling microdomains, especially those concerning calcium. As discussed in the previous chapter, Kv2.1 enhances ER calcium store recovery, perhaps this nanostructure is in some way involved in that process.

Future studies will need to begin to quantify the structures and events laid out in this chapter. While the observations within this chapter are certainly of note, and certainly provide insight into a novel nanodomain, a better appreciation of these phenomenon will come from enumerating their existence and behavior.

Chapter Five: Regulation of Endoplasmic Reticulum / Plasma Membrane Junctions in Hippocampal Neurons

Chapter Overview

Endoplasmic reticulum / plasma membrane (ER/PM) junctions are highly regulated microdomains, with a variety of conditions and stimuli that influence not only their composition but also their very presence or absence within cells. Recently, ER/PM junctions in rat hippocampal cultures and brain slices were shown to be regulated by activity as assessed using electron microscoopy. Here we examine the mechanisms regulating two ER/PM junction forming proteins widely expressed in excitable cells: Kv2 potassium ion channels and the junctophilins (JPHs). The Kv2 channels form ER/PM junctions by interacting with ER resident VAP proteins mediated by an unconventional FFAT motif on the channel C-terminus as discussed in Chapter 2. This interaction is sensitive to glutamate, with the Kv2-VAP interaction being disrupted during glutamate application in a calcineurin-mediated manner leading to junction dispersal. Using a series of CD4-Kv2.1 chimeric proteins, we identified two serine residues outside of the C-terminal FFAT motif which regulate Kv2-VAP disassociation during glutamate treatment. Mutation of these residues to aspartic acid, mimicking phosphorylation, results in a construct that forms glutamate-resistant ER/PM junctions. The JPHs create junction microdomains by binding to phospholipids in the PM. Here we find that glutamate treatment will also result in junctophilin junction disassembly in hippocampal neurons. This disruption is calcium-dependent and occurs at a faster rate than Kv2-VAP junction loss. ER/PM junctions are known to play roles in trafficking, calcium homeostasis, and lipid homeostasis. In excitable cells they have been found to localize L-type calcium channels and ryanodine receptors. Knock-out of the JPHs leads to deficits in memory.

Knock-out of Kv2.1 also results in learning impairment in mice. In addition, in humans point mutations in Kv2.1 which are predicted to effect junction forming ability but not channel electrical properties are associated with developmental delay. Uncovering the mechanisms underlying ER/PM microdomain assembly and disassembly represents a large step towards understanding the regulation of these contact sites.

Introduction

Stimulus-induced recruitment and/or expulsion of protein residents from ER/PM junctional microdomains is a common occurrence at these sites. In Chapter Three of this dissertation we explored Nir2 recruitment to Kv2.1 junctions during angiotensin activation, as well as STIM/Orai assembly at these locations during calcium store recovery. ER/PM junction concentration of oxysterol-binding protein (OSBP)-related proteins (ORP) 5 and 8 depends on PM PI4P levels (228) and extended synaptotagmin 1 localization is dependent on Ca^{2+} influx into the cytosol (91). In addition to regulation of protein localization within these microdomains, ER/PM junctions are themselves regulated, with stimuli leading to either their enlargement, or their total dissolution.

Individual Kv2.1 channels are capable of switching between being freely diffusive or clustered under homeostatic conditions (173), suggesting constant dynamic control over the very presence of these ER/PM microdomains. In COS-1 cells, Kv2.1 junctions ebb and flow depending on cell cycle (40). In rat α-motoneurons, peripheral nerve injury results in Kv2.1 clustering disruption in both ipsilateral and contralateral limbs (9, 166, 229, 230). Cellular insult and disease also influence Kv2/VAP junctions, as Kv2-induced ER/PM junctions are dispersed in response to hypoxic or ischemic conditions (32, 33). Kv2.2 appears to be less sensitive to this insult-induced declustering (7) and this sensitivity or resistance to ER/PM junction rearrangement may be one

reason cells have opted to use one channel over the other. Kv2.1 clusters are enlarged in some rat models of Alzheimer's disease with a coupled decrease in K^+ current density that may be due to increased oxidative stress during development (231). Human mutations predicted to disrupt Kv2.1-VAP interaction without impacting channel electrical activity are associated with developmental delay (197). ER/PM junctions within different compartments of a single cell may display different properties. For example Kv2.1-induced junctions on the AIS are more resistant to CO_2- and kainate-induced declustering than junctions on the soma (196).

Recently, endogenous ER/PM junctions in both rat hippocampal culture and in brain slices were found to be regulated by activity, with a significant decrease in both size and number of junctions as activity increases (93, 94). This suggests a common mechanism that impacts all tethering proteins in hippocampal neurons, uniting them in a singular response to activity or injury. Here, we examine the regulation of two widely expressed ER/PM tethers in excitable cells, the Kv2 channels and the junctophilins (JPHs) and their response to neuronal activity. It is already established that Kv2.1-induced junctions are regulated by activity due to calcineurin-mediated dephosphorylation (40, 46, 47, 127-129, 232), although the exact molecular mechanisms have yet to be fully established, especially considering the newly uncovered Kv2-VAP interaction which serves to tether the PM and ER membranes together. Regulation of the junctophilins by activity has never before been shown, but such a mechanism could have profound repercussions concerning the location of L-type calcium channels and ryanodine receptors, which the JPHs serve to stabilize (118-121).

Materials and Methods

DNA Constructs The luminal ER marker dsRedER has been previously described (44, 46). mCherry-JPH4 was provided by Yousang Gwack (Addgene 79599). mCherry-JPH3 was a kind gift provided by Kurt Beam. Kv2.1loopBAD has been previously described (46) and when expressed, was always cotransfected with BirA to ensure robust biotinylation of the BAD domain prior to extracellular labeling. VAPB-mRuby2 was created using standard techniques from a construct provided by Axel Brunger (Addgene plasmid 18874). CD4-Kv2.1:445-609, CD4-Kv2.1:573-609, and CD4-Kv2.1:573-598 have been previously described (Johnson et al. 2018). Briefly, the single pass transmembrane CD4 has β2-microglobulin sequence appended to it to create a rigid structure of the correct length to span the intramembrane distance. To the end of this, a flexible $(Gly_4Ser)_n$ linker is attached that leads into the Kv2.1 amino acids of interest. This combination of β2-microglobulin and flexible linker is based on work done by the Bjorkman laboratory(178). The CD4-Kv2.1:445-609SallD was designed using our previously synthesized CD4-Kv2.1:445-609 construct as a template. An aspartic acid residue was substituted for each serine within the Kv2.1 sequence and the DNA was created by Genewiz. For the CD4-Kv2.1:S601D, CD4-Kv2.1:S603D, CD4-Kv2.1:S607D, CD4-Kv2.1:S609D, and CD4-Kv2.1:S601,603,607,609D constructs, our previously described CD4-Kv2.1:573-609 construct was used as a template. That construct was chosen as a backbone to these phosphomimic substitutions as it contained the fewest amino acids necessary that we had yet found that still resulted in a glutamate-sensitive response. For the sake of consistency, we have opted to retain the amino acid numbering used primarily throughout the Kv2.1 literature, although an additional methionine five residues upstream has also been deemed amino acid 1 in other publications and may be the true start codon.

Cell culture, transfection, and labeling of surface constructs Culturing of HEK 293 cells [passage 42-50, American Type Culture Collection (ATCC)] was performed in Dulbecco's Modified Eagle's Medium supplemented with 10% FBS (Atlanta Biologicals). Cells were transfected via electroporation and plated on 35 mm glass bottom dishes (Matsunami Glass Corporation) coated with Matrigel. Transfection of HEK cells occurs 24 hrs prior to imaging. For experiments using a Kv2.1loopBAD construct for extracellular labeling, BirA was cotranfected to insure robust biotinylation of the BAD motif. Labeling of channels was done using a 1:1000 dilution of CF640-conjugated streptavidin (CF640-SA; Biotium) for 10 minutes in HEK physiological imaging saline (NIS; 146 mM NaCl, 4.7 mM KCl, 2.5 mM $CaCl_2$, 0.6 mM $MgSO_4$, 1.6 mM $NaHCO_3$, 0.15 mM NaH_2PO_4, 0.1 mM ascorbic acid, 8 mM glucose, and 20 mM 4-(2-hydroxyethyl)-1-piperazineethanesulfonic acid (HEPES), pH of 7.4). Washes were performed after labeling to remove excess label. For CD4 chimera labeling, a 10 minute incubation in 1:1000 dilution of CF640-conjugated, extracellular epitope targeted, anti-CD4 antibody in HIS was used.

Hippocampal neurons were isolated from embryonic (E18) rats anesthetized using isoflurane and sacrificed in accordance with a protocol approved by the Institutional Animal Care and Use Committee of Colorado State University (Protocol ID: 15-6130A). Embryos were collected from both sexes and therefore the neuronal cultures used are of a mixed population of male and female cells. Dissociation of neurons was performed as previously described (46, 174, 175). Cells were plated at a density $5x10^5$ of onto glass bottom coverslips coated for 1 hr with poly-L-Lysine (P4707, Sigma) that had been diluted 1:2 in 0.15 M pH 8.4 borate butter. Neurons were fed with Neurobasal media (Gibco by Life Technologies, REF# 21163-049) that had been supplemented with 1:100 GlutaMAX (100x) (Gibco by Life Technologies, REF# 35050-061),

1:100 Pen-Strep (HyClone, CAT# SV30010, 100 units/mL, 100 µg/ml respectively) and 1:500 NeuroCult SM1 (Stem Cell Technologies, CAT# 05711).

Neuronal cultures were transfected on DIV5 using 2 µl of Lipofectamine 2000. On DIV7 dishes were washed in neuronal imaging saline (NIS; 126 mM NaCl, 4.7 mM KCl, 2.5 $CaCl_2$, 0.6 mM $MgSO_4$, 0.15 mM NaH_2PO_4, 0.1 mM ascorbic acid, 8 mM glucose, and 20 mM HEPES, pH 7.4). Labeling was performed using a 10 minute incubation with either CF640-conjugated streptavidin or anti-CD4 antibody as described above. Anti-neurofascin monoclonal antibodies were used to identify the axon initial segment when required. Anti-NF186 antibody (Neuromab) was used at a 1/1000 dilution for 10 min, followed by NIS wash and a 10 min incubation with fluorescent (Alexa 594 or 647) goat anti-mouse secondary antibody diluted 1/1000. Dishes were washed in NIS to remove excess label and imaged immediately. For calcium imaging, cells were incubated in 1:100 Fluo4-AM (Life Technologies, REF# F14201) for ten minutes before washing and imaging.

Microscopy TIRF microscopy was performed on a Nikon Eclipse Ti fluorescence microscope equipped with 100 mW 405, 488, 561, and 633 nm diode laser split evenly between TIRF and photoactivation pathways. Images were collected through a Plan Apo 100x, NA 1.49 TIRF objective on an Andor iXon EMCCD DU-897 camera. Stage and objective were both temperature controlled. Focus was kept constant using the Nikon Perfect-Focus system. This system runs using NIS AR software. Where noted, spinning disk confocal microscopy was performed using a Yokogawa-based CSUX1 system built around an Olympus IX83 inverted stand and a laser launch by Andor with 100-150 mW 405, 488, 561, and 637 nm lasers. Images were collected through a 100X Plan Apo, 1.4 NA objective on an Andor iXon EMCCD camera (DU-897). ZDC constant focus was used to maintain focus and temperature was controlled via a Tokai Hit chamber and

objective heater. This system runs using Metamorph imaging software. With both systems spectral detectors, sequential exicitation, dichroics, and bandpass filters were used to separate flourophores. Additional details have been described previously (46, 174, 175).

Image processing and analysis ImageJ was used for both image processing and analysis. Images were pseudo-colored, cropped, and adjusted for contrast and brightness. Details specific to each experiment are presented in the Results section or Figure legends.

Glutamate Treatment of Hippocampal Neurons DIV7-8 rat hippocampal neurons were treated with 20 µM glutamate (Sigma, REF: G1251) made up in NIS as performed in previous publications (46). There are reports that NMDA receptor activation can cause fission of the ER (233), but we did not observe this occurring in our cells during glutamate application.

Results

VAP Expression Levels Do Not Impact Kv2.1/VAP Junction Disassembly Dynamics

We have previously established that 20 µM glutamate treatment results in Kv2.1 junction disassembly ((46); see Fig. 5.1A & B). To examine if intracellular VAP levels effect this dispersal, we expressed VAPB at increasing concentrations and again treated with glutamate. As shown in Fig. 5.1C & D, overexpression of VAP by transfecting either 1 or 3 µg exogenous VAP DNA had no effect on the rate of junction loss nor the level of final junction disassembly. As concentration of DNA used for transfection is not a reliable measure of VAP concentration within the individual cells imaged however, we next plotted VAP fluorescence at junctions before glutamate against that individual junction's level of dispersal (Fig. 5.1E). We found no correlation between these measures with an R^2 value of 0.055, indicating no relationship between the concentration of VAP within a junction and its sensitivity to glutamate.

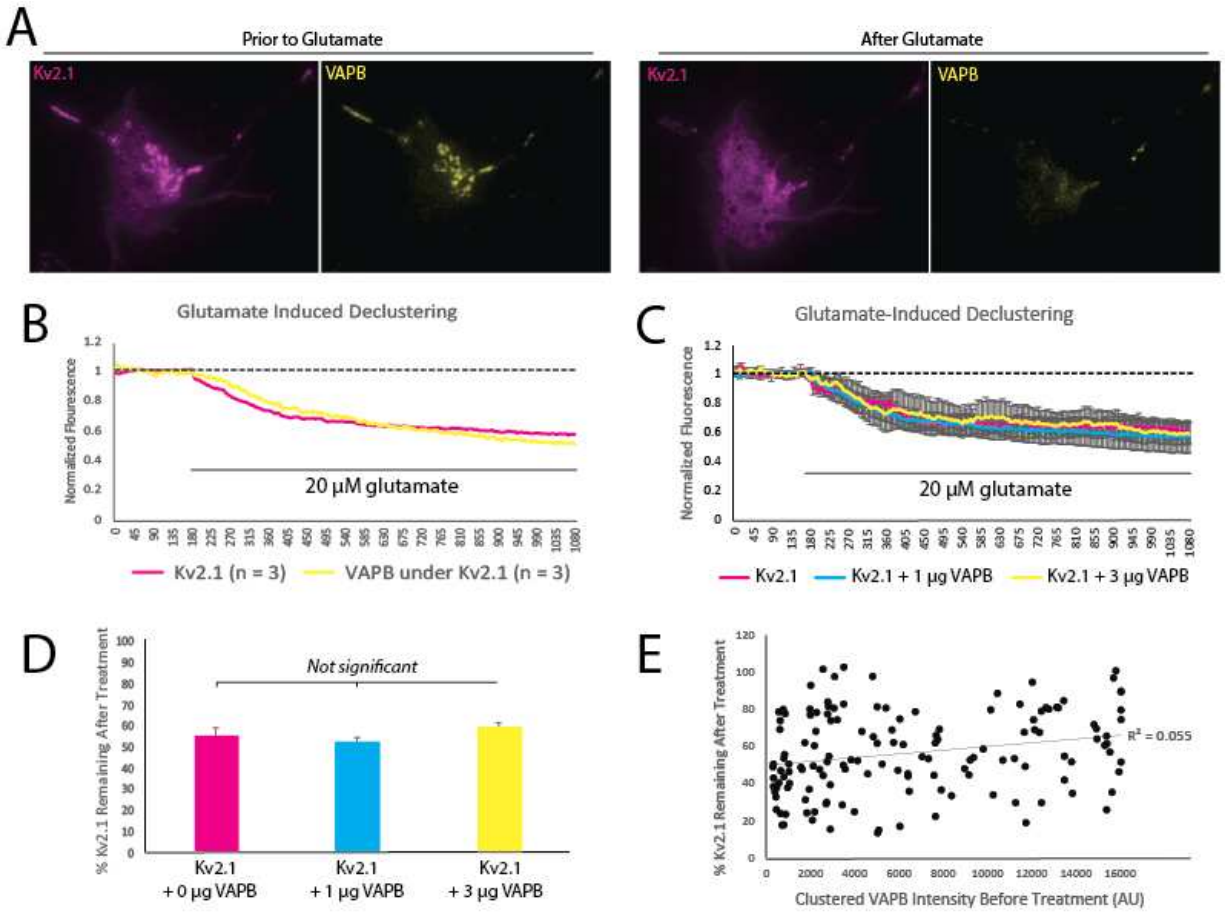

Figure 5.1 VAP concentration has no effect on glutamate-induced Kv2.1/VAP junction disassembly in cultured rat hippocampal neurons. (A) Representative TIRF images of GFP-Kv2.1 and VAPB-mRuby2 before and after 20 µM glutamate treatment. (B) Time course of GFP-Kv2.1 and VAPB-mRuby2 fluorescence loss during glutamate treatment. (C) Time course of GFP-Kv2.1 fluorescence loss from junctions when coexpressed with 0, 1, or 3 µg of exogenous VAPB-mRuby2 DNA. (D) Post glutamate treatment fluorescence measurements of Kv2.1 in the presence of 0, 1, or 3 µg of exogenous VAPB-mRuby2 DNA. (E) No correlation was found between VAP fluorescence intensity at junctions and the level of Kv2.1 dispersal with an R^2 value of 0.055. Error bars indicate SEM.

Kv2.1/VAP Junctions within the Axon Initial Segment are Not More Stable Due to a Secondary Clustering Motif

Kv2.1 displays differences in sensitivity to glutamate between subcellular compartments with junctions in the AIS being more resilient to disassembly than junctions on the soma (196). It

has been recently published that Kv2.1 contains a secondary amino acid domain downstream from its FFAT motif and together these motifs are responsible for the clustering behavior within the AIS compartment (190). While this secondary motif (amino acids 720-745) has been reported as sufficient to generate clusters, both it and the FFAT motif must be eliminated in order to fully disrupt AIS clustering and clusters within the AIS generate ER/PM junctions through interaction with the VAP proteins just as those on the soma (47). To test if this secondary motif is responsible for the enhanced resistance to glutamate-induced declustering seen in the AIS, we expressed a CD4-Kv2.1 chimera that contains the FFAT motif but lacks this downstream AIS motif in rat hippocampal neurons. This was a construct that we have previously used (47) and combines the single transmembrane spanning CD4 with a portion of Kv2.1 C-terminus containing the Kv2.1 FFAT motif, in this case amino acids 573-609. The AIS was identified by neurofascin labeling (see Figure 5.2A).

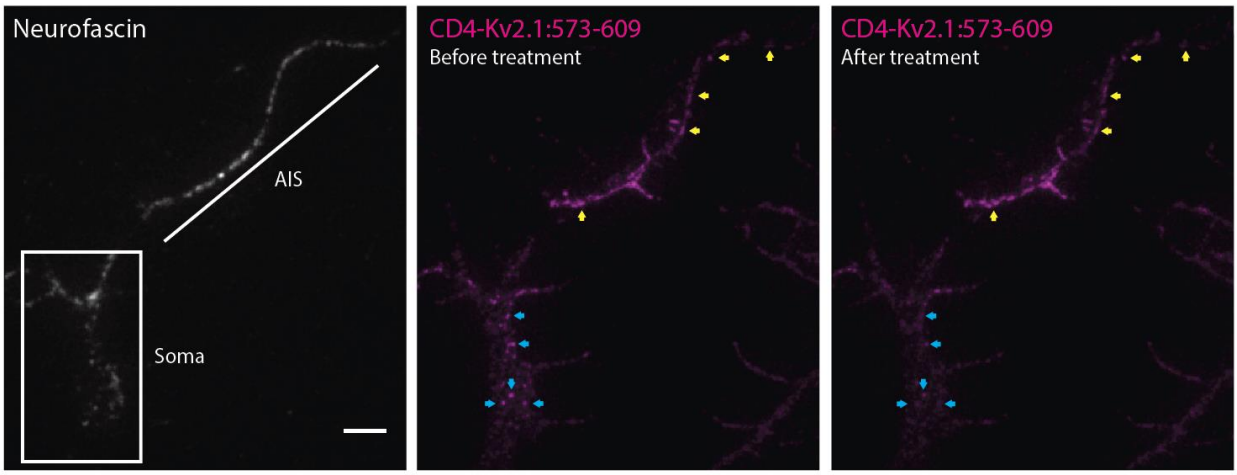

Figure 5.2. CD4-Kv2.1:573-609 junctions on the soma disperse during glutamate treatment while those on the AIS remain intact. (Left panel) The AIS is marked in a DIV7 rHN through neurofascin labeling. (Middle panel) Prior to 20 µM glutamate treatment, CD4-Kv2.1:573-609 forms ER/PM junctions in both the soma (blue arrows) and AIS (yellow arrows) compartments. (Right panel) After treatment, junctions on the soma have dispersed while those in the AIS remain. Scale bar represents 5 µm.

As depicted in Figure 5.2, the CD4-Kv2.1:573-609 construct forms clusters on both the soma and the AIS. After treatment with 20 μM glutamate, clusters on the soma (blue arrows) fully disperse while junctions on the AIS (yellow arrows) remain fully intact. This finding that AIS clusters retain their resistance to glutamate application while soma clusters disassemble suggests two things: 1, sensitivity to disassembly is due to a mechanism contained within the CD4-Kv2.1:573-609 chimera, and 2, resistance to disassembly within the AIS compartment is not conferred to the channel by the downstream AIS motif.

Regulation of Kv2.1/VAP Junction Sensitivity to Glutamate Occurs Outside of the FFAT Motif

As VAP concentration had no effect on cluster dispersal, and the AIS motif was not necessary to confer differences in sensitivity across subcellular compartments, we next further examined Kv2.1 sequence itself as a possible regulatory mechanism. Returning to the knowledge that dephosphorylation is a precursor to junction disassembly, and using our CD4-Kv2.1:445-609 construct as a template, we mutated every serine within the Kv2.1 sequence to aspartic acid to mimic phosphorylation. This new construct, CD4-Kv2.1:445-609SallD was also capable of forming ER/PM junctions on the surface of cells through VAP interaction (see Fig. 5.3), indicating that these serine to aspartic acid substitutions had no effect on VAP interaction.

Comparing the CD4-Kv2.1:445-609SallD construct to other chimeras we had previously created, we found that while CD4-Kv2.1:445-609 was sensitive to glutamate in a manner not significantly different than the full length channel, CD4-Kv2.1:445-609SallD was resistant to declustering in rat hippocampal neurons (see Fig. 5.4A & B), once again illustrating the importance of dephosphorylation in breaking the Kv2-VAP interaction. Based on these findings, it became

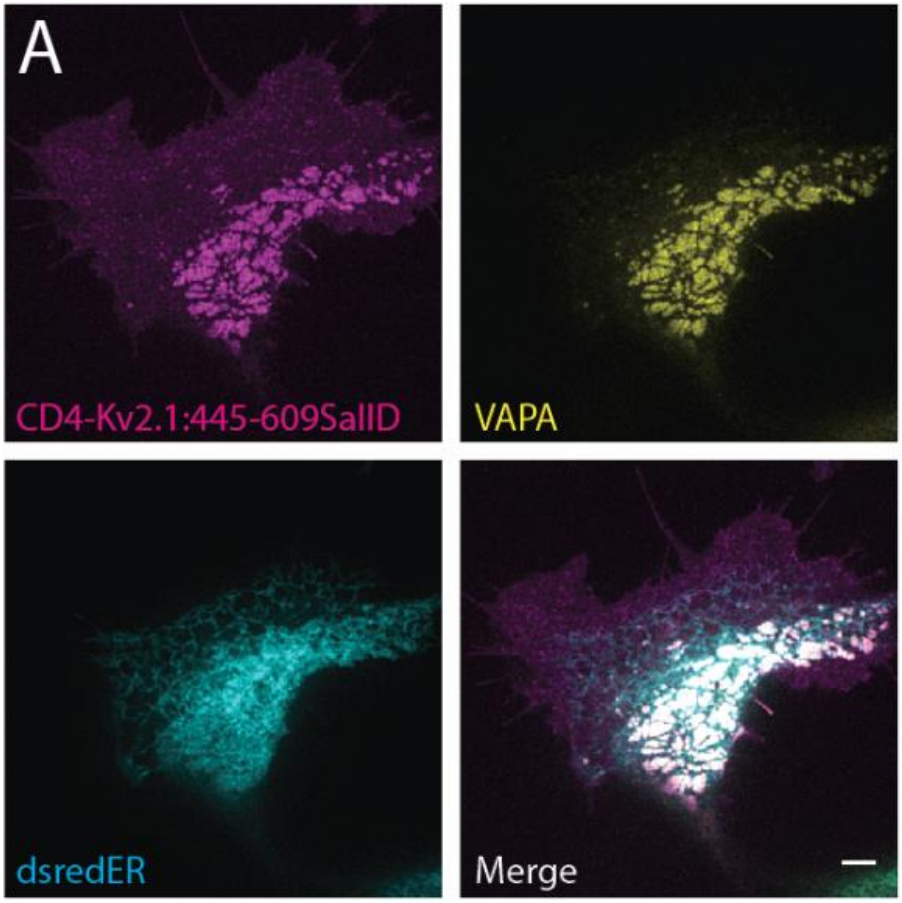

Figure 5.3 CD4-Kv2.1:445-609SallD interacts with VAPs to form ER/PM junctions. (A) Expression of CD4-Kv2.1:445-609SallD led to the formation of clusters and recruitment of mRuby-VAPA to form ER/PM junctions. Representative spinning disk microscopy images of the basal surface. Scale bars represent 5 µm.

apparent that serine dephosphorylation of serine residues within the 445-609 sequence was regulating this dispersal. Narrowing down the sequence regulating sensitivity to glutamate, we also tested the response of constructs with fewer Kv2.1 amino acids. Excitingly, while CD4-Kv2.1:579-609 was sensitive to treatment, CD4-Kv2.1:579-598 was resistant to glutamate application and retained junction integrity throughout the treatment time course. Together, these data indicated that one or more serine residues contained within amino acids 599 to 609 were critical for glutamate-induced junction disassembly (see Fig. 5.4C). Within this short sequence there are four serine residues, S601, S603, S607, and S609. Each of these serine residues resides

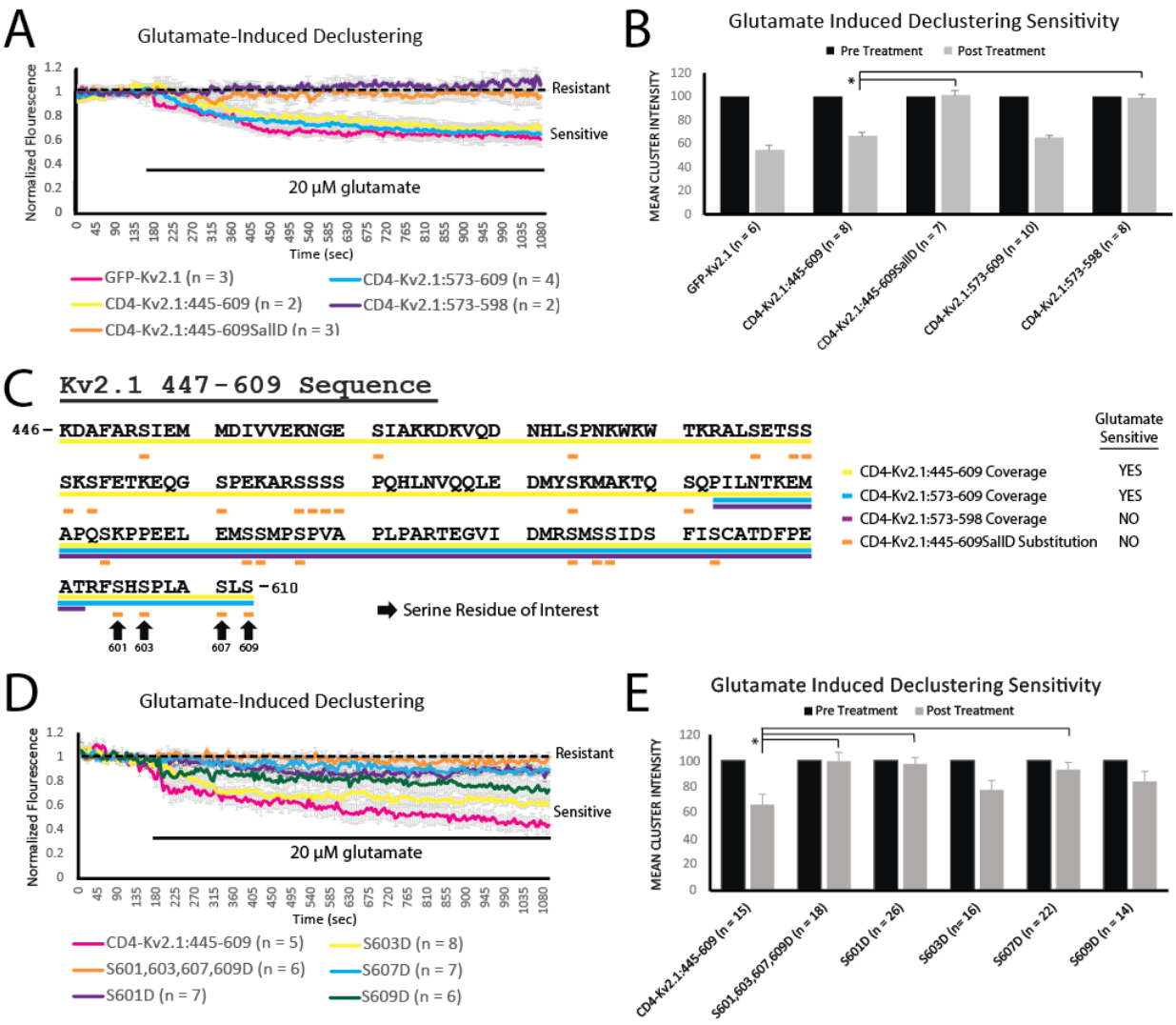

Figure 5.4 Identification of amino acids outside the Kv2.1 FFAT motif which regulate glutamate-induced disassembly of junctions in hippocampal neurons. (A) Time course of junction fluorescence during 20 µM glutamate treatment of various CD4-Kv2.1 constructs. (B) Pre and post glutamate treatment fluorescence measurements of constructs from A. (C) Sequence comparisons of the various CD4-Kv2.1 chimeras. Based on results in A and B, four serine residues are identified that may be involved in the regulation of Kv2.1-VAP disruption due to glutamate. (D) Time course of fluorescence during glutamate treatment of new CD4-Kv2.1 chimeras testing residues of interest. (E) Pre and post glutamate treatment fluorescence measurements of constructs from D. * represents *p*-values of less than 0.05; true values can be found in text. Error bars indicate SEM.

outside of the FFAT motif, at locations ranging from nine to seventeen amino acids downstream.

Only one of these residues, S603, has previously been found to be a phosphorylation site (176).

We next created CD4-chimera constructs where each of these serine residues was mutated to aspartic acid individually, as well as creating a construct with all four mutated in case multiple of these residues were required to be dephosphorylated in a combinatorial effect in order to confer sensitivity to glutamate. This last construct would also serve as an internal control. As expected, mutating all four of these residues to aspartic acid (S601,603,607,609D) resulted in an ER/PM junction tether that did not break apart from VAP upon glutamate application (see Fig 5.4D & E). S601D and S607D were also significantly resistant to dispersal. While both S603D and S609D resulted in what appeared to be an intermediate phenotype, they were not found to be significantly different than that of a CD4-Kv2.1:445-609 control. These results suggest dephosphorylation of S601 and/or S607 in some way mediates the disassociation of VAP from the channel's FFAT motif, located nine and fifteen amino acids upstream from these residues, respectively.

Junctophilin Junctions Disassemble During Glutamate-Induced Cytosolic Calcium Increases

As endogenous junctions in the hippocampus are regulated by activity, and these junctions should contain both Kv2 channels as well as JPH3 and JPH4, we next examined the junctophilin response to glutamate treatment. As shown in Figure 5.5A & B, glutamate treatment resulted in the disassembly of JPH4-induced ER/PM junctions. This loss of the junction microdomain occurred at a faster rate than Kv2.1-induced ER/PM junction loss due to glutamate (Fig. 5.5B). JPH3 was also sensitive to glutamate application (Fig. 5.5B) with a rate of loss perhaps faster than JPH4, although more experiments will need to be performed to confirm this. While the presence of Kv2.1 within these same junctions slowed the rate of JPH4 loss to the same rate as Kv2.1, this

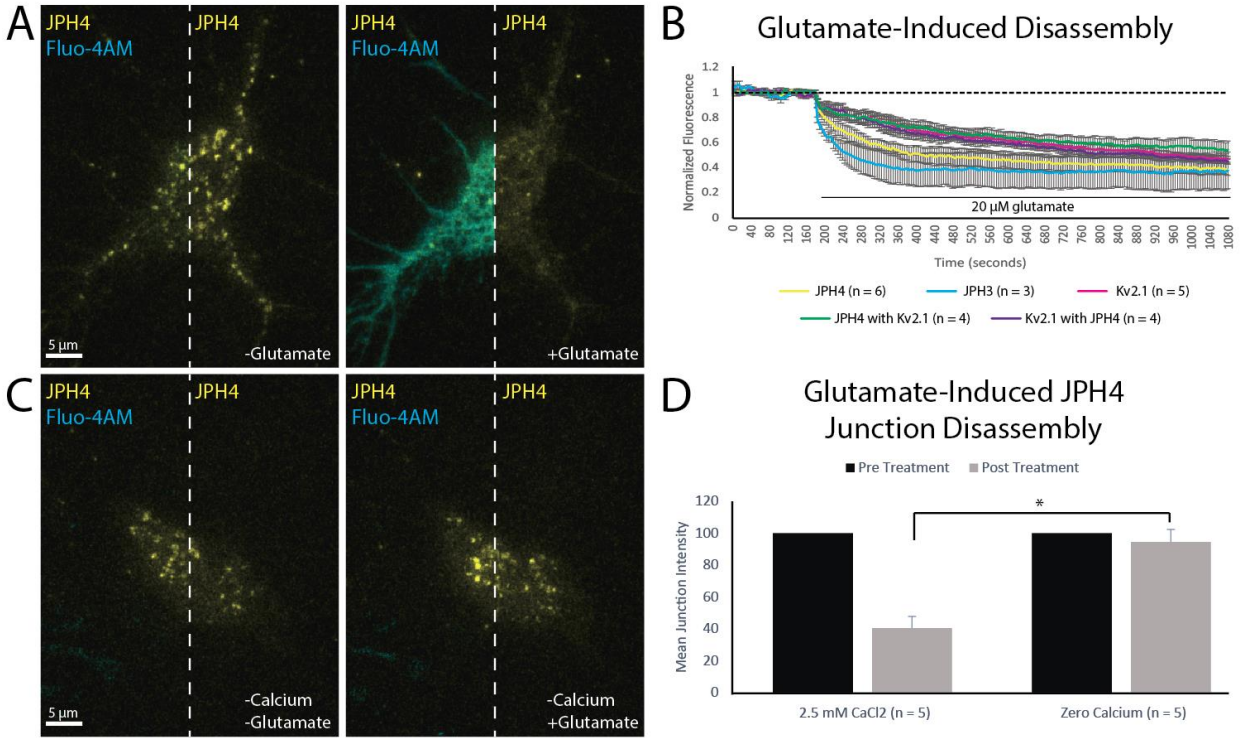

Figure 5.5 JPH junctions in hippocampal neurons disassemble due to glutamate in a calcium-dependent manner. (A) mCherry-JPH junctions disassemble after 20 µM glutamate treatment. Fluo-4AM was used to visualize increases in cytosolic calcium concentrations within cells. Representative TIRF images. (B) Time course of JPH and Kv2.1 junction disruption. JPH loss occurs at a faster rate than Kv2.1 loss. When coexpressed, JPH4 loss mirrors the rate at which Kv2.1 is lost. (C) JPH4 junction disassembly requires an increase in cytosolic calcium levels. Note the lack of Fluo-4AM response after glutamate application in the righthand panel. (D) Mean junction fluorscence intensities pre and post glutamate treatment when solutions contained either 2.5 mM or zero $CaCl_2$. Scale bars are 5 µM. Error bars indicate SEM. * represents $p \leq 0.05$; true values can be found in text.

may be due to the channel holding the ER, and thus the ER resident JPH4 proteins, within the TIRF field until the channel junctions fully disperse.

Disruption of JPH4 contacts required calcium, as using zero-calcium solutions combined with the calcium chelator EGTA resulted in JPH4 maintaining junctional integrity during glutamate treatment (Fig. 5.5C & D). In these experiments we used the calcium indicator Fluo-4AM to observe calcium levels within the cellular cytosol. In Figure 5.5A an increase in cytosolic calcium is paired with JPH4 junction disassembly, whereas in Figure 5.5C, using calcium-free

solutions results in no cytosolic calcium increase and JPH4 junctions remain significantly intact ($p = 0.000968$).

Discussion

The observation that dephosphorylation of serine residues outside of the FFAT motif and upstream flanker region can regulate the Kv2.1-VAP interaction is a novel finding. While we still believe phosphorylation within or immediately upstream of the FFAT motif is critical for Kv2-VAP interaction, dephosphorylation of these residues was difficult to explain as it was hard to imagine phosphatases gaining entry to these sites while VAP was bound at this same location. The existence of a secondary site whose dephosphorylation mediates the Kv2-VAP interaction solves this conundrum. It does, however, raise questions about the three-dimensional structure of this area and how dephosphorylation of these downstream residues is transduced upstream to the FFAT motif in order to generate disassociation.

VAP has a long list of interactors, some of these are already known to be regulated in a phosphorylation-mediated manner (109, 111, 234). If an additional domain outside of the FFAT motif can mediate the Kv2.1-VAP interaction, an examination of other proteins to see if such a mechanism is common is certainly warranted. Such a mechanism could go far to explain the regulated nature of a number of VAP interactors.

MORN motifs bind strongly to phosphatidic acid, and to a lesser extent to both PI4P and $PI(4,5)P_2$ (116). It's possible that loss of JPH-induced ER/PM junctions is due to changes in the lipid composition of the PM, perhaps in a phospholipase-mediated manner. Glutamate-induced, calcium-influx activated, phospholipases do exist within the hippocampus and play a role in neuronal vulnerability during ischemic injury (235-237). There are also reports that the JPHs can

undergo calpain-dependent cleavage during cytosolic calcium increases (238-240), though these findings have so far been confined to JPH1 and JPH2 within cardiac and skeletal cells.

The JPHs are known to stabilize L-type calcium channels at ER/PM junctions (118). They are also known to play a role in ryanodine receptor localization to these areas (119-121). Future investigation will be required to investigate L-type calcium channel and ryanodine receptor behavior during glutamate-induced JPH junction dispersal. Glutamate is known to result in Cav1.2 internalization in hippocampal neurons (241). The loss of junctophilin junctions could be one possible mechanism for this, although preliminary data on this subject are puzzling (see Appendix III). JPH3/4 double knockout mice display defects in memory and hind-limb reflex (83), and the JPHs are becoming recognized as potential therapeutic targets for a number of neurological diseases (122). Additional studies are required given this activity-dependent regulation.

Redundancy and compensation are common with ER/PM tethers and knockout of a single tether often results in no discernable phenotype (73, 85-88). In yeast, concurrent knockout of Ist2, Tcb1, Tcb2, Tcb3, Scs2 and Scs22 must be performed in order to observe any change in ER/PM junction morphology (73). It has been hypothesized that this redundancy serves to ensure ER/PM junction structural integrity even as individual components may exhibit shifting tethering behavior (50). A common mechanism regulating binding of tethers in the hippocampus is an interesting finding in light of this.

The extended synaptotagmins can also induce ER/PM junctions and are also regulated by calcium (91, 92, 136, 199), yet it seems that increases in cytosolic calcium results in increased ER/PM tethering in this case. How the extended synaptotagmins fit into this story requires more study, but given that activity results in junction disassembly throughout the hippocampus in culture

and slices (93, 94), it doesn't seem like the extended synaptotagmins are major players in keeping these sites intact during activity.

Chapter Six: Summary of Dissertation and Future Directions

The work within this dissertation has examined the protein residents of ER/PM junctions, how those components assemble into a functional microdomain from both a compositional and structural viewpoint, and how this microdomain is regulated in neuronal cells. Chapter 2 identified the mechanism by which Kv2 channels interact with VAP proteins to form ER/PM junction microdomains. First, FRET and siRNA knockdown approaches were used to confirm a Kv2-VAP interaction, and then an FFAT motif was identified in the channel using a series of CD4-Chimeric constructs.

Now that we are aware that ion channels are capable of forming ER/PM junctions through VAP interaction (see Figure 6.1 for model summarizing Chapter 2 findings), the idea that other channels may be operating in a similar manner becomes an intriquing proposition.

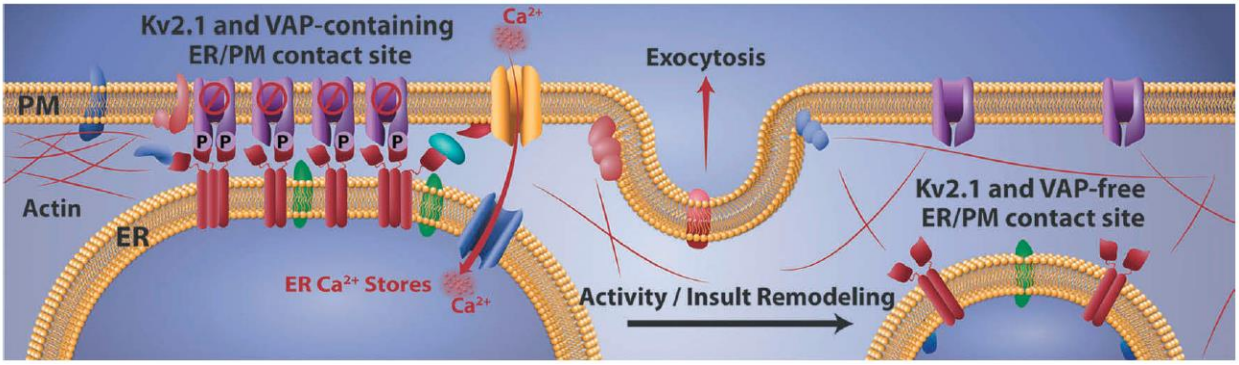

Figure 6.1, Model of the Kv2.1-induced ER/PM junction. Calcineurin-dependent dephosphorylation of the Kv2.1 C-terminus results in release from the ER VAPs, Kv2.1 declustering, loss of the ER/PM junction, VAP redistribution, and cortical ER retraction. The clustered Kv2.1 channels are proposed to be non-conducting under resting conditions. Both the Kv2.1-containing and Kv2.1-free ER/PM junctions are trafficking hubs where dense core vesicle exocytosis and membrane protein delivery is concentrated, perhaps in part due to these membrane contact sites residing in, or forming, "holes" in the cortical actin.

The transient receptor potential (TRP) channels, for instance, are known to play a role in calcium homeostasis alongside STIM and Orai. How they might localize to ER/PM junctions is

still a matter open to debate. However, analysis of two TRP N-termini sequences reveals possible FFAT motifs (see Table 3.1).

Table 3.1. Comparison of Putative TRPC3 and TRPC6 FFAT motifs.

Protein	Flanker & FFAT sequence	Levine's Suboptimal Elements Score[1]
OSBP	DEDDEN**EFFDAPE**	0
TRPC3	LTAEEE**RFLDAAE**	3.5
TRPC6	LSIEEE**RFLDAAE**	3.5
Kv2.1	SMSSID**SFISCAT**	4
N/A	RANDOM SEQUENCE	11.2 ± 1.8

[1]Levine's suboptimal elements score for flankers and FFAT motifs as well as for random amino acid sequence generated using methodology described in (110).

Using analysis developed by Dr. Levine of UCL (Levine) which assigns a suboptimal score to each amino acid within the putative FFAT motif as well as the upstream flanker, both TRPC3 and TRPC6 are awarded scores of 3.5. In context, a perfect FFAT motif and flanker region such as that found in OSBP is given a score of 0, Kv2.1 is given a score of 4, and randomly generated sequences of amino acids would be scored as 11.2 ± 1.8. While the upstream negative charge required for VAP binding is likely provided through phosphorylation of upstream serine residues in the case of Kv2.1, for TRPC3 and TRPC6 this negative charge is intrinsic to the TRP FFAT flanker amino acid sequence in a manner similar to the OSBP flanker sequence. There is, however, one serine residue in the case of TRPC6 and one threonine residue in the case of TRPC3 within the flanker that could possibly be phosphorylated.

While we have observed TRP channels localizing into 'clusters' (data not shown), this behavior cannot be consistently reproduced in our cells. As we are using immature rat hippocampal neurons for the majority of these experiments an additional protein regulator not yet expressed, or some localizing stimulus not yet tested could possibly explain this behavior. For instance, ER store depletion has been reported as necessary for some TRP channel trafficking to the PM (242, 243).

Futher research is clearly required to test the localization of the TRP channels as it pertains to the VAPs.

TRP channels are far from being the only ion channels with the potential for this type of interaction. Other voltage-gated potassium ion channels, for instance, may contain uncharacterized FFAT motifs yet to be discovered (see Table 3.2).

Table 3.2. Comparison of Putative Potassium Channel FFAT motifs.

Protein	Flanker & FFAT sequence	Levine's Suboptimal Elements Score[1]
Kv6.3	RMSDTY**TFYSADE**	2
EAG1	ALQKVL**EFYTAFS**	2.5
Kv6.1	SQDSDI**LFGSASS**	3.5
Kv7.4	DPDITS**DYHSPVD**	4
TASK-2	TFTSTE**SELSVPY**	5.5
N/A	RANDOM SEQUENCE	11.2 ± 1.8

[1]Levine's suboptimal elements score for flankers and FFAT motifs as well as for random amino acid sequence generated using methodology described in (110). Channels examined were selected based on communications with Dr. Tim Levine of University College London.

There are a host of potassium ion channels whose behavior and localization will need to be re-examined in light of these findings. Clearly ion channel-VAP interaction is an area of research that needs to be further investigated.

Chapter 3 built off the idea of a VAP platform and sought to identify additional resident proteins within these microdomains. While a number of VAP interactors were not found to be located within Kv2-induced junctions to a degree discernable by the techniques used here, MOSPD3, a VAP-like protein, was significantly concentrated at these locations when coexpressed with Kv2.1. This may be the first evidence of a Kv2.1-MOSPD interaction that serves to tether the PM and ER membranes together in a manner similar to the Kv2-VAP interaction. More work will need to be accomplished on this front. Chapter 2 also established Kv2-VAP junctions as sites where a variety of proteins will relocalize to upon stimulation. Nir2 was observed concentrating

to these locations when activated by angiotensin. Interestingly, this same Nir2 concentration will displace JPH4 from these sites. The exact molecular mechanism behind this is still unknown as is the functional significance of JPH loss during Nir2 activation.

As has been previously found, STIM and Orai will also localize to these Kv2.1-induced ER/PM junctions during calcium depletion (46). These studies determined that the presence of Kv2.1 enhances the rate of store recovery after store depletion. This was not simply due to the generation of ER/PM contact sites, as our CD4-Kv2.1:445-609 construct displayed an intermediate phenotype. This suggests that another portion of the potassium channel is responsible for the higher rate beyond what is seen in the chimera. What this aspect of the channel is, however, remains unknown. While CD4 is capable of forming dimers (187), perhaps the tetramerization of the Kv2 channel protein confers additional properties in the form of domain structural aspects or VAP redistribution effects. There is also the possibility that the non-conducting channels within junctions are able to activate under these conditions, possibly providing a counter flux of current to that of calcium.

Chapter 4 sought to examine the structure and nanoarchitecture of these sites using super resolution techniques. A cursory examination of actin behavior surround junctions was performed, and the internal dynamics of the ER at junctions was observed. The induction of Kv2.1 'donut' structures via STIM activation was first examined. This arrangement of Kv2.1 surrounding a protein has been previously described as existing in hippocampal neurons, but this is the first time this localization pattern has been induced and offers the first putative explanations for its occurrence. Future studies will need to parse apart potential functional significances behind this bit of domain nanoarchitecture.

Chapter 5 identified mechanisms underlying the activity-dependent regulation of ER/PM junctions in excitable cells. The phospho-dependence of the Kv2-VAP interaction was further explored, and a short sequence outside the FFAT motif and flanker region was identified as a possible regulatory domain that mediate VAP disassociation from the channel during neuronal activity. In addition, JPH4-induced ER/PM junctions were found to be impacted by glutamate stimulation in a calcium-dependent manner.

A quick sequence alignment of FFAT motifs and downstream residues finds a number of VAP interactors with possible phosphorylation sites or negatively charged residues landing at position FFAT+9 and/or FFAT+15 (residues S601 and S607 in Kv2.1 sequence; see Appendix IV). If found to be a common mechanism, an outside domain regulating the FFAT motif is an exciting prospect for VAP interactions.

What this dissertation has avoided addressing for the most part, is why use a voltage-gated potassium channel to form these junctions at all? Could the ion flux be generated under certain conditions from these largely non-conducting channels? We know that the S4 voltage sensor still moves in response to depolarization. Could the Kv2 channels be transducing the action potential to the ER in some way? And what of the Kv2 channel beta subunit AMIGO? Clusters are known to be sites of cell-cell contact, so are these domains not just conducting signals from the PM to the ER and vice versa, but also across cells?

The work within this dissertation marks a small step towards understanding an enigmatic microdomain. Though ER/PM junctions have been known for decades, and are best characterized in yeast, the true scope of their function is yet to be determined, especially within the mammalian CNS. This work represents the first forays into understanding the Kv2-VAP microdomain, and we

look forward to future investigations that further the role of Kv2.1 within the ER/PM field and perhaps beyond.

REFERENCES

1. Singer SJ, Nicolson GL. The fluid mosaic model of the structure of cell membranes. Science. 1972;175(4023):720-31. Epub 1972/02/18. PubMed PMID: 4333397.
2. Frech GC, VanDongen AM, Schuster G, Brown AM, Joho RH. A novel potassium channel with delayed rectifier properties isolated from rat brain by expression cloning. Nature. 1989;340(6235):642-5. Epub 1989/08/24. doi: 10.1038/340642a0. PubMed PMID: 2770868.
3. Hwang PM, Glatt CE, Bredt DS, Yellen G, Snyder SH. A Novel K+ Channel with Unique Localizations in Mammalian Brain - Molecular-Cloning and Characterization. Neuron. 1992;8(3):473-81. doi: Doi 10.1016/0896-6273(92)90275-I. PubMed PMID: WOS:A1992HK67500007.
4. Hwang PM, Cummingham AM, Peng YW, Snyder SH. CDRK and DRK1 K+ channels have contrasting localizations in sensory systems. Neuroscience. 1993;55(3):613-20.
5. Hwang PM, Fotuhi M, Bredt DS, Cunningham AM, Snyder SH. Contrasting immunohistochemical localizations in rat brain of two novel K+ channels of the Shab subfamily. J Neurosci. 1993;13(4):1569-76. Epub 1993/04/01. PubMed PMID: 8463836.
6. Kihira Y, Hermanstyne TO, Misonou H. Formation of heteromeric Kv2 channels in mammalian brain neurons. J Biol Chem. 2010;285(20):15048-55. Epub 2010/03/06. doi: 10.1074/jbc.M109.074260. PubMed PMID: 20202934; PMCID: PMC2865335.
7. Bishop HI, Guan D, Bocksteins E, Parajuli LK, Murray KD, Cobb MM, Misonou H, Zito K, Foehring RC, Trimmer JS. Distinct Cell- and Layer-Specific Expression Patterns and Independent Regulation of Kv2 Channel Subtypes in Cortical Pyramidal Neurons. J Neurosci. 2015;35(44):14922-42. Epub 2015/11/06. doi: 10.1523/JNEUROSCI.1897-15.2015. PubMed PMID: 26538660; PMCID: PMC4635138.
8. Du J, Tao-Cheng JH, Zerfas P, McBain CJ. The K+ channel, Kv2.1, is apposed to astrocytic processes and is associated with inhibitory postsynaptic membranes in hippocampal and cortical principal neurons and inhibitory interneurons. Neuroscience. 1998;84(1):37-48. Epub 1998/04/02. PubMed PMID: 9522360.
9. Muennich EAL, Fyffe REW. Focal aggregation of voltage-gated, Kv2.1 subunit-containing, potassium channels at synaptic sites in rat spinal motoneurones. Journal of Physiology-London. 2004;554(3):673-85. doi: 10.1113/jphysiol.2003.056192. PubMed PMID: WOS:000188829800010.
10. Yazulla S, Studholme KM. Differential distribution of Shaker-like and Shab-like K+-channel subunits in goldfish retina and retinal bipolar cells. J Comp Neurol. 1998;396(1):131-40. Epub 1998/06/12. PubMed PMID: 9623892.
11. O'Connell KM, Whitesell JD, Tamkun MM. Localization and mobility of the delayed-rectifer K+ channel Kv2.1 in adult cardiomyocytes. Am J Physiol Heart Circ Physiol. 2008;294(1):H229-37. Epub 2007/10/30. doi: 10.1152/ajpheart.01038.2007. PubMed PMID: 17965280.
12. Amberg GC, Santana LF. Kv2 channels oppose myogenis constriction of rat cerebral arteries. Am J Physiol Cell Physiol. 2006;291(2):C348-C56.

13. Epperson A, Bonner HP, Ward SM, Hatton WJ, Bradley KK, Bradley ME, Trimmer JS, Horowitz B. Molecular diversity of Kvα- and β-subunit expression in canine gastrointestinal smooth muscles. Neuroregulation and Motility. 1999;277(1):G127-G36.
14. Fu J, Dai X, Plummer G, Suzuki K, Bautista A, Githaka JM, Senior L, Jensen M, Greitzer-Antes D, Manning Fox JE, Gaisano HY, Newgard CB, Touret N, MacDonald PE. Kv2.1 Clustering Contributes to Insulin Exocytosis and Rescues Human beta-Cell Dysfunction. Diabetes. 2017;66(7):1890-900. Epub 2017/06/14. doi: 10.2337/db16-1170. PubMed PMID: 28607108; PMCID: PMC5482075.
15. Greitzer-Antes D, Xie L, Qin T, Xie H, Zhu D, Dolai S, Liang T, Kang F, Hardy AB, He Y, Kang Y, Gaisano HY. Kv2.1 clusters on beta-cell plasma membrane act as reservoirs that replenish pools of newcomer insulin granule through their interaction with syntaxin-3. J Biol Chem. 2018;293(18):6893-904.
16. Du J, Haak LL, Phillips-Tansey E, Russell JT, McBain CJ. Frequency-dependent regulation of rat hippocampal somato-dendritic excitability by the K+ channel subunit Kv2.1. The Journal of Physiology. 2004;522(1):19-31.
17. Xu H, Barry DM, Li H, Brunet S, Guo W, Nerbonne JM. Attenuation of the slow component of delayed rectification, action potential prolongation, and triggered activity in mice expressing a dominant-negative Kv2 alpha subunit. Circ Res. 1999;85(7):623-33. Epub 1999/10/03. PubMed PMID: 10506487.
18. Jacobson DA, Kuznetsov A, Lopez JP, Kash S, Ammala CE, Philipson LH. Kv2.1 ablation alters glucose-induced islet electrical activity, enhancing insulin secretion. Cell Metab. 2007;6(3):229-35. Epub 2007/09/05. doi: 10.1016/j.cmet.2007.07.010. PubMed PMID: 17767909; PMCID: PMC2699758.
19. Pal S, Hartnett KA, Nerbonne JM, Levitan ES, Aizenman E. Mediation of neuronal apoptosis by Kv2.1-encoded potassium channels. J Neurosci. 2003;23(12):4798-802. Epub 2003/07/02. PubMed PMID: 12832499; PMCID: PMC2945225.
20. Pal SK, Takimoto K, Aizenman E, Levitan ES. Apoptotic surface delivery of K+ channels. Cell Death Differ. 2006;13(4):661-7. Epub 2005/11/08. doi: 10.1038/sj.cdd.4401792. PubMed PMID: 16273079; PMCID: PMC1403161.
21. Redman PT, Hartnett KA, Aras MA, Levitan ES, Aizenman E. Regulation of apoptotic potassium currents by coordinated zinc-dependent signalling. J Physiol. 2009;587(Pt 18):4393-404. Epub 2009/07/23. doi: 10.1113/jphysiol.2009.176321. PubMed PMID: 19622611; PMCID: PMC2766646.
22. Redman PT, He K, Hartnett KA, Jefferson BS, Hu L, Rosenberg PA, Levitan ES, Aizenman E. Apoptotic surge of potassium currents is mediated by p38 phosphorylation of Kv2.1. Proc Natl Acad Sci U S A. 2007;104(9):3568-73. Epub 2007/03/16. doi: 10.1073/pnas.0610159104. PubMed PMID: 17360683; PMCID: PMC1805571.
23. Thiffault I, Speca DJ, Austin DC, Cobb MM, Eum KS, Safina NP, Grote L, Farrow EG, Miller N, Soden S, Kingsmore SF, Trimmer JS, Saunders CJ, Sack JT. A novel epileptic encephalopathy mutation in KCNB1 disrupts Kv2.1 ion selectivity, expression, and localization. J Gen Physiol. 2015;146(5):399-410. Epub 2015/10/28. doi: 10.1085/jgp.201511444. PubMed PMID: 26503721; PMCID: PMC4621747.
24. Torkamani A, Bersell K, Jorge BS, Bjork RL, Jr., Friedman JR, Bloss CS, Cohen J, Gupta S, Naidu S, Vanoye CG, George AL, Jr., Kearney JA. De novo KCNB1 mutations in epileptic encephalopathy. Ann Neurol. 2014;76(4):529-40. Epub 2014/08/29. doi: 10.1002/ana.24263. PubMed PMID: 25164438; PMCID: PMC4192091.

25. Speca DJ, Ogata G, Mandikian D, Bishop HI, Wiler SW, Eum K, Wenzel HJ, Doisy ET, Matt L, Campi KL, Golub MS, Nerbonne JM, Hell JW, Trainor BC, Sack JT, Schwartzkroin PA, Trimmer JS. Deletion of the Kv2.1 delayed rectifier potassium channel leads to neuronal and behavioral hyperexicitability. Genes, Brain and Behavior. 2014;13:394-408.
26. Trimmer JS. Immunological identification and characterization of a delayed rectifier K+ channel polypeptide in rat brain. Proc Natl Acad Sci U S A. 1991;88(23):10764-8. Epub 1991/12/01. PubMed PMID: 1961744; PMCID: PMC53011.
27. Scannevin RH, Murakoshi H, Rhodes KJ, Trimmer JS. Identification of a cytoplasmic domain important in the polarized expression and clustering of the Kv2.1 K+ channel. J Cell Biol. 1996;135(6 Pt 1):1619-32. Epub 1996/12/01. PubMed PMID: 8978827; PMCID: PMC2133974.
28. Shi G, Kleinklaus AK, Marrion NV, Trimmer JS. Properties of Kv2.1 K+ channels expressed in transfected mammalian cells. The Journal of Biological Chemistry. 1994;269(37):23204-11.
29. Lim ST, Antonucci DE, Scannevin RH, Trimmer JS. A novel targeting signal for proximal clustering of the Kv2.1 K+ channel in hippocampal neurons. Neuron. 2000;25(2):385-97. Epub 2000/03/17. PubMed PMID: 10719893.
30. Antonucci DE, Lim ST, Vassanelli S, Trimmer JS. Dynamic localization and clustering of dendritic Kv2.1 voltage-dependent potassium channels in developing hippocampal neurons. Neuroscience. 2001;108(1):69-81. Epub 2001/12/12. PubMed PMID: 11738132.
31. Misonou H, Mohapatra DP, Park EW, Leung V, Zhen D, Misonou K, Anderson AE, Trimmer JS. Regulation of ion channel localization and phosphorylation by neuronal activity. Nat Neurosci. 2004;7(7):711-8. Epub 2004/06/15. doi: 10.1038/nn1260. PubMed PMID: 15195093.
32. Misonou H, Mohapatra DP, Menegola M, Trimmer JS. Calcium- and metabolic state-dependent modulation of the voltage-dependent Kv2.1 channel regulates neuronal excitability in response to ischemia. J Neurosci. 2005;25(48):11184-93. Epub 2005/12/02. doi: 10.1523/JNEUROSCI.3370-05.2005. PubMed PMID: 16319318.
33. Misonou H, Mohapatra DP, Trimmer JS. Kv2.1: a voltage-gated k+ channel critical to dynamic control of neuronal excitability. Neurotoxicology. 2005;26(5):743-52. Epub 2005/06/14. doi: 10.1016/j.neuro.2005.02.003. PubMed PMID: 15950285.
34. Surmeier DJ, Foehring R. A mechanism for homeostatic plasticity. Nat Neurosci. 2004;7(7):691-2. Epub 2004/06/29. doi: 10.1038/nn0704-691. PubMed PMID: 15220926.
35. O'Connell KM, Rolig AS, Whitesell JD, Tamkun MM. Kv2.1 potassium channels are retained within dynamic cell surface microdomains that are defined by a perimeter fence. J Neurosci. 2006;26(38):9609-18. Epub 2006/09/22. doi: 10.1523/JNEUROSCI.1825-06.2006. PubMed PMID: 16988031.
36. O'Connell KM, Loftus R, Tamkun MM. Localization-dependent activity of the Kv2.1 delayed-rectifier K+ channel. Proc Natl Acad Sci U S A. 2010;107(27):12351-6. Epub 2010/06/23. doi: 10.1073/pnas.1003028107. PubMed PMID: 20566856; PMCID: PMC2901471.
37. Benndorf K, Koopman R, Lorra C, Pongs O. Gating and conductance properties of a human delayed rectifier K+ channel expressed in frog oocytes. Journal of Physiology. 1994;477(1):1-14.

38. Baver SB, O'Connell KM. The C-terminus of neuronal Kv2.1 channels is required for channel localization and targeting but not for NMDA-receptor-mediated regulation of channel function. Neuroscience. 2012;217:56-66. Epub 2012/05/05. doi: 10.1016/j.neuroscience.2012.04.054. PubMed PMID: 22554782; PMCID: PMC3383376.
39. Fox PD, Loftus RJ, Tamkun MM. Regulation of Kv2.1 K(+) conductance by cell surface channel density. J Neurosci. 2013;33(3):1259-70. Epub 2013/01/18. doi: 10.1523/JNEUROSCI.3008-12.2013. PubMed PMID: 23325261; PMCID: PMC3711267.
40. Cobb MM, Austin DC, Sack JT, Trimmer JS. Cell Cycle-dependent Changes in Localization and Phosphorylation of the Plasma Membrane Kv2.1 K+ Channel Impact Endoplasmic Reticulum Membrane Contact Sites in COS-1 Cells. J Biol Chem. 2015;290(49):29189-201. Epub 2015/10/08. doi: 10.1074/jbc.M115.690198. PubMed PMID: 26442584; PMCID: PMC4705925.
41. Feinshreiber L, Singer-Lahat D, Friedrich R, Matti U, Sheinin A, Yizhar O, Nachman R, Chikvashvili D, Rettig J, Ashery U, Lotan I. Non-conducting function of the Kv2.1 channel enables it to recruit vesicles for release in neuroendocrine and nerve cells. J Cell Sci. 2010;123(Pt 11):1940-7. Epub 2010/05/21. doi: 10.1242/jcs.063719. PubMed PMID: 20484665.
42. Singer-Lahat D, Sheinin A, Chikvashvili D, Tsuk S, Greitzer D, Friedrich R, Feinshreiber L, Ashery U, Benveniste M, Levitan ES, Lotan I. K+ channel facilitation of exocytosis by dynamic interaction with syntaxin. J Neurosci. 2007;27(7):1651-8. Epub 2007/02/16. doi: 10.1523/JNEUROSCI.4006-06.2007. PubMed PMID: 17301173.
43. Deutsch E, Weigel AV, Akin EJ, Fox P, Hansen G, Haberkorn CJ, Loftus R, Krapf D, Tamkun MM. Kv2.1 cell surface clusters are insertion platforms for ion channel delivery to the plasma membrane. Mol Biol Cell. 2012;23(15):2917-29. Epub 2012/06/01. doi: 10.1091/mbc.E12-01-0047. PubMed PMID: 22648171; PMCID: PMC3408418.
44. Fox PD, Haberkorn CJ, Weigel AV, Higgins JL, Akin EJ, Kennedy MJ, Krapf D, Tamkun MM. Plasma membrane domains enriched in cortical endoplasmic reticulum function as membrane protein trafficking hubs. Molecular Biology of the Cell. 2013;24(17):2703-13. doi: 10.1091/mbc.E12-12-0895. PubMed PMID: WOS:000324493800011.
45. Tanabe T, Mikami A, Numa S, Beam KG. Cardiac-type excitation-contraction coupling in dysgenic skeletal muscle injected with cardiac dihydropyridine receptor cDNA. Nature. 1990;344(6265):451-3. Epub 1990/03/29. doi: 10.1038/344451a0. PubMed PMID: 2157159.
46. Fox PD, Haberkorn CJ, Akin EJ, Seel PJ, Krapf D, Tamkun MM. Induction of stable ER-plasma-membrane junctions by Kv2.1 potassium channels. J Cell Sci. 2015;128(11):2096-105. Epub 2015/04/25. doi: 10.1242/jcs.166009. PubMed PMID: 25908859; PMCID: PMC4457025.
47. Johnson B, Leek AN, Sole L, Maverick EE, Levine TP, Tamkun MM. Kv2 potassium channels form endoplasmic reticulum/plasma membrane junctions via interaction with VAPA and VAPB. Proc Natl Acad Sci U S A. 2018;115(31):E7331-E40. Epub 2018/06/27. doi: 10.1073/pnas.1805757115. PubMed PMID: 29941597; PMCID: PMC6077746.
48. Kirmiz M, Palacio S, Thapa P, King AN, Sack JT, Trimmer JS. Remodeling neuronal ER-PM junctions is a conserved nonconducting function of Kv2 plasma membrane ion channels. Molecular Biology of the Cell. 2018;29(20):2410-32. doi: 10.1091/mbc.E18-05-0337. PubMed PMID: WOS:000451910900006.
49. Berridge MJ. Neuronal calcium signaling. Neuron. 1998;21(1):13-26.

50. Gallo A, Vannier C, Galli T. Endoplasmic reticulum-plasma membrane associations: structures and functions. Annu Rev Cell Dev Biol. 2016;32:279-301.
51. Wu YM, Whiteus C, Xu CS, Hayworth KJ, Weinberg RJ, Hess HF, De Camilli P. Contacts between the endoplasmic reticulum and other membranes in neurons. Proceedings of the National Academy of Sciences of the United States of America. 2017;114(24):E4859-E67. doi: 10.1073/pnas.1701078114. PubMed PMID: WOS:000403179300018.
52. Verkhratsky A. Physiology and pathology of the calcium store in the endoplasmic reticulum of neurons. Phys Rev. 2005;85:201-79.
53. Nixon-Abell J, Obara CJ, Weigel AV, Li D, Legant WR, Xu CS, Pasolli A, Harvey K, Hess HF, Betzig E, Blackstone C, Lippincott-Schwartz J. Increased spatiotemporal resolution reveals highly dynamic dense tubular matrices in the peripheral ER. Science. 2016;354(6311):aaf3928.
54. Berridge MJ. The endoplasmic reticulum: a multifunctional signaling organelle. Cell Calcium. 2002;32(5-6):235-49.
55. Tajiri S, Oyadomari S, Yano S, Morioka M, Gotoh T, Hamada J-I, Ushio Y, Mori M. Ischemia-induced neuronal cell death is mediated by the endoplasmic reticulum stress pathway involving CHOP. Cell Death & Diff. 2004;11:403-15.
56. de Juan-Sanz J, Holt GT, Schreiter ER, de Juan F, Kim DS, Ryan TA. Axonal Endoplasmic Reticulum Ca(2+) Content Controls Release Probability in CNS Nerve Terminals. Neuron. 2017;93(4):867-81.e6. doi: 10.1016/j.neuron.2017.01.010. Epub Feb 2.
57. Bliss TVP, Collingridge GL. A synaptic model of memory: long-term potentiation in the hippocampus. Nature. 1993;361:31-9.
58. Katayama T, Imaizumi K, Manabe T, Hitomi J, Kudo T, Tohyama M. Induction of neuronal death by ER stress in Alzheimer's disease. J Chem Neuroanat. 2004;28(1-2):67-78.
59. Fasana E, Fossati M, Ruggiano A, Brambillasca S, Hoogenraad CC, Navone F, Francolini M, Borgese N. A VAPB mutant linked to amyotrophis lateral sclerosis generates a novel form of organized smooth endoplasmic reticulum. FASEB J. 2010;24(5):1419-30.
60. Lindholm D, Wootz H, Korhonen L. ER stress and neurodegenerative diseases. Cell Death & Diff. 2006;13:385-92.
61. Park SH, Zhu P-P, Parker RL, Blackstone C. Hereditary spastic paraplegia proteins REEP1, spastin, and atlasting-1 coordinate microtubule interactions with the tubular ER network. J Clin Invest. 2010;120(4):1097-110.
62. Montenegro G, Rebelo AP, Connell J, Allison R, Babalini C, D'Aloia M, Montieri P, Schüle R, Ishiura H, Price J, Strickland A, Gonzalez MA, Baumbach-Reardon L, Deconinck T, Huang J, Bernardi G, Vance JM, Rogers MT, Tsuji S, De Jonghe P, Pericak-Vance MA, Schöls L, Orlacchio A, Reid E, Züchner S. Mutations in the ER-shaping protein reticulon 2 cause the axon-degenerative disorder hereditary spastic paraplegia type 12. J Clin Invest. 2012;122(2):538-44.
63. Porter KR, Palade GE. Studies on the Endoplasmic Reticulum. The Journal of Cell Biology. 1957;3(2):269-300.
64. Rosenbluth J. Subsurface Cisterns and their Relationship to the Neuronal Plasma Membrane. The Journal of Cell Biology. 1962;13(3):405-21.
65. Henkart M, Landis DM, Reese TS. Similarity of junctions between plasma membranes and endoplasmic reticulum in muscle and neurons. J Cell Biol. 1976;20(1):338-47.

66. Phillips MJ, Voeltz GK. Structure and function of ER membrane contact sites with other organelles. Nat Rev Mol Cell Biol. 2015;17:69-82.
67. Ramírez OA, Couve A. The endoplasmic reticulum and protein trafficking in dendrites and axons. Trends Cell Biol. 2011;21(4):P219-27.
68. Luik RM, Wu MM, Buchanan J, Lewis RS. The elementary unit of store-operated Ca2+ entry: local activation of CRAC channels by STIM1 at ER-plasma membrane junctions. Journal of Cell Biology. 2006;174(6):815-25. doi: DOI 10.1083/jcb.200604015. PubMed PMID: WOS:000240697100011.
69. Wu MM, Buchanan J, Luik RM, Lewis RS. Ca2+ store depletion causes STIM1 to accumulate in ER regions closely associated with the plasma membrane. J Cell Biol. 2006;174(6):803-13. Epub 2006/09/13. doi: 10.1083/jcb.200604014. PubMed PMID: 16966422; PMCID: PMC2064335.
70. Kim YJ, Guzman-Hernandez ML, Wisniewski E, Balla T. Phosphatidylinositol-Phosphatidic Acid Exchange by Nir2 at ER-PM Contact Sites Maintains Phosphoinositide Signaling Competence. Developmental Cell. 2015;33(5):549-61. doi: 10.1016/j.devcel.2015.04.028. PubMed PMID: WOS:000356055500010.
71. Kim YJ, Guzman-Hernandez ML, Wisniewski E, Echeverria N, Balla T. Phosphatidylinositol and phosphatidic acid transport between the ER and plasma membrane during PLC activation requires the Nir2 protein. Biochemical Society Transactions. 2016;44(1):197-201. doi: 10.1042/Bst20150187. PubMed PMID: WOS:000374119800027.
72. Dickson EJ, Jensen JB, Vivas O, Kruse M, Traynor-Kaplan AE, Hille B. Dynamic formation of ER-PM junctions presents a lipid phosphatase to regulate phosphoinositides. J Cell Biol. 2016;213(1):33-48. Epub 2016/04/06. doi: 10.1083/jcb.201508106. PubMed PMID: 27044890; PMCID: PMC4828688.
73. Manford AG, Stefan CJ, Yuan HL, MacGurn JA, Emr SD. ER-to-plasma membrane tethering proteins regulate cell signaling and ER morphology. Dev Cell. 2012;23(6):1129-40.
74. Paschen W, Mengesdorf T. Endoplasmic reticulum stress response and neurodegeneration. Cell Calcium. 2005;38(3-4):409-15.
75. Stefan CJ, Manford AG, Emr SD. ER-PM connections: sites of information transfer and inter-organelle communication. Curr Opin Cell Biol. 2013;25(4):434-42.
76. Weigel AV, Tamkun MM, Krapf D. Quantifying the dynamic interactions between a clathrin-coated pit and cargo molecules. Proceedings of the National Academy of Sciences of the United States of America. 2013;110(48):E4591-E600. doi: 10.1073/pnas.1315202110. PubMed PMID: WOS:000327390400012.
77. Zhang D, Bidone TC, Vavylonis D. ER-PM contacts define actomyosin kinetics for proper contractile ring assembly. Curr Biol. 2016;26:647-53.
78. Zhang D, Vjestica A, Oliferenko S. Plasma membrane tethering of the cortical ER necessitates its finely reticulated architecture. Curr Biol. 2012;22(21):2048-52.
79. Thillaiappan NB, Chavda AP, Tovey SC, Prole DL, Taylor CW. Ca2+ signals initiate at immobile IP3 receptors adjacent to ER-plasma membrane junctions. Nat Commun. 2017;8:1505.
80. Weigel AV, Simon B, Tamkun MM, Krapf D. Ergodic and nonergodic processes coexist in the plasma membrane as observed by single-molecule tracking. Proc Natl Acad Sci U S

A. 2011;108(16):6438-43. Epub 2011/04/06. doi: 10.1073/pnas.1016325108. PubMed PMID: 21464280; PMCID: PMC3081000.
81. Wu MM, Covington ED, Lewis RS. Single-molecule analysis of diffusion and trapping of STIM1 and Orai1 at enoplasmic reticulum-plasma membrane junctions. Mol Biol Cell. 2014;25(22):3437-716.
82. Deller T, Bas Orth C, Del Turco D, Vlachos A, Burbach GJ, Drakew A, Chabanis S, Korte M, Schwegler H, Haas CA, Frotscher M. A role for synaptopodin and the spine apparatus in hippocampal synaptic plasticity. Ann Anat. 2007;189(1):5-16.
83. Moriguchi S, Nishi M, Komazaki S, Sakagami H, Miyazaki T, Masumiya H, Saito S, Watanabe M, Kondo H, Yawo H, Fukunaga K, Takeshima H. Functional uncoupling between Ca2+ release and afterhyperpolarization in mutant hippocampal neurons lacking junctophilins. Proc Natl Acad Sci USA. 2006;103(28):10811-6.
84. Bas Orth C, Schultz C, Müller CM, Frotscher M, Deller T. Loss of the cisternal organelle in the axon intial segment of cortical neurons in synaptopodin-deficient mice. J Comp Neurol. 2007;504(5):441-9.
85. Takeshima H, Hoshijima M, Song LS. Ca2+ microdomains organized by junctophilins. Cell Calcium. 2015;58(4):349-56.
86. Herdman C, Tremblay MG, Mishra PK, Moss T. Loss of extended synaptotagmins ESyt2 and ESyt3 does not affect mouse development or viability, but in vitro cell migration and survival under stress are affected. Cell Cycle. 2014;13(16):2616-25.
87. Tremblay MG, Moss T. Loss of all 3 extended synaptotagmins does not affect normal mouse development, viability or fertility. Cell Cycle. 2016;15(17):2360-6.
88. Helle SCJ, Kanfer G, Kolar K, Lang A, Michel AH, Kornmann B. Organization and function of membrane contact sites. Biochim Biophys Acta. 2013;1833(11):2526-41.
89. Eisenberg-Bord M, Shai N, Schuldiner M, Bohnert M. A tether is a tether is a tether: tethring at membrane contact sites. Dev Cell. 2016;39(4):395-409.
90. Deng X, Wang Y, Zhou Y, Soboloff J, Gill DL. STIM and Orai: dynamic intermembrane coupling to control cellular calcium signals. J Biol Chem. 2009;284:22501-5.
91. Idevall-Hagren O, Lü A, Xie B, De Camilli P. Triggered Ca2+ influx is required for extended synaptotagmin 1-induced ER-plasma membrane tethering. EMBO J. 2015;34:2291-305.
92. Chang C-L, Hsieh TS, Yang TT, Rothberg KG, Azizoglu DB, Volk E, Liao J-C, Liou J. Feedback regulation of receptor-induced Ca2+ signaling mediated by E-Syt1 and Nir2 at endoplasmic reticulum-plasma membrane junctions. Cell Rep. 2013;5(3):813-25.
93. Tao-Cheng J-H. Activity-dependent decrease in contact areas between subsurface cisterns and plasma membrane of hippocampal neurons. Molecular Brain. 2018;11(23).
94. Tao-Cheng J-H. Stimulation-induced structural changes at the nucleus, endoplasmic reticulum and mitochondria of hippocampal neurons. Molecular Brain. 2018;11(44).
95. Skehel PA, Martin KC, Kandel ER, Bartsch D. A VAMP-binding protein from Aplysia required for neurotransmitter release. Science. 1995;269(5230):1580-3. Epub 1995/09/15. PubMed PMID: 7667638.
96. Nishimura Y, Hayashi M, Inada H, Tanaka T. Molecular cloning and characterization of mammalian homologues of vesicle-associated membrane protein-associated (VAMP-associated) proteins. Biochem Biophys Res Commun. 1999;254(1):21-6. Epub 1999/01/28. doi: 10.1006/bbrc.1998.9876. PubMed PMID: 9920726.

97. Loewen CJR, Levine TP. A highly conserved binding site in Vesicle-associated membrane protein-Associated Protein (VAP) for the FFAT motif of lipid-binding proteins. The Journal of Biological Chemistry. 2005;280(14):14097-104.
98. Kaiser SE, Brickner JH, Reilein AR, Fenn TD, Walter P, Brunger AT. Structural basis of FFAT motif-mediated ER targeting. Structure. 2005;13(7):1035-45. Epub 2005/07/12. doi: 10.1016/j.str.2005.04.010. PubMed PMID: 16004875.
99. Lev S, Ben Halevy D, Peretti D, Dahan N. The VAP protein family: from cellular functions to motor neuron disease. Trends Cell Biol. 2008;18(6):282-90. Epub 2008/05/13. doi: 10.1016/j.tcb.2008.03.006. PubMed PMID: 18468439.
100. Amarilio R, Ramachandran S, Sabanay H, Lev S. Differential regulation of endoplasmic reticulum structure through VAP-Nir protein interaction. The Journal of Biological Chemistry. 2005;280(7):5934-44.
101. Nishimura AL, Mitne-Neto M, Silva HCA, Richieri-Costa A, Middleton S, Cascio D, Kok F, Oliveira JRM, Gillingwater T, Webb J, Skehel P, Zatz M. A mutation in the vesical-trafficking protein VAPB causes late-onset spinal muscular atrophy and amyotrophic lateral sclerosis. The American Journal of Human Genetics. 2004;75(5):822-31.
102. Teuling E, Ahmed S, Haasdijk E, Demmers J, Steinmetz MO, Akhmanova A, Jaarsma D, Hoogenraad CC. Motor neuron disease-associated mutant vesicle-associated membrane protein-associated protein (VAP) B recruits wild-type VAPs into endoplasmic reticulum-derived tubular aggregates. Journal of Neuroscience. 2007;27(36):9801-15. doi: 10.1523/Jneurosci.2661-07.2007. PubMed PMID: WOS:000249393900027.
103. Mitne-Neto M, Machado-Costa M, Marchetto MC, Bengtson MH, Joazeiro CA, Tsuda H, Bellen HJ, Silva HC, Oliveira AS, Lazar M, Muotri AR, Zatz M. Downregulation of VAPB expression in motor neurons derived from induced pluripotent stem cells of ALS8 patients. Hum Mol Genet. 2011;20(18):3642-52. Epub 2011/06/21. doi: 10.1093/hmg/ddr284. PubMed PMID: 21685205; PMCID: PMC3159551.
104. Pennetta G, Hiesinger PR, Fabian-Fine R, Meinertzhagen IA, Bellen HJ. Drosophila VAP-33A directs bouton formation at neuromuscular junction in a dosage-dependent manner. Neuron. 2002;25(2):291-306.
105. Appel N, Schaller T, Penin F, Bartenschlager R. From Structure to Function: New Insights into Hepatitis C Virus RNA Replication. The Journal of Biological Chemistry. 2006;281:9833-6.
106. Barajas D, Xu K, de Castro Martin IF, Sasvari Z, Brandizzi F, Risco C, Nagy PD. Co-opted oxysterol-binding ORP and VAP proteins channel sterols to RNA virus replication sites via membrane contact sites. PLoS Pathog. 2014;10(10):e1004388. Epub 2014/10/21. doi: 10.1371/journal.ppat.1004388. PubMed PMID: 25329172; PMCID: PMC4199759.
107. McCune BT, Tang W, Lu J, Eaglesham JB, Thorne L, Mayer AE, Condiff E, Nice TJ, Goodfellow I, Krezel AM, Virgin HW. Noroviruses Co-opt the Function of Host Proteins VAPA and VAPB for Replication via a Phenylalanine-Phenylalanine-Acidic-Tract-Motif Mimic in Nonstructural Viral Protein NS1/2. MBio. 2017;8(4):e00668-17. Epub 2017/07/13. doi: 10.1128/mBio.00668-17. PubMed PMID: 28698274; PMCID: PMC5513711.
108. Mikitova V, Levine TP. Analysis of the Key Elements of FFAT-Like Motifs Identifies New Proteins That Potentially Bind VAP on the ER, Including Two AKAPs and FAPP2. Plos One. 2012;7(1):e30455. doi: 10.1371/journal.pone.0030455. Epub 2012 Jan 19. doi: ARTN e30455

109. Kumagai K, Kawano-Kawada M, Hanada K. Phosphorylation of the cerimide transport protein CERT at serine 315 in the interaction with VAMP-associated protein (VAP) for inter-organelle trafficking of ceramide in mammalian cells. The Journal of Biological Chemistry. 2014;289(15):10748-60.
110. Murphy SE, Levine TP. VAP, a Versatile Access Point for the Endoplasmic Reticulum: Review and analysis of FFAT-like motifs in the VAPome. Biochim Biophys Acta. 2016;1861(8 Pt B):952-61. Epub 2016/02/24. doi: 10.1016/j.bbalip.2016.02.009. PubMed PMID: 26898182.
111. Weber-Boyvat M, Kentala H, Lilja J, Vihervaara T, Hanninen R, Zhou Y, Peranen J, Nyman TA, Ivaska J, Olkkonen VM. OSBP-related protein 3 (ORP3) coupling with VAMP-associated protein A regulates R-Ras activity. Exp Cell Res. 2015;331(2):278-91. Epub 2014/12/03. doi: 10.1016/j.yexcr.2014.10.019. PubMed PMID: 25447204.
112. Takeshima H, Komazaki S, Nishi M, Iion M, Kangawa K. Junctophilins: A novel family of junctional membrane complex proteins. Molecular Cell. 2000;6(1):11-22.
113. Nishi M, Sakagami H, Komazaki S, Kondo H, Takeshima H. Coexpression of junctophilin type 3 and type 4 in brain. Mol Brain Res. 2003;118(1-2):102-10.
114. Landstrom AP, Beavers DL, Wehrens XH. The junctophilin family of proteins: from bench to bedside. Trends Mol Med. 2014;20(6):353-62.
115. Garbino A, van Oort RJ, Dixit SS, Landstrom AP, Ackerman MJ, Wehrens XH. Molecular evolution of the junctophilin gene family. Physiol Genomics. 2009;37(3):175-86. Epub 2009/03/26. doi: 10.1152/physiolgenomics.00017.2009. PubMed PMID: 19318539; PMCID: PMC2685503.
116. Ma H, Lou Y, Lin WH, Xue HW. MORN motifs in plant PIPKs are involved in the regulation of subcellular localization and phospholipid binding. Cell Research. 2006;16:466-78.
117. Varnai P, Toth B, Toth DJ, Hunyady L, Balla T. Visualization and manipulation of plasma membrane-endoplasmic reticulum contact sites indicates the presence of additional molecular components within the STIM1-Orai1 complex. Journal of Biological Chemistry. 2007;282(40):29678-90. doi: 10.1074/jbc.M704339200. PubMed PMID: WOS:000249788000064.
118. Nakada T, Kashihara T, Komatsu M, Kojima K, Takeshita T, Yamada M. Physical interaction of junctophilin and the Cav1.1 C terminus is crucial for skeletal muscle contraction. Proc Natl Acad Sci U S A. 2018;115(17):4507-12.
119. Phimister AJ, Lango J, Lee EH, Ernst-Russell MA, Takeshima H, Ma J, Allen PD, Pessah IN. Conformational-dependent stability of Junctophilin 1 (JP1) and ryanodine receptor type 1 (RyR1) channel complex is mediated by their hyper-reactive thiols. J Biol Chem. 2007;282:8667-77.
120. Jayasinghe ID, Baddeley D, Kong CHT, Wehrens XHT, Cannell MB, Soeller C. Nanoscale organization of Junctophilin-2 and ryanodine receptors within peripheral couplings of rat ventricular cardiomyocytes. Biophys J. 2012;102(5):L19-L21.
121. Kakizawa S, Moriguchi S, Ikeda A, Iino M, Takeshima H. Functional crosstalk between cell-surface and intracellular channels mediated by Junctophilins essential for neuronal functions. Cerebellum. 2008;7(3):385-91.
122. Jiang J, Tang M, Huang Z, Chen L. Junctophilins emerge as novel therapeutic targets. J Cell Physiol. 2019;[Epub ahead of print].

123. Burgoyne T, Patel S, Eden ER. Calcium signaling at ER membrane contact sites. Biochimica Et Biophysica Acta-Molecular Cell Research. 2015;1853(9):2012-7. doi: 10.1016/j.bbamcr.2015.01.022. PubMed PMID: WOS:000359960400012.
124. Dittmer PJ, Wild AR, Dell'Acqua ML, Sather WA. STIM1 Ca(2+) Sensor Control of L-type Ca(2+)-Channel-Dependent Dendritic Spine Structural Plasticity and Nuclear Signaling. Cell Rep. 2017;19(2):321-34. doi: 10.1016/j.celrep.2017.03.056.
125. Hewavitharana T, Deng X, Soboloff J, Gill DL. Role of STIM and Orai proteins in the store-operated calcium signaling pathway2007.
126. Hogan PG, Lewis RS, Rao A. Molecular basis of calcium signaling in lymphocytes: STIM and ORAI. Annu Rev Immunol. 2010;28(doi):491-533. Epub 2010/03/24. doi: 10.1146/annurev.immunol.021908.132550. PubMed PMID: 20307213; PMCID: PMC2861828.
127. Huang GN, Zeng W, Kim JY, Yuan JP, Han L, Muallem S, Worley PF. STIM1 carboxyl-terminus activates native SOC, I(crac) and TRPC1 channels. Nat Cell Biol. 2006;8(9):1003-10. Epub 2006/08/15. doi: 10.1038/ncb1454. PubMed PMID: 16906149.
128. Korzeniowski MK, Manjarres IM, Varnai P, Balla T. Activation of STIM1-Orai1 involves an intramolecular switching mechanism. Sci Signal. 2010;3(148):ra82. Epub 2010/11/18. doi: 10.1126/scisignal.2001122. PubMed PMID: 21081754; PMCID: PMC3408607.
129. Korzeniowski MK, Popovic MA, Szentpetery Z, Varnai P, Stojilkovic SS, Balla T. Dependence of STIM1/Orai1-mediated calcium entry on plasma membrane phosphoinositides. J Biol Chem. 2009;284(31):21027-35. Epub 2009/06/02. doi: 10.1074/jbc.M109.012252. PubMed PMID: 19483082; PMCID: PMC2742867.
130. Lu B, Fivaz M. Neuronal SOCE: Myth or Reality? Trends Cell Biol. 2016;26(12):890-3. Epub 2016/10/11. doi: 10.1016/j.tcb.2016.09.008. PubMed PMID: 27720332.
131. Park CY, Hoover PJ, Mullins FM, Bachhawat P, Covington ED, Raunser S, Walz T, Garcia KC, Dolmetsch RE, Lewis RS. STIM1 clusters and activates CRAC channels via direct binding of a cytosolic domain to Orai1. Cell. 2009;136(5):876-90. Epub 2009/03/03. doi: 10.1016/j.cell.2009.02.014. PubMed PMID: 19249086; PMCID: PMC2670439.
132. Spassova MA, Soboloff J, He LP, Hewavitharana T, Xu W, Venkatachalam K, van Rossum DB, Patterson RL, Gill DL. Calcium entry mediated by SOCs and TRP channels: variations and enigma. Biochim Biophys Acta. 2004;1742(1-3):9-20. Epub 2004/12/14. doi: 10.1016/j.bbamcr.2004.09.001. PubMed PMID: 15590052.
133. Wang Y, Deng X, Zhou Y, Hendron E, Salvatore M, Ritchie MF, Tang XD, Baba Y, Kurosaki T, Mori Y, Soboloff J, Gill DL. STIM protein coupling in the activation of Orai channels. Proc Natl Acad Sci U S A. 2009;106(5):7391-6.
134. Feske S, Gwack Y, Prakriya M, Srikanth S, Puppel S-H, Tanasa B, Hogan PG, Lewis RS, Daly M, Rao A. A mutation in Orai1 causes immune deficiency by abrogating CRAC channel function. Nature. 2006;441(7090):179-85.
135. Orci L, Ravazzola M, Le Coadic M, Shen W-w, Demaurex N, Cosson P. STIM1-induced precortical and cortical subdomains of the endoplasmic reticulum. Proc Natl Acad Sci U S A. 2009;106(46):19358-62.
136. Fernández-Busnadiego R, Saheki Y, De Camilli P. Three-dimensional architecture of extended synaptotagmin-mediated endoplasmic reticulum-plasma membrane contact sites. Proc Natl Acad Sci U S A. 2015;112(16):E2004-E13.

137. Poteser M, Leitinger G, Pritz E, Platzer D, Frischauf I, Romanin C, Groschner K. Live-cell imaging of ER-PM contact architecture by a novel TIRFM approach reveals extension of junctions in response to store-operate Ca2+-entry. Sci Rep. 2016;6:35656.
138. Ishikawa K, Tamura K, Ueda H, Ito Y, Nakano A, Hara-Nishimura I, Shimada T. Synaptotamin-associated endoplasmic reticulum-plasma membrane contact sites are localized to immobile ER tubules. Plant Phys. 2018;178:641-53.
139. West M, Zurek N, Hoenger A, Voeltz GK. A 3D analysis of yeast ER structure reveals how ER domains are organized by membrane curvature. J Cell Biol. 2011;193(2):333.
140. Zurek N, Sparks L, Voeltz GK. Reticulon short hairpin transmembrane domains are used to shape ER tubules. Traffic. 2011;12(1):28-41.
141. Ando R, Hama H, Yamamoto-Hino M, Mizuno H, Miyawaki A. An optical marker based on the UV-induced green-to-red photoconversion of a fluorescent protein. Proc Natl Acad Sci U S A. 2002;99(20):12651-6.
142. Huang B, Bates M, Zhuang X. Super-resolution fluorescence microscopy. Ann Rev Biochem. 2009;78:993-1016.
143. Betzig E, Patterson GH, Sougrat R, O.W. L, Olenych S, Bonifacino JS, Davidson MW, Lippincott-Schwartz J, Hess HF. Imaging intracellular fluorescent proteins at nanometer resolution. Science. 2006;313(5793):1642-5.
144. Rust MJ, Bates M, Zhuang X. Sub-diffraction-limit imaging by stochastic optical reconstruction microscopy (STORM). Nat Methods. 2006;3:793-6.
145. Patterson GH, Lippincott-Schwartz J. A photoactivatable GFP for selective photolabeling of proteins and cells. Science. 2002;297(5588):1873-7. Epub 2002/09/14. doi: 10.1126/science.1074952. PubMed PMID: 12228718.
146. Patterson GH, Lippincott-Schwartz J. Selective photolabeling of proteins using photoactivatable GFP. Methods. 2004;32(4):445-50.
147. Gustafsson N, Culley S, Ashdown G, Owen DM, Pereira PM, Henriques R. Fast live-cell conventional fluorophore nanoscopy with ImageJ through super-resolution radial fluctuations. Nature Communications. 2016;7(doi):10.1038/ncomms12471. doi: ARTN 12471
148. Culley S, Tosheva KL, Pereira PM, Henriques R. SRRF: Universal live-cell super-resolution microscopy. Int J Biochem Cell Biol. 2018;101:74-9.
149. Roux KJ, Kim DI, Raida M, Burke B. A promiscuous biotin ligase fusion protein identifies proximal and interacting proteins in mammalian cells. J Cell Biol. 2012;196:801-10.
150. Jing J, He L, Sun A, Quintana A, Ding Y, Ma G, Tan P, Liang X, Zheng X, Chen L, Shi X, Zhang SL, Zhong L, Huang Y, Dong M-Q, Walker CL, Hogan PG, Wang Y, Zhou Y. Proteomic mapping of ER-PM junctions identifies STIMATE as a regulator of Ca2+ influx. Nat Cell Biol. 2015;17:1339-47.
151. Lee SY, Kang MG, Park JS, Lee G, Ting AY, Rhee HW. APEX fingerprinting reveals the subcellular localization of proteins of interest. Cell Rep. 2016;15(8):1837-47.
152. Mavylutov T, Chen X, Guo L, Yang J. APEX2-tagging of Sigma 1-receptor indicates subcellular proein topology with cytosolic N-terminus and ER luminal C-terminus. Protein Cell. 2018;9(8):733-7.
153. Cronan JE. Biotination of proteins in vivo. A post-translational modification to label, purify, and study proteins. J Biol Chem. 1990;265:10327-33.
154. Hung V, Zou P, Rhee HW, Udeshi ND, Cracan V, Svinkina T, Carr SA, Mootha VK, Ting AY. Proteomic mapping of the human mitochondrial intermembrane space in live cells via

ratiometric APEX tagging. Mol Cell. 2014;55(2):332-41. Epub 2014/07/09. doi: 10.1016/j.molcel.2014.06.003. PubMed PMID: 25002142; PMCID: PMC4743503.
155. Choi-Rhee E, Schulman H, Cronan JE. Promiscuous protein biotinylation by Escherichia coli biotin protein ligase. Protein Sci. 2004;13(11):3043-50.
156. Green NM. Avidin. 1. The use of [14C]biotin for kinetic studies and for assay. Biochem J. 1963;89(3):585-91.
157. Howarth M, Takao K, Hayashi Y, Ting AY. Targeting quantum dots to surface proteins in living cells with biotin ligase. Proc Natl Acad Sci U S A. 2005;102(21):7583-8.
158. Varnaitė R, MacNeill SA. Meet the neighbors: Mapping local protein interactomes by proximity-dependent labeling with BioID. Proteomics. 2016;16(19):2503-18.
159. Trinkle-Mulcahy L. Recent advances in proximity-based labeling methods for interactome mapping. F1000Research. 2019;8((F1000 Faculty Rev)):135.
160. Mechold U, Gilbert C, Ogryzko V. Codon optimization of the BirA enzyme gene leads to higher expression and an improved effiency of biotinylation of target proteins in mammalian cells. J Biotechology. 2005;116(3):245-9.
161. Hung V, Udeshi ND, Lam SS, Loh KH, Cox KJ, Pedram K, Carr SA, Ting AY. Spatially resolved proteomic mapping in living cells with the engineered peroxidase APEX2. Nat Protoc. 2016;11:456-75.
162. Lam SS, Martell JD, Kamer KJ, Deerinck TJ, Ellisman MH, Mootha VK, Ting AY. Directed evolution of APEX2 for electron microscopy and proximity labeling. Nat Methods. 2015;12(1):51-4. Epub 2014/11/25. doi: 10.1038/nmeth.3179. PubMed PMID: 25419960; PMCID: PMC4296904.
163. Han S, Udeshi ND, Deerinck TJ, Svinkina T, Ellisman MH, Carr SA, Ting AY. Proximity biotinylation as a method for mapping proteins associated with mtDNA in living cells. Cell Chem Biol. 2017;24:404-14.
164. Sarmiere PD, Weigle CM, Tamkun MM. The Kv2.1 K+ channel targets to the axon initial segment of hippocampal and cortical neurons in culture and in situ. BMC Neurosci. 2008;9:112. Epub 2008/11/19. doi: 10.1186/1471-2202-9-112. PubMed PMID: 19014551; PMCID: PMC2592246.
165. Misonou H, Trimmer JS. Determinants of voltage-gated potassium channel surface expression and localization in Mammalian neurons. Crit Rev Biochem Mol Biol. 2004;39(3):125-45. Epub 2004/12/15. doi: 10.1080/10409230490475417. PubMed PMID: 15596548.
166. Romer SH, Deardorff AS, Fyffe RE. Activity-dependent redistribution of Kv2.1 ion channels on rat spinal motoneurons. Physiol Rep. 2016;4(22):e13039. Epub 2016/11/26. doi: 10.14814/phy2.13039. PubMed PMID: 27884958; PMCID: PMC5358001.
167. Saheki Y, De Camilli P. Endoplasmic Reticulum-Plasma Membrane Contact Sites. Annu Rev Biochem. 2017;86:659-84. Epub 2017/03/17. doi: 10.1146/annurev-biochem-061516-044932. PubMed PMID: 28301744.
168. Irie T, Trussell LO. Double-Nanodomain Coupling of Calcium Channels, Ryanodine Receptors, and BK Channels Controls the Generation of Burst Firing. Neuron. 2017;96(4):856-70 e4. Epub 2017/11/18. doi: 10.1016/j.neuron.2017.10.014. PubMed PMID: 29144974; PMCID: PMC5758055.
169. Huttlin EL, Ting L, Bruckner RJ, Gebreab F, Gygi MP, Szpyt J, Tam S, Zarraga G, Colby G, Baltier K, Dong R, Guarani V, Vaites LP, Ordureau A, Rad R, Erickson BK, Wuhr M, Chick J, Zhai B, Kolippakkam D, Mintseris J, Obar RA, Harris T, Artavanis-Tsakonas S,

Sowa ME, De Camilli P, Paulo JA, Harper JW, Gygi SP. The BioPlex Network: A Systematic Exploration of the Human Interactome. Cell. 2015;162(2):425-40. Epub 2015/07/18. doi: 10.1016/j.cell.2015.06.043. PubMed PMID: 26186194; PMCID: PMC4617211.

170. Chattopadhyay D, Sengupta S. First evidence of pathogenicity of V234I mutation of hVAPB found in Amyotrophic Lateral Sclerosis. Biochemical and Biophysical Research Communications. 2014;448(1):108-13. doi: 10.1016/j.bbrc.2014.04.102. PubMed PMID: WOS:000336558800018.
171. Kabashi E, El Oussini H, Bercier V, Gros-Louis F, Valdmanis PN, McDearmid J, Mejier IA, Dion PA, Dupre N, Hollinger D, Sinniger J, Dirrig-Grosch S, Camu W, Meininger V, Loeffler JP, Rene F, Drapeau P, Rouleau GA, Dupuis L. Investigating the contribution of VAPB/ALS8 loss of function in amyotrophic lateral sclerosis. Hum Mol Genet. 2013;22(12):2350-60. Epub 2013/03/01. doi: 10.1093/hmg/ddt080. PubMed PMID: 23446633.
172. O'Connell KM, Tamkun MM. Targeting of voltage-gated potassium channel isoforms to distinct cell surface microdomains. J Cell Sci. 2005;118(Pt 10):2155-66. Epub 2005/04/28. doi: 10.1242/jcs.02348. PubMed PMID: 15855232.
173. Tamkun MM, O'Connell K M, Rolig AS. A cytoskeletal-based perimeter fence selectively corrals a sub-population of cell surface Kv2.1 channels. J Cell Sci. 2007;120(Pt 14):2413-23. Epub 2007/07/04. doi: 10.1242/jcs.007351. PubMed PMID: 17606996.
174. Akin EJ, Sole L, Dib-Hajj SD, Waxman SG, Tamkun MM. Preferential targeting of Nav1.6 voltage-gated Na+ Channels to the axon initial segment during development. PLoS One. 2015;10(4):e0124397. Epub 2015/04/16. doi: 10.1371/journal.pone.0124397. PubMed PMID: 25874799; PMCID: PMC4398423.
175. Akin EJ, Sole L, Johnson B, Beheiry ME, Masson JB, Krapf D, Tamkun MM. Single-Molecule Imaging of Nav1.6 on the Surface of Hippocampal Neurons Reveals Somatic Nanoclusters. Biophys J. 2016;111(6):1235-47. Epub 2016/09/23. doi: 10.1016/j.bpj.2016.08.016. PubMed PMID: 27653482; PMCID: PMC5034717.
176. Park KS, Mohapatra DP, Misonou H, Trimmer JS. Graded regulation of the Kv2.1 potassium channel by variable phosphorylation. Science. 2006;313(5789):976-9. Epub 2006/08/19. doi: 10.1126/science.1124254. PubMed PMID: 16917065.
177. Suzuki H, Kanekura K, Levine TP, Kohno K, Olkkonen VM, Aiso S, Matsuoka M. ALS-linked P56S-VAPB, an aggregated loss-of-function mutant of VAPB, predisposes motor neurons to ER stress-related death by inducing aggregation of co-expressed wild-type VAPB. J Neurochem. 2009;108(4):973-85. Epub 2009/02/03. doi: 10.1111/j.0022-3042.2008.05857.x. PubMed PMID: 19183264.
178. Klein JS, Jiang S, Galimidi RP, Keeffe JR, Bjorkman PJ. Design and characterization of structured protein linkers with differing flexibilities. Protein Eng Des Sel. 2014;27(10):325-30. Epub 2014/10/11. doi: 10.1093/protein/gzu043. PubMed PMID: 25301959; PMCID: PMC4191447.
179. Becker JW, Reeke GN, Jr. Three-dimensional structure of beta 2-microglobulin. Proc Natl Acad Sci U S A. 1985;82(12):4225-9. Epub 1985/06/01. PubMed PMID: 3889925; PMCID: PMC397969.
180. Xia ZP, Liu YH. Reliable and global measurement of fluorescence resonance energy transfer using fluorescence microscopes. Biophysical Journal. 2001;81(4):2395-402. doi: Doi 10.1016/S0006-3495(01)75886-9. PubMed PMID: WOS:000171205100052.

181. Hoppe A, Christensen K, Swanson JA. Fluorescence resonance energy transfer-based stoichiometry in living cells. Biophys J. 2002;83(6):3652-64. Epub 2002/12/24. doi: 10.1016/S0006-3495(02)75365-4. PubMed PMID: 12496132; PMCID: PMC1302440.
182. Chung JJ, Li M. Biochemical characterization of the native Kv2.1 potassium channel. FEBS J. 2005;272(14):3743-55. Epub 2005/07/13. doi: 10.1111/j.1742-4658.2005.04802.x. PubMed PMID: 16008572.
183. Simons K, Ikonen E. Functional rafts in cell membranes. Nature. 1997;387(6633):569-72. Epub 1997/06/05. doi: 10.1038/42408. PubMed PMID: 9177342.
184. Bishop HI, Cobb MM, Kirmiz M, Parajuli LK, Mandikian D, Philp AM, Melnik M, Kuja-Panula J, Rauvala H, Shigemoto R, Murray KD, Trimmer JS. Kv2 Ion Channels Determine the Expression and Localization of the Associated AMIGO-1 Cell Adhesion Molecule in Adult Brain Neurons. Front Mol Neurosci. 2018;11(doi):1. Epub 2018/02/07. doi: 10.3389/fnmol.2018.00001. PubMed PMID: 29403353; PMCID: PMC5780429.
185. Peltola MA, Kuja-Panula J, Lauri SE, Taira T, Rauvala H. AMIGO is an auxiliary subunit of the Kv2.1 potassium channel. Embo Reports. 2011;12(12):1293-9. doi: 10.1038/embor.2011.204. PubMed PMID: WOS:000297809500019.
186. Kim S, Leal SS, Ben Halevy D, Gomes CM, Lev S. Structural Requirements for VAP-B Oligomerization and Their Implication in Amyotrophic Lateral Sclerosis-associated VAP-B(P56S) Neurotoxicity. Journal of Biological Chemistry. 2010;285(18):13839-49. doi: 10.1074/jbc.M109.097345. PubMed PMID: WOS:000276987700059.
187. Wu H, Kwong PD, Hendrickson WA. Dimeric association and segmental variability in the structure of human CD4. Nature. 1997;387(6632):527-30. Epub 1997/05/29. doi: 10.1038/387527a0. PubMed PMID: 9168119.
188. Johnston J, Griffin SJ, Baker C, Skrzypiec A, Chernova T, Forsythe ID. Initial segment Kv2.2 channels mediate a slow delayed rectifier and maintain high frequency action potential firing in medial nucleus of the trapezoid body neurons. J Physiol. 2008;586(14):3493-509. Epub 2008/05/31. doi: 10.1113/jphysiol.2008.153734. PubMed PMID: 18511484; PMCID: PMC2538803.
189. Sanchez-Ponce D, DeFelipe J, Garrido JJ, Munoz A. Developmental Expression of Kv Potassium Channels at the Axon Initial Segment of Cultured Hippocampal Neurons. Plos One. 2012;7(10):e48557. doi: 10.1371/journal.pone.0048557. Epub 2012 Oct 31. doi: ARTN e48557
190. Jensen CS, Watanabe S, Stas JI, Klaphaak J, Yamane A, Schmitt N, Olesen SP, Trimmer JS, Rasmussen HB, Misonou H. Trafficking of Kv2.1 Channels to the Axon Initial Segment by a Novel Nonconventional Secretory Pathway. J Neurosci. 2017;37(48):11523-36. Epub 2017/10/19. doi: 10.1523/JNEUROSCI.3510-16.2017. PubMed PMID: 29042434.
191. Shaw G, Morse S, Ararat M, Graham FL. Preferential transformation of human neuronal cells by human adenoviruses and the origin of HEK 293 cells. FASEB J. 2002;16(8):869-71. Epub 2002/04/23. doi: 10.1096/fj.01-0995fje. PubMed PMID: 11967234.
192. Mohapatra DP, Trimmer JS. The Kv2.1 C terminus can autonomously transfer Kv2.1-like phosphorylation-dependent localization, voltage-dependent gating, and muscarinic modulation to diverse Kv channels. Journal of Neuroscience. 2006;26(2):685-95. doi: 10.1523/Jneurosci.4620-05.2006. PubMed PMID: WOS:000234556200037.
193. Bajar BT, Wang ES, Zhang S, Lin MZ, Chu J. A Guide to Fluorescent Protein FRET Pairs. Sensors (Basel). 2016;16(9):s16091488. doi: 10.3390/s. Epub 2016/09/21. doi: 10.3390/s16091488. PubMed PMID: 27649177; PMCID: PMC5038762.

194. Misonou H, Menegola M, Mohapatra DP, Guy LK, Park KS, Trimmer JS. Bidirectional activity-dependent regulation of neuronal ion channel phosphorylation. J Neurosci. 2006;26(52):13505-14. Epub 2006/12/29. doi: 10.1523/JNEUROSCI.3970-06.2006. PubMed PMID: 17192433.
195. Cerda O, Trimmer JS. Activity-dependent phosphorylation of neuronal Kv2.1 potassium channels by CDK5. J Biol Chem. 2011;286(33):28738-48. Epub 2011/06/30. doi: 10.1074/jbc.M111.251942. PubMed PMID: 21712386; PMCID: PMC3190682.
196. King AN, Manning CF, Trimmer JS. A unique ion channel clustering domain on the axon initial segment of mammalian neurons. J Comp Neurol. 2014;522(11):2594-608. Epub 2014/01/31. doi: 10.1002/cne.23551. PubMed PMID: 24477962; PMCID: PMC4133991.
197. de Kovel CGF, Syrbe S, Brilstra EH, Verbeek N, Kerr B, Dubbs H, Bayat A, Desai S, Naidu S, Srivastava S, Cagaylan H, Yis U, Saunders C, Rook M, Plugge S, Muhle H, Afawi Z, Klein KM, Jayaraman V, Rajagopalan R, Goldberg E, Marsh E, Kessler S, Bergqvist C, Conlin LK, Krok BL, Thiffault I, Pendziwiat M, Helbig I, Polster T, Borggraefe I, Lemke JR, van den Boogaardt MJ, Moller RS, Koeleman BPC. Neurodevelopmental Disorders Caused by De Novo Variants in KCNB1 Genotypes and Phenotypes. JAMA Neurol. 2017;74(10):1228-36. Epub 2017/08/15. doi: 10.1001/jamaneurol.2017.1714. PubMed PMID: 28806457; PMCID: PMC5710242.
198. Dickson EJ, Jensen JB, Hille B. Regulation of calcium and phosphoinositides at endoplasmic reticulum-membrane junctions. Biochemical Society Transactions. 2016;44(2):467-73. doi: 10.1042/Bst20150262. PubMed PMID: WOS:000377518000021.
199. Bian X, Saheki Y, De Camilli P. Ca(2+) releases E-Syt1 autoinhibition to couple ER-plasma membrane tethering with lipid transport. EMBO J. 2018;37(2):219-34. doi: 10.15252/embj.201797359. Epub 2017 Dec 8.
200. Lees JA, Messa M, Sun EW, Wheeler H, Torta F, Wenk MR, De Camilli P, Reinisch KM. Lipid transport by TMEM24 at ER-plasma membrane contacts regulates pulsatile insulin secretion. Science. 2017;355(6326):355/6326/eaah171. doi: 10.1126/science.aah6171. doi: ARTN eaah6171
201. Olkkonen VM. OSBP-Related Protein Family in Lipid Transport Over Membrane Contact Sites. Lipid Insights. 2015;8(Suppl 1):1-9. Epub 2015/12/31. doi: 10.4137/LPI.S31726. PubMed PMID: 26715851; PMCID: PMC4685180.
202. Olkkonen VM, Levine TP. Oxysterol binding proteins: in more than one place at one time? Biochem Cell Biol. 2004;82(1):87-98.
203. Stradalova V, Blazikova M, Grossmann G, Opekarová M, Tanner W, Malinsky J. Distribution of cortical endoplasmic reticulum determines positioning of endocytic events in yeast plasma membrane. PLoS One. 2012;7(4):e35132.
204. Stefan CJ. Building ER-PM contacts: keeping calm and ready on alarm. Curr Opin Cell Biol. 2018;53:1-8.
205. Hanada K, Kumagai K, Yasuda S, Miura Y, Kawano M, Fukasawa M, Nishijima M. Molecular machinery for non-vesicular trafficking of ceramide. Nature. 2003;426(6968):803-9.
206. Kawano M, Kumagai K, Nishijima M, Hanada K. Efficient trafficking of ceramide from the endoplasmic reticulum to the Golgi apparatus requires a VAMP-associated protein-interacting FFAT motif of CERT. J Biol Chem. 2006;281(40):30279-88.
207. Leung YM, Kang Y, Gao X, Xia F, Xie H, Sheu L, Tsuk S, Lotan I, Tsushima RG, Gaisano HY. Syntaxin 1A binds to the cytoplasmic C terminus of Kv2.1 to regulate channel gating

and trafficking. J Biol Chem. 2003;278(19):17532-8. Epub 2003/03/07. doi: 10.1074/jbc.M213088200. PubMed PMID: 12621036.
208. Leung YM, Kang Y, Xia F, Sheu L, Gao X, Xie H, Tsushima RG, Gaisano HY. Open form of syntaxin-1A is a more potent inhibitor than wild-type syntaxin-1A of Kv2.1 channels. Biochem J. 2005;387(Pt 1):195-202. Epub 2004/11/03. doi: 10.1042/BJ20041625. PubMed PMID: 15518587; PMCID: PMC1134947.
209. Furuse M, Hirase T, Itoh M, Nagafuchi A, Yonemura S, Tsukita S, Tsukita S. Occludin: a novel integral membrane protein localizing at tight junctions. J Cell Biol. 1993;123(6):1777-88.
210. Furuse M, Itoh M, Nagafuchi A, Yonemura S, Tsukita S, Tsukita S. Direct association of occludin with ZO-1 and its possible involvement in the localization of occludin at tight junctions. J Cell Biol. 1994;127(6):1617-26.
211. Lapierre LA, Tuma PL, Navarre J, Goldenring JR, J.M. A. VAP-33 localizes to both an intracellular vesicle population and with occludin at the tight junction. J Cell Sci. 1999;112(Pt 21):3723-32.
212. Di Mattia T, Tomasetto C, Alpy F. A third musketeer on the ER: MOSPD2 is a novel VAP-related receptor for FFAT motifs. Contact. 2018;1.
213. Fan Z, Makielski JC. Anionic phospholipids activate ATP-sensitive potassium channels. J Biol Chem. 1997;272:5388-95.
214. Hilgemann DW, Ball R. Regulation of cardiac Na+, Ca2+ exchange and KATP potassium channels by PIP2. Science. 1996;273(5277):956-9.
215. Weingarth M, Prokofyev A, van der Cruijsen EAW, Nand D, Bonvin AMJJ, Pongs O, Baldus M. Structural determinants of specific lipid binding to potassium channels. J Am Chem Soc. 2013;135(10):3983-8.
216. Delgado-Ramírez M, De Jesús-Pérez JJ, Aréchiga-Figueroa IA, Arreola J, Adney SK, Villalba-Galea CA, Logothetis DE, Rodríguez-Menchaca AA. Regulation of Kv2.1 channel inactivation by phosphatidylinositol 4,5-biphosphate. Sci Rep. 2018;8:1769.
217. Okeke E, Dingsdale H, Parker T, Voronina S, Tepikin AV. Endoplasmic reticulum-plasma membrane junctions: structure, function and dynamics. J Physiol. 2016;594(11):2837-47.
218. Vullhorst D, Mitchell RM, Keating C, Roychowdhury S, Karavanova I, Tao-Cheng JH, Buonanno A. A negative feedback loop controls NMDA receptor function in cortical interneurons via neuregulin 2/ErbB4 signalling. Nat Commun. 2015;6:7222. Epub 2015/06/02. doi: 10.1038/ncomms8222. PubMed PMID: 26027736; PMCID: PMC4451617.
219. Casanovas A, Salvany S, Lahoz V, Tarabal O, Piedrafita L, Sabater R, Hernández S, Calderó J, Esquerda JE. Neuregulin 1-ERB module in C-bouton synapses on somatic motor neurons: molecular compartmentation and response to peripheral nerve injury. Scientific Reports. 2017;7:Article number: 40155.
220. Hsieh TS, Chen YJ, Chang CL, Lee WR, Liou J. Cortical actin contributes to spatial organization of ER-PM junctions. Mol Biol Cell. 2017;28(23):3171-80. Epub 2017/09/29. doi: 10.1091/mbc.E17-06-0377. PubMed PMID: 28954864; PMCID: PMC5687020.
221. Encinar Del Dedo J, Idrissi FZ, Fernandez-Golbano IM, Garcia P, Rebollo E, Krzyzanowski MK, Grotsch H, Geli MI. ORP-Mediated ER Contact with Endocytic Sites Facilitates Actin Polymerization. Dev Cell. 2017;43(5):588-602 e6. Epub 2017/11/28. doi: 10.1016/j.devcel.2017.10.031. PubMed PMID: 29173820.

222. Delgado-Ramírez M, Rodríguez-Menchaca AA. Cytoskeleton disruption affects Kv2.1 channel function and its modulation by PIP2. J Physiol Sci. 2019;69(3):513-21.
223. Ovesny M, Krizek P, Borkovec J, Svindrych Z, Hagen GM. ThunderSTORM: a comprehensive ImageJ plug-in for PALM and STORM data analysis and super-resolution imaging. Bioinformatics. 2014;30(16):2389-90. Epub 2014/04/29. doi: 10.1093/bioinformatics/btu202. PubMed PMID: 24771516; PMCID: PMC4207427.
224. Sadegh S, Higgins JL, Mannion PC, Tamkun MM, Krapf D. Plasma Membrane is Compartmentalized by a Self-Similar Cortical Actin Meshwork. Phys Rev X. 2017;7(1):011031-1--10. Epub 2017/07/12. doi: 10.1103/PhysRevX.7.011031. PubMed PMID: 28690919; PMCID: PMC5500227.
225. van Vliet AR, Agostinis P. PERK and filamin A in actin cytoskeleton remodeling at ER-plasma membrane contact sites. Mol Cell Oncol. 2017;4(5):e1340105. doi: 10.1080/23723556.2017.1340105. eCollection 2017.
226. van Vliet AR, Giordano F, Gerlo S, Segura I, Van Eygen S, Molenberghs G, Rocha S, Houcine A, Derua R, Verfaillie T, Vangindertael J, De Keersmaecker H, Waelkens E, Tavernier J, Hofkens J, Annaert W, Carmeliet P, Samali A, Mizuno H, Agostinis P. The ER Stress Sensor PERK Coordinates ER-Plasma Membrane Contact Site Formation through Interaction with Filamin-A and F-Actin Remodeling. Mol Cell. 2017;65(5):885-99.e6. doi: 10.1016/j.molcel.2017.01.020. Epub Feb 23.
227. Asanov A, Sherry R, Sampieri A, Vaca L. A relay mechanism between EB1 and APC facilitate STIM1 puncta assembly at endoplasmic reticulum-plasma membrane junctions. Cell Calcium. 2013;54(3):246-56.
228. Chung J, Torta F, Masai K, Lucast L, Czapla H, Tanner LB, Narayanaswamy P, Wenk MR, Nakatsu F, De Camilli P. PI4P/phospatidylserine countertransport at ORP5- and ORP8-mediated ER-plasma membrane contacts. Science. 2015;349(6246):428-32.
229. Deardorff AS, Romer SH, Sonner PM, Fyffe RE. Swimming against the tide: investigations of the C-bouton synapse. Front Neural Circuits. 2014;8(doi):106. Epub 2014/10/04. doi: 10.3389/fncir.2014.00106. PubMed PMID: 25278842; PMCID: PMC4167003.
230. Romer SH, Dominguez KM, Gelpi MW, Deardorff AS, Tracy RC, Fyffe RE. Redistribution of Kv2.1 ion channels on spinal motoneurons following peripheral nerve injury. Brain Res. 2014;1547(doi):1-15. Epub 2013/12/21. doi: 10.1016/j.brainres.2013.12.012. PubMed PMID: 24355600; PMCID: PMC3970712.
231. Frazzini V, Guarnieri M, Bomba M, Navarra R, Morabito C, Mariggiò MA, Sensi SL. Altered Kv2.1 functioning promotes increased excitability in hippocampal neurons of an Alzheimer's disease mouse model. Cell Death & Disease. 2016;7(e2100).
232. Kirmiz M, Vierra NC, Palacio S, Trimmer JS. Identification of VAPA and VAPB as Kv2 Channel-Interacting Proteins Defining Endoplasmic Reticulum-Plasma Membrane Junctions in Mammalian Brain Neurons. Journal of Neuroscience. 2018;38(35):7562-84. doi: 10.1523/Jneurosci.0893-18.2018. PubMed PMID: WOS:000442995700003.
233. Kucharz K, Krogh M, Ng AN, Toresson H. NMDA receptor stimulation induces reversible fission of the neuronal endoplasmic reticulum. PloS One. 2009;4(4):e5250.
234. Alli-Balogun GO, Levine TP. Regulation of targeting determinants in interorganelle communication. Curr Opin Cell Biol. 2019;57:106-14.
235. Arai K, Ikegaya Y, Nakatani Y, Kudo I, Nishiyama N, Matsuki N. Phospholipase A2 mediates ischemic injury in the hippocampus: a regional difference of neuronal vulnerability. Eur J Neurosci. 2001;13(12):2319-23.

236. Brady KM, Texel SJ, Kishimoto K, Koehler RC, Sapirstein A. Cytosolic phospholipase A2 alpha modulates NMDA neurotoxicity in mouse hippocampal cultures. Eur J Neurosci. 2006;24(12):3381-6.
237. Shen Y, Kishimoto K, D.J. L, Sapirstein A. Cytosolic phospholipase A2 alpha mediates electrophysiologic responses of hippocampal pyramidal neurons to neurotoxic NMDA treatment. Proc Natl Acad Sci U S A. 2007;104(14):6078-83.
238. Guo A, Hall D, Zhang C, Peng T, Miller JD, Kutschke W, Grueter CE, Johnson FL, Lin RZ, Song L-S. Molecular determiniants of calpain-dependent cleavage of Junctophilin-2 protein in cardiomyocytes. J Biol Chem. 2015;290:17946-55.
239. Murphy RM, Dutka TL, Horvath D, Bell JR, Delbridge LM, Lamb GD. Ca2+-dependent proteolysis of junctophilin-1 and junctophilin-2 in skeletal and cardiac muscle. J Physiol. 2012;591(3):719-29.
240. Toral-Ojeda I, Aldanonda G, Vallejo-Illarramendi A. Junctophilins and μ-calpain: partners in excitation–contraction uncoupling. J Physiol. 2013;591(15):3679-80.
241. Green EM, Barret CF, Bultynck G, Shamah SM, Dolmetsch RE. The tumor suppressor eIF3e mediates calcium-dependent internalization of the L-type calcium channel Cav1.2. Neuron. 2007;55(4):615-32.
242. Cayouette S, Boulay G. Intracellular trafficking of TRP channels. Cell Calcium. 2007;42(2):225-32.
243. Cayouette S, Lussier MP, Mathieu EL, Bousquet SM, Boulay G. Exocytotic insertion of TRPC6 channel into the plasma membrane upon Gq protein-coupled receptor activation. J Biol Chem. 2004;279(8):7241-6. Epub 2003/12/10. doi: 10.1074/jbc.M312042200. PubMed PMID: 14662757.

APPENDIX I: The presence of Kv2.2 and junctophilin-4 do not alter the concentration of VAPs at Kv2.1-induced ER/PM contact sites

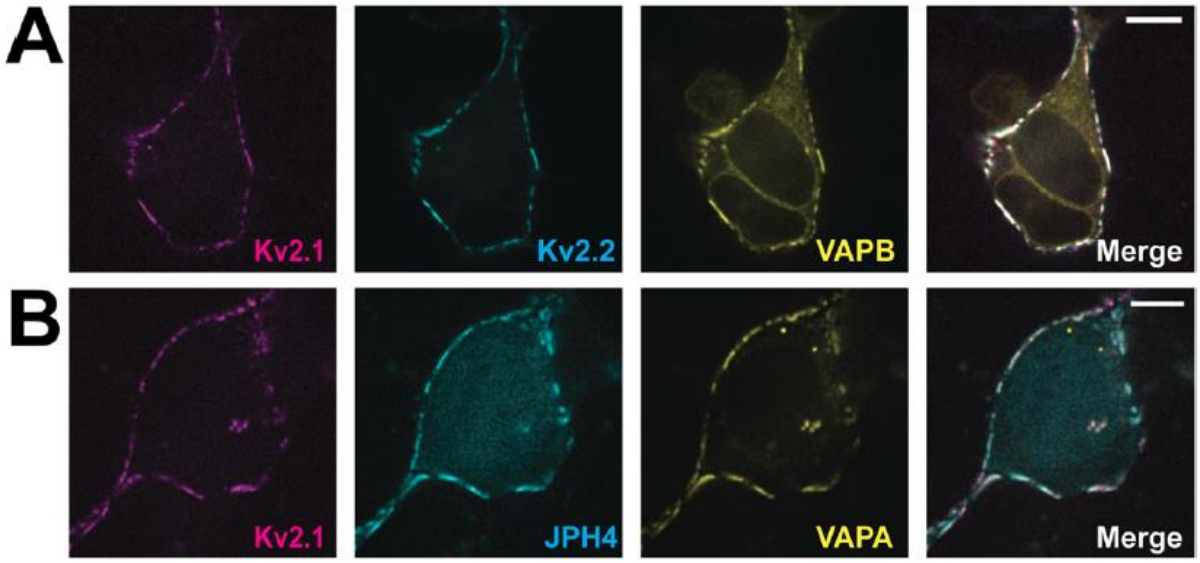

Figure 7.1. The presence of Kv2.2 and junctophilin-4 do not alter the concentration of VAPs at Kv2.1-induced ER/PM contact sites. (A) Co-expression of Kv2.1loopBad labeled with streptavidin-CF640, GFP-Kv2.2, and mRuby-VAPB. (B) Coexpression of Kv2.1loopBAD labeled with streptavidin-CF640, mCherry-JPH4, and VAPA-GFP. Scale bars represent 10 µm.

APPENDIX II: Kv2.1, Kv2.2, and Kv2.1:573-598 colocalization with VAPs in the axon initial segment

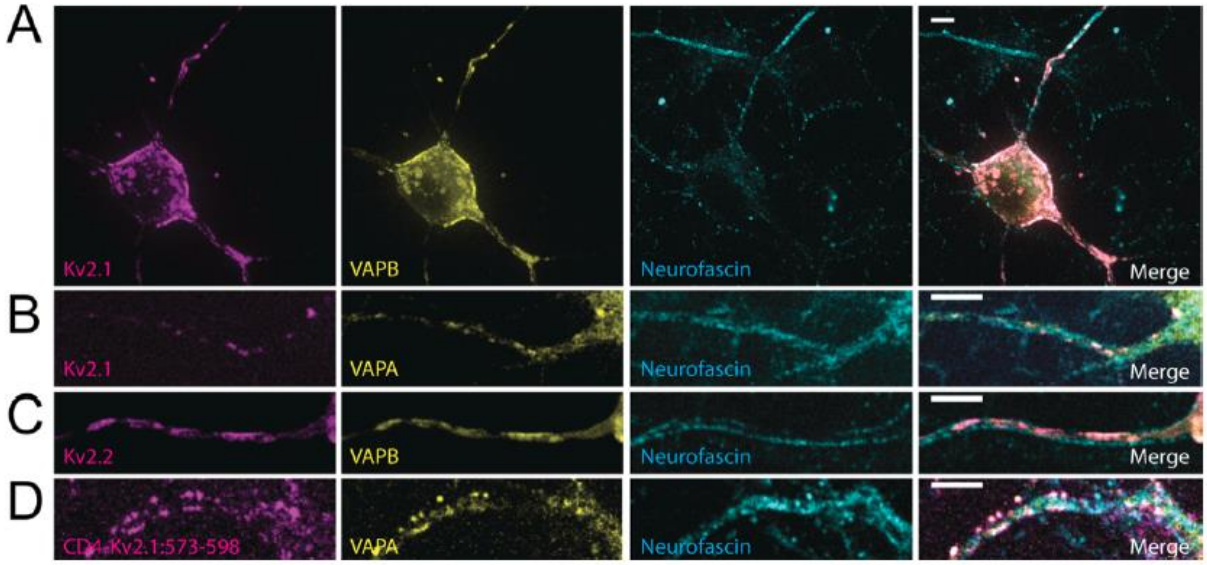

Figure 7.2. Use of neurofascin immunostaining to identify the axon initial segment. (A) Representative image showing the localization of transfected Kv2.1loopBAD, VAPB-GFP and neurofascin immune-staining in live DIV7 rat hippocampal neurons. Surface Kv2.1loopBAD was visualized with CF640-conjugated streptavidin and antibody binding to extracellular neurofascin was detected using Alexa 594-conjugated goat anti mouse secondary antibody. Note that the neurofascin-positive axon initial segment (AIS) in the top left corner is derived from a non-transfected neuron. (B) Colocalization of VAPA-GFP with Kv2.1 within the neurofascin-positive AIS. (C) Colocalization of VAPB-mRuby2 with GFP-Kv2.2 within the neurofascin-positive AIS (labeled with Alexa-647 secondary antibody). (D) Colocalization of VAPA-GFP with the CD4-Kv2.1:573-598 chimera (labeled with CF640-conjugated anti-CD4 antibody) within the neurofascin-positive AIS (labeled with Alexa 594). All images are maximum intensity projections. Scale bars represent 5 µm.

APPENDIX III: Cav1.2 channel density increases during glutamate stimulation in hippocampal neurons

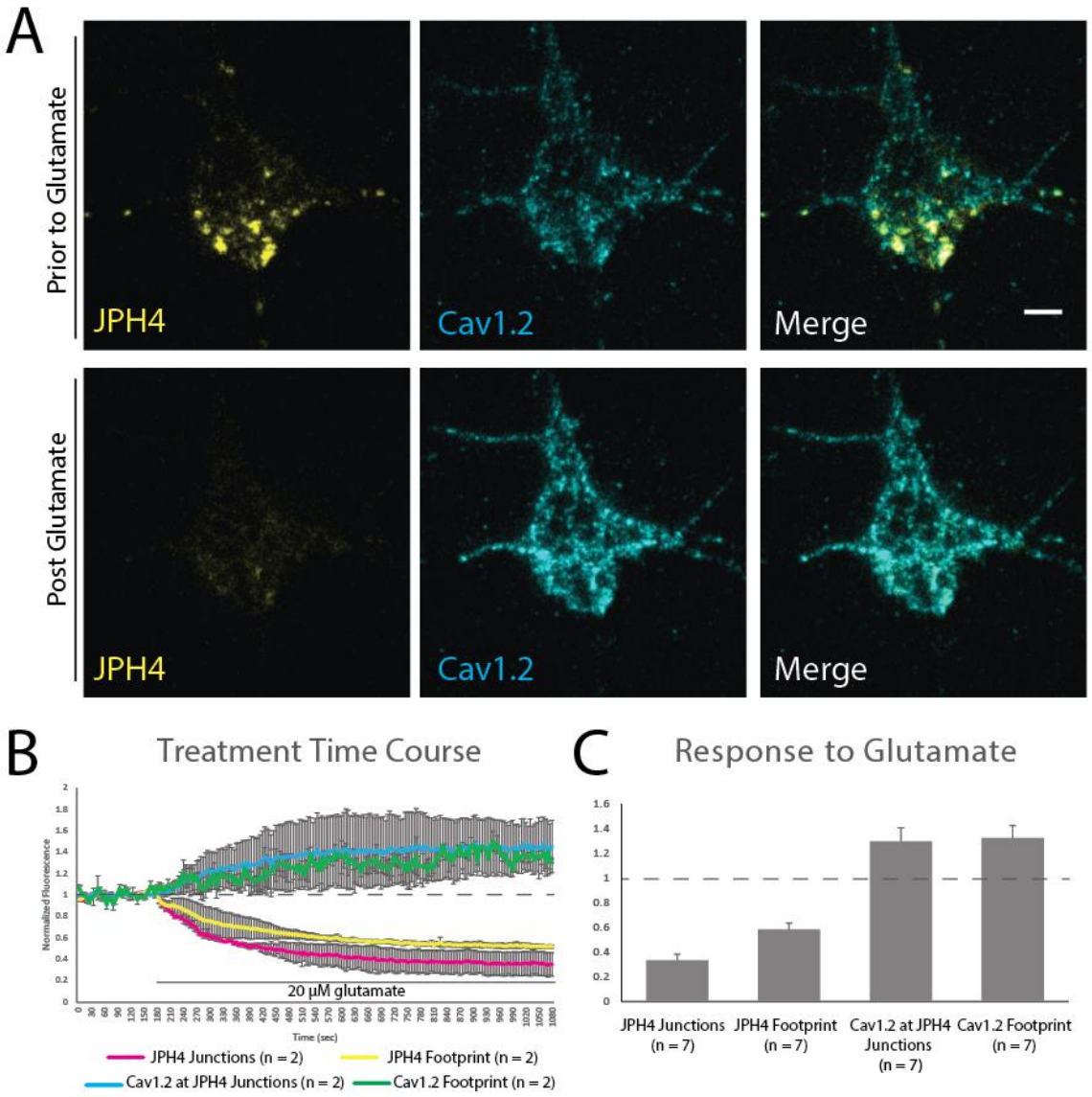

Figure 7.3. Cav1.2 channel density increases during glutamate stimulation in hippocampal neurons. (A) Prior to treatment with 20 µM glutamate, mCherry-JPH4 forms ER/PM junctions at the surface of rat hippocampal neurons. Cav1.2HA labeled with anti-HA488 antibody demonstrate a preference for colocalization to these areas. Post glutamate treatment, JPH4 junctions are disassembled and Cav1.2 fluorescence across the entirety of the basal surface increases. (B) Fluorescence time course during glutamate treatment. mCherry-JPH4 fluorescence at junctions decreases rapidly during treatment, as does measurements of mCherry-JPH4 across the entire cellular footprint. Cav1.2 fluorescence at JPH4 junctions increases during glutamate treatment. This increase is mirrored in measurements of the total cellular footprint. (C) Normalized fluorescence changes after glutamate treatment. Scale bar represents 5 µm. Error bars indicate SEM.

APPENDIX IV: Sequence Alignment of FFAT Motifs and Downstream Sequences in Known VAP Interactors

Figure 7.4 Sequence Alignment of FFAT Motifs and Downstream Sequences in Known VAP Interactors. Kv.21 residues S601 (FFAT +9) and S607 (FFAT +15) are involved in mediating VAP-Kv2 unbinding. A number of other known VAP interactors have serines/threonines or negatively charged residues at these locations or immediately adjacent. Whether this is a conserved mechanism remains to be tested.

APPENDIX V: Gifts from Google Scholar Alert: AMIGO

Scholar Alert: [AMIGO]

Holistic Goat Care: A Comprehensive Guide to Raising Healthy Animals, Preventing Common Ailments, and Troubleshooting Problems
G Caldwell - 2017
... needs. I kept those Pygmy or Pygmy-cross goats simply as cute pets and companions for my horses. Fortunately for me, my cavalier treatment had no ill effects on them, and Sundance, **Amigo**, and Goatee-goat lived full lives. It ...

Scholar Alert: [AMIGO]

Hey **amigo**! Do you want to go on a trip? Do you want mushrooms?
LZ Montalvo - Australasian Journal of Popular Culture, 2017
The Mazatec people from the northern highlands of the Mexican State of Oaxaca are known for the syncretism of their religion, which combines pre-Hispanic culture and Catholic religion introduced with Spanish colonization in the sixteenth century. Nowadays, Mazatec

Scholar Alert: [AMIGO]

Monitoring the staling of wheat bread using 2D MIR-NIR correlation spectroscopy
T Ringsted, HW Siesler, SB Engelsen - Journal of Cereal Science, 2017
... Gray and Bemiller, 2003). The industrial reference measurement to bread staling and the most direct correlation to sensory evaluation is texture profile analysis (TPA) (**Amigo** et al., 2016 ; Bourne, 1978). Several other methods ...

Scholar Alert: [AMIGO]

" A White Lady is Like Gold for Us": Economic and Emotional Dimensions of Kenyan-German Romantic Relations
N Berman - German Studies Review, 2017
... Even though Diani Agriculture and Research Development, which was scandal-ridden throughout (and in fact linked to the "**Amigo**-Affäre" that forced Bavarian Ministerpräsident Max Streibl to resign in 1993), was dissolved in the 1990s, the [End Page 129] question regarding ...

[PDF] A new micro-baking method for determination of crumb firmness properties in fresh bread and bread made from frozen dough
J Frauenlob, M Nava, S D'Amico, H Grausgruber...
... The Avrami exponent n indicates the nucleation type and describes the behavioral approach to reach the final state of staling (**Amigo** et al., 2016). Both parameters revealed
big differences between waxy wheat and standard bread wheat. ...

[PDF] Hangover relieving effect of Sanghwang mushroom mycelium cultured in germinated buckwheat

YJ An, SM Cho, MS Kim, HH Moon, DS Park, NG Jeon... - Korean J Vet Res, 2017

... Korean J Med Crop Sci 1999, 7, 263-268. Korean. 2. Carbon S, Ireland A, Mungall CJ, Shu S, Marshall B, Lewis S; **AmiGO** Hub; Web Presence Working Group. **AmiGO**: online access to ontology and annotation data. Bioinformatics 2009, 25, 288-289. ...

The virtual reality simulator-based catheter training system with haptic feedback

S Guo, M Yu, Y Song, L Zhang - Mechatronics and Automation (ICMA), 2017 IEEE ..., 2017

... Even some commercial companies like Hansen Medical and Catheter Robotics Inc. have developed catheter robotic systems such as Sensi (Hansen Medical) [1],[2] and **Amigo** (Catheter Robotics Inc.) [3] to assist surgeons. ...

Detecting semen stains on fabrics using near infrared hyperspectral images and multivariate models

CS Silva, MF Pimentel, JM **Amigo**, RS Honorato... - TrAC Trends in Analytical ..., 2017

Abstract Identification of semen stains is a critical step in evidence analysis in cases of sexual assaults (rape, child molestation, sexual harassments, etc). Presumptive and confirmatory methodologies that are nondestructive and can be used at crime scenes are

The Man on the Beach

JS Sibara - Ploughshares, 2018

... Each time he turned the wide, flat paddle over to me, he wiggled his eyebrows and his mustache in unison, pointed at the bulge of muscle under his rolled-up sleeve, and said, Only muscle will win over your little sweetheart, **amigo**-amico. He meant my friend Emelia ...

The sign-off

G Page - Quadrant, 2017

... How long, we ask, does "ever" last? "Warm wishes" stokes a winter fire but sounds a bit too cosy.

"God bless" may frighten atheists. "Inshallah" can be OK but just a little scary. Unfazed by our fatuities, the future wanders where it will. Adios, **amigo**. Geoff Page

…Adios, amigos